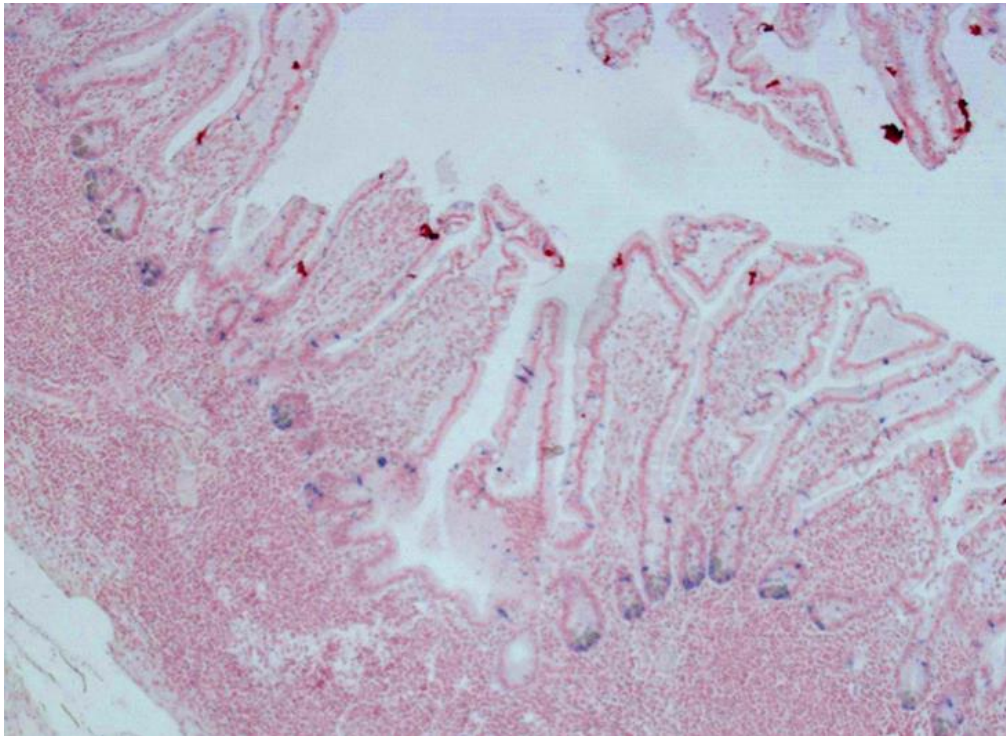Master Thesis in Medical and Molecular Biology

Characterization of two microRNAs in endocrine tissue

Dår Kristian Sarusie

Juni 2015

Center for Genomic Medicine
Rigshospitalet, Copenhagen University Hospital
&
Medical and Molecular Biology
Department of Science, System and Models
Roskilde University

Submitted 1th June 2015

Front Cover:

A section of the small intestine that is stained for miR-375

Paraffinized tissue section of the small intestine with villi projections and adherent crypts. Cells are stained with double DIG-labeled miRCURY miR-375 LNA detection probe (blue), showing miR-375 expressing cells, near the crypt base and along the villi. Nuclear Fast Red™ is used as nuclear counterstain (red).

Acknowledgements

Acronyms

5-HIAA – 5-hydroxyindoleacetate

5-HT – 5-hydroxytryptamine (serotonin)

5-HTP – 5-hydroxytryptophan

ATP – adenosine triphosphate

bHLH – basic helix loop helix

Cg – chromogranin

CT – computed tomography

C-terminal – carboxyl terminal

CCK – cholecystokinin

CS – carcinoid syndrome

Dll – delta like ligand

DNA – deoxyribonucleic acid

DNES – diffuse neuroendocrine system

DSL - delta/serrate/lag-2

ECL – enterochromaffin-like

EGF – epidermal growth factor

ELISA – enzyme-linked immunosorbent assay

ETM – epithelial to mesenchymal transition

EUS – endoscopic ultrasonography

FDG – fluorodeoxyglucose

FSG – fasting serum gastrin

GEP-NET – gastroenteropancreatic neuroendocrine tumor

GI-tract – gastrointestinal tract

IRMA – immunoradiometric assay

LDCV – large dense-core vesicle

LNA – locked nucleic acid

MEN – multiple endocrine neoplasia

MIBG – *meta*-iodobenzylguanidine

miRNA – microRNA

MRI – magnetic resonance imaging

NECD – notch extracellular domain

NE – neuroendocrine

NF – non functional

NICD – notch intracellular domain

NME – necrolytic migratory erythema

NSE – neuron specific enolase

N-terminal – amino terminal

PET – positron emission tomography

PNET – pancreatic neuroendocrine tumor

PP – pancreatic polypeptide

PPI – proton pump inhibitor

Pre-miRNA – precursor microRNA

Pri-miRNA – primary microRNA

PRRT – peptide receptor radionuclide therapy

PS – primitive streak

RBP-Jκ – recombination signal binding protein for immunoglobulin kappa J region

RFA – radiofrequency ablation

RISC – RNA-induced silencing complex

RNA – ribonucleic acid

RT-PCR – reverse transcription PCR

SCLC – small cell lung cancer

SLMV – synaptic-like microvesicle

SPECT – single photon emission computed tomography

SRS – somatostatin receptor scintigraphy

3'UTR – 3'-untranslated region

VIP – vasoactive intestinal polypeptide

VPA - valproic acid

WDHA – watery diarrhea, hypokalemia, achlorhydria (Verner-Morrison syndrome)

ZES – zollinger ellison syndrome

Summary

Gastroenteropancreatic neuroendocrine tumors (GEP-NETs) are heterogeneous group of tumors that originate from various cell types belonging to the diffuse neuroendocrine system (DNES), which is ultimately derived from the endodermal primitive gut. The malignant transformations of these cells are caused by genetic alternation as for instance in the tumor suppressor *MEN1* gene; however for most tumors the causation is not identified. GEP-NETs are generally well-differentiated with a benign course and can occur with typical syndromes due to hormone hypersecretion. But in most cases, the symptoms are nearly absent or vague that often results in delayed diagnosis (7-10 years), with an increased risk of developing metastasis.

The most abundant type of GEP-NETs are carcinoids, which are neoplastic lesions derived from neuroendocrine cells of the gastrointestinal mucosa (55%); the remainder being pancreatic (PNETs), originating in most cases from the head (Insulinoma, Gastrinoma, Somatostatinoma and Non-functional PNETs) and tail (Glucagonoma and VIPoma) of the pancreas. Although these two subgroups differ in their histology and location, there are many diagnostic and therapeutic similarities between them. Today, clinical diagnostic is preferentially achieved by using serum/plasma CgA assay, advanced endoscopic and radiological imaging and due to their availability and routinely use, the diagnosis of benign and incidentally identified lesions have been increased over few decades, suggesting GEP-NETs not as rare as previously thought. Furthermore due to better treatments available, the survival of GEP-NET patients has been improved for the well-differentiated. The only potential curative solution for GEP-NETs is complete surgical resection. But as the majorities are metastatic lesions, more aggressive resection and embolization therapy are considered. The somatostatin-analogs, octreotide and lanreotide offer symptomatic relief and radiolabel somatostatin-analogs (PRRT) improve survival rate in most patients whereas conventional chemotherapy has only limited effect.

Notch pathway is known to be involved in the control of cell fate choice between proliferation and differentiation in intestinal epithelial lineages and thus play an important role in both intestinal homeostasis and tumorigenesis. In most GEP-NETs investigated, Notch appears to be absent or minimal expressed, suggesting Notch to act as tumor suppressor.

In thesis I examined the impact of miR-375 and miR-7-5p on the Notch mediator, RBP-Jκ in GEP-NETs with focus on its role in promoting tumorigenesis. Furthermore the prognostic value of miR-375 was considered in GEP-NET biopsy samples.

First, miRNA expression profile of carcinoids was compared to normal tissue and it was observed that miR-375 and miR-7-5p was among the most upregulated. miR-375 and miR-7-5p are both identified as important for endocrine cells differentiation of islet pancreas. The miRNA expression profile was furthermore studied using laser capture microdissection and real-time RT–PCR analysis on ileal carcinoids were miRNA-375 expression in carcinoid tissue was increased compared to normal mucosal endocrine cells. In addition *in situ* hybridization in normal and tumor tissue samples showed that endocrine cells expressed miRNA-375 and miR-7-5p. Both in carcinoids from the upper and lower part of the intestinal tract and pancreatic islet tumors expressed miRNA-375 and miR-7-5p.To investigate the effect of miR-375 and miR-7-5p on GEP-NETs, NCI-H727 and CNDT2 cell lines was used as a model for carcinoids *in vitro* and cell proliferation was measured by xCELLigence system. In this thesis, knockdown of miR-375 in NCI-H727 induced cell proliferation compared to miR-375 and miR-7-5p overexpression. For CNDT2, cell proliferation only increased when miR-375 and miR-7-5p was overexpressed. Next, global analysis was used to predict miR-375 targets and the direct binding of miR-375 and miR-7-5p was studied using the 3'-untranslated region (3'UTR) of RBP-Jκ containing the binding sites, predicted by TargetScan. Luciferase reporter assay confirmed that miR-375 and miR-7-5p directly binds to RBP-Jκ 3'UTR, however western blot analysis could not confirm that the protein is negatively regulated by the miRNAs in NCI-H727 cell line.

In conclusion, miR-375 and miR-7-5p are upregulated in different GEP-NETs and are exclusively found in endocrine cells, which seem not to be dependent on the actual differentiation stage the cell are in. The specific location of the miR may be due to their importance for endocrine cell differentiation in tumors by negative regulating RBP-Jκ and thus keeping progenitor cells in differentiated state.

Resume

Neuroendokrine tumore fra mavetarmkanalen og bugspytkirtelen er en gruppe heterogene tumorer som stammer fra forskellige typer celler i det diffuse endokrine system med oprindelse fra det endoderme lag af den primitive gut. Ondartet forandring af disse celler skyldes genetisk ændring som for eksempel tumor undertrykker genet *MEN1*, dog er de fleste tumores årsag ukendt. Normal er disse tumorer højt differenterede, godartet og kan associeres med syndromer skyldes høj hormon sekretion. Men i fleste tilfælde er der meget få symptomer eller slet ingen, hvilket er med til at forsinke diagnosen i 7-10 år. Forsinket diagnose medfører også øget risiko for at tumoren spreder sig.

De fleste tumorer af den art er karcinoider som skyldes neoplasi af endokrine celler fra mavetarm kanalen (55%). Resten stammer fra bugspytkirtelens hoved- (Insulinom, Gastrinom, Somatostatinom og ikke funktionelle tumorer) og hale sektionen (Glukagonom og VIPom). Selvom tumorene varierer i deres histologi og placering er der mange lighedspunkter når tumoren skal diagnoseres og behandles. I dag sker den kliniske diagnose ved måling af serum/plasma chromogranin A (CgA) samt endoskopiske og radiologiske metoder. På grund større tilgængelighed af diagnostiske metoder og større rutine mæssig brug er opdagelsen af neuroendokrine tumorer steget over de få årtier, og derfor anses tumorene ikke mere for at være særligt sjældne. Desuden er overlevelsen hos patienter med højt differenterede neuroendokrine tumor blevet forbedret på grund af bedre behandlinger. Den eneste mulighed for helbredelse af disse tumorer er ved kirurgisk resektion, dog er de fleste metastaseret efter diagnosen og derfor kræver et mere aggressivt indgreb med mulighed for embolisering. Somatostatin analoger som octreotid og lanreotid er med til at mindske symptomerne, mens radioaktive somatostation analoger (PRRT), i modsætning til kemoterapi øger overlevelsen.

Celle skæbnen bliver kontrolleret af Notch signalering, der bestemmer om tarm epitel cellerne skal differentere eller vokse. Derfor spiler Notch ikke kun en vigtig rolle i cellulær homeostase af tarmen, men også for udviklingen af cancer. I neuroendokrine tumorer er Notch i de fleste tilfælde ikke tilstede eller kun minimalt udtrykt, som tyder på at Notch virker som tumor undertrykker.

I denne afhandling undersøges, hvilken betydning miR-375 og miR-7-5p har på RBP-Jκ fra Notch signalerings vejen, med fokus på neuroendokrin tumor udviklingen. Desuden diskuteres betydningen af miR-375 som prognose faktor i tumor væv.

Først bliver miRNA profilen undersøgt for karcinoider i sammenligning med normal væv, hvor der blev bemærket af miR-375 og miR-7-5p var blandt de mest overudtrykt. Både miR-375 og miR-7-5p er identificeret som vigtige for den endokrine differentering i bugspytkirtelen. Udtrykket af begge miRNA blev også yderligere undersøg vha. mikrodissektion og real-time PCR analyse af tyndtarm karcinoider, hvor udtrykket af miR-375 i vævet var øget i forhold til celler i normal væv. Desuden viste *in situ* hybridisering i normal og tumor væv at endokrine celler udtrykker miR-375 og miR-7-5p – både i karcinoider fra øverste og nederste del af tarmen og forskellige neuroendokrine tumorer fra bugspytkirtelen. For at undersøge effekten af begge miRNAer i tumorene blev celle linjerne NCI-H727 og CNDT2 brugt til at undersøge *in vitro*, hvilken betydning begge miRNAer for celle væksten, målt vha. xCELLigence systemet. Der ses at hæmning af miR-375 udtryk inducere væksten i NCI-H727 i forhold til miR-375 og miR-7-5p overudtryk. Modsat i CNDT2 celle linjen øges væksten når miR-375 og miR-7-5p overudtrykkes. Bagefter undersøges mulige targets for miR-375 vha. en global miRNA analyse og den bekræfter RBP-Jκ fra Notch som target. Derfor bliver den forventet RBP-Jκ 3'UTR sekvens til begge miR forudsagt vha. TargetScan. Luciferase reporter bekræfter at begge miR binder direkte til RBP-Jκ mRNA, dog kunne western blot analysen ikke eftervise at proteinet nedreguleres i NCI-H727 celle linjen der blev transfekteret med miR-375 eller miR-7-5p.

Konklusionen er at miR-375 og miR-7-5p er opreguleret i neuroendokrine tumorer og disse er udelukkende fundet i endokrine celler og dette synes uafhængigt af differenteringsstadiet. Den specifikke placering i tumor vævet kan skyldes begge miRNA har betydning for den endokrine differentering ved at de negativt regulerer RBP-Jκ og derved opretholde endokrine celler i tumoren i differenteret tilstand.

Table of Contents

1 Introduction

1.1 The diffuse neuroendocrine system

The term "endocrine cells" refers to a type of cells that possess the ability to secrete regulatory molecules or factors, called hormones into the "inner" circulatory system, thereby affecting target cells, distant from site of origin. The circulatory system refers not only to the bloodstream, but includes also lymphatic capillaries. Hormones are either simple structured, such as modified amino acids or fatty acids, or contains a more complex structure, such as peptides/proteins and steroids. Many regulatory molecules also act outside vessels, locally by being released into the extracellular fluid, affecting neighboring cells (paracrine) or the particular cell that secreted the regulatory molecule (autocrine). Similarly to autocrine, regulatory factors can also be derived from precursors and act intracrine without being secreted. For example progesterone and other steroids are synthesized from cholesterol and converted within the same cell to its active form[1]. However it is important to note that other cell types are secretory by nature, but generally are not considered as endocrine such as macrophages and mast cells, releasing immunological and regulatory substances respectively[2,3]. In contrast to the endocrine feature described above, exocrine cells release products that are exported towards the lumen of the corresponding tract (digestive, respiratory or urogenital), glands such as pancreas and salivary gland or towards the surface of the skin.

The synthesis of hormones may take place in secreting cells grouped together, forming endocrine glands or within specialized cells. Within these glands, endocrine cells are arranged in irregular groups or cords but also in follicles[4,5]. In contrast to endocrine glands, endocrine cells can also be scattered within the epithelium of various organs, such as in the intestine where enteroendocrine cells releases peptides to regulate metabolism of oral nutrients. Another example is adipocytes release of leptin to regulate the food-intake in the brain and influence fat mobilization in nearby adipocytes[6]. In 1938, Friedrich Feyrter introduced the basic concepts of diffuse neuroendocrine system (DNES). The term 'neuroendocrine' was introduced later as it became more evident that these cells store hormonal content similarly to neurons[7]. DNES consist of endocrine cells that are spread as single cells or as clusters of cells, among non-endocrine cells throughout the gastrointestinal tract (GI-tract), bronchopulmonary system and urogenital tract[8]. These observations revolutionized, the initially assumption of the endocrine system, are only composed of pure endocrine organs or ductless glands such as the thyroid and adrenal gland, although it still used in some extent in the literature[9,10].

Endocrine cells of the DNES can be distinguished in open or closed cell types, according to their shape and epithelial location. The 'open cells' refer to cells that reach the lumen, they have microvilli that enable these

cells to sense directly the luminal content and trigger hormone release into the blood, activate extrinsic or intrinsic afferent nerves or paracrine action on nearby cells. In contrast closed cells do not reach the apical surface of the epithelium and can therefore only be indirectly affected by nerves or signals emanating from the bloodstream. G cells in the stomach and I cells in the upper small intestine are examples of open endocrine cells that release gastrin and Cholecystokinin (CCK) respectively in response to luminal content. Gastrin enters the circulation and induces release of histamine by binding to CCK2 receptors on enterochromaffin-like (ECL) cells, which stimulates gastric acid secretion. CCK triggers the release pancreatic juice from the pancreas and emptying of bile salts from the gallbladder into the duodenum to induce protein and fat digestion. Somatostatin is instead released from closed D cells of the gastric corpus upon stimulation of intestinal hormones or neurotransmitters and inhibits gastric acid release and histamine release[11,12].

Hormonal substances are stored in sub-organelles called secretory vesicles which can release amines and hormones upon stimulation. There are two main types of secretory vesicles: the large dense-core vesicle (LDCV) and the synaptic-like microvesicle (SLMV). In β-cells for example, the Insulin is synthesized and stored in LDCV granules, and upon elevation of Ca^{2+} the release is triggered[13]. In contrast Synaptophysin is contained in SLMV in different types of endocrine cells, including β-cells[14]. In addition to specific peptides and hormones stored in LDCV, these granules also contain one or more members of the chromogranin/secretogranin family, consisting mainly of chromogranin A (CgA), B (CgB) and secretogranin II (sometimes called CgC). Chromogranins are then co-secreted with resident hormones, such as catecholamine and calcitonin[15,16]. The best studied granin in humans is CgA; it was first isolated in 1965 as water soluble peptide in the chromaffin cells of the adrenal medulla. The adrenal medulla is the main source of CgA where it is stored in catecholamine secretory granules. The immunoreactivity of CgA has been found in endocrine cells of all parts of the GI-tract, including the pancreas, however CgA is not present in exocrine cells[17]. Furthermore CgA has also been demonstrated in neurons and in the central nervous system[18]. CgA is an acidic glycoprotein of 439 amino acids with a molecular weight of 49 kilodalton (kDa). Importantly, the prohormone of CgA can generate multiple bioactive fragments by splicing into smaller fragments such as vasostatin, chromostatin and pancreastatin. Although the exact biological function of CgA is not fully elucidated studies have shown that CgA or its derivatives have vast roles in the body[19,20]. Intracellularly, CgA is thought to have role in controlling vesicle formation and facilitate the sorting of other regulated secretory proteins; including hormones[21].

1.2 Endoderm formation and development of the intestine and pancreas

1.2.1 Endodermal origin, development and gut tube formation

In the human embryo endoderm formation occurs during the third week of gestation, where all three layers are established by a process called gastrulation. Endoderm is one of the three principal germ layers that contribute to all organs of the alimentary tract, whereas ectoderm forms the skin and central nervous system, and mesoderm; the blood capillary, bone and muscle tissue. The process of gastrulation is found to be similar in all vertebrates, including mice, chick and humans which begin by formation of the primitive streak (PS).

In the first two weeks the formation of the PS on the surface of epiblast begins. Initially, the streak is vaguely defined, but as it becomes thicker and midline groove appears it forms an oval shape. Eventually the PS elongates to occupy half the length of the embryonic disc and cranial end of the streak, expand to a structure called primitive node. The node also contains a depression called primitive pit. The PS has been proven necessary for defining embryonic axis as well as accomplishing gastrulation[22]. The epithelial cells in this tissue express E-cadherin and exhibit apical-basal polarity. After the streak is fully formed, the epiblast cells starts to migrate towards the PS. As the epiblast cells moves into the PS, they undergo epithelial-to-mesenchymal transition (ETM). In other words the epiblast cells go from tightly connected regular shaped cells (epithelial) to more irregular shaped and loosely connected cells (mesenchymal). During this process, cells become flask-shaped and detach from the other epiblast cells as they creates pseudopodia protrusions, allowing them to migrate away from the PS, to a space between the epiblast and hypoblast, where they term the embryonic mesoderm. Some of the mesenchymal cells further invades the hypoblast and displace it to become the embryonic endodermal layer. The remaining cells in the epiblast form the ectoderm (Figure 1).
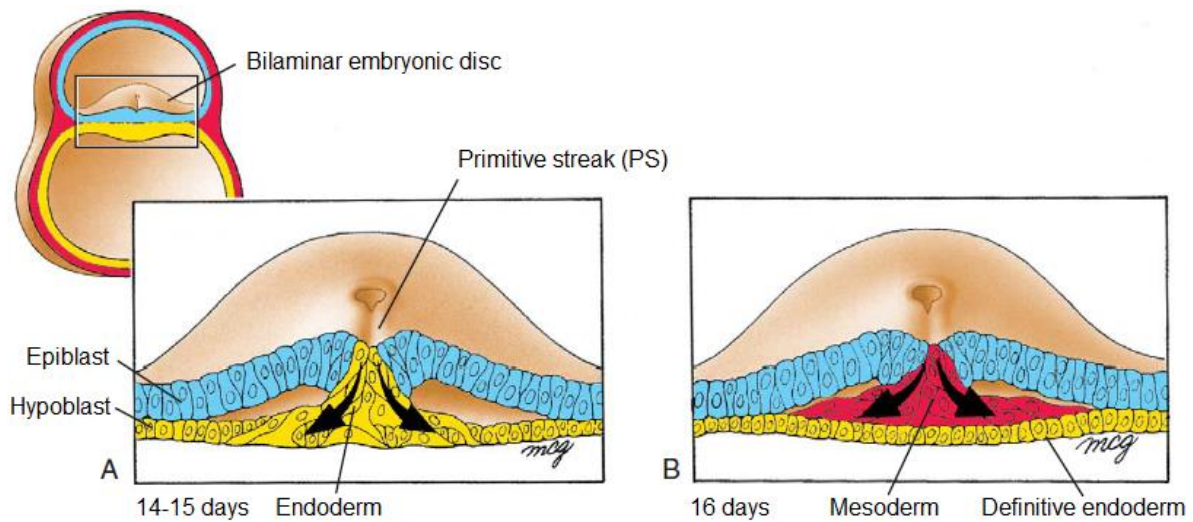
Figure 1: Definitive endoderm and mesoderm formation in the bilaminar embryonic disc. A: During gastrulation in humans at the day 14-15, epiblast cells become loosely connected and begin to ingress along the primitive streak (PS). First, these cells migrate and displace the hypoblast and form the endoderm. B: Subsequently after (day 16) the epiblast cells migrate between epiblast and definitive endoderm to form mesoderm. Adapted from[23].

Evidence suggests that the choice between endodermal and mesodermal fate may be influenced by different soluble factors produced in the PS and node. These soluble factors includes members of the fibroblast growth factors (FGF), transforming growth factor beta (TGFβ) superfamily members and canonical Wnt growth factors, which may act in various combination to induce either endoderm or mesoderm transition[24–26]. Specifically, cell migration and specification have been shown to be controlled by FGF. During gastrulation the FGF4 and FGF8 are co-expressed in the PS, where they control the cell movement by down-regulation E-cadherin which is a protein that normally binds epiblast together. In absence of both FGF4 and FGF8, epiblast cells are able to move towards the PS and undergo epithelial-to-mesenchymal transition, but fails to move away from the streak, leading to no embryonic endoderm and mesoderm formation[27]. As a consequence of continuing migration of cells between the epiblast and hypoblast layers, cells spreads laterally and cranially and migrate beyond the margin of the disc to establish contact with the extraembryonic mesoderm, covering the yolk sac and amnion. Additionally during embryonic development, the EMT also takes place in the epithelial cells of the neuroectoderm, which give rise to migratory neural crest cells[28]. This EMT occurring in the neural crest is triggered by signaling pathways similarly to the EMT, associated with gastrulation[29].

In the cranial direction however, prenotochordal cells of the primitive node extent in the cranial midline direction into a hollow tube structure, the process of elongation is called the notochordal process (Figure 2A, B). The tube elongates as primitive node cells migrates towards the proximal end of the tube. The notochordal process is fully complete on day 20 of the human development, eventually leading to the

formation of the notochord. At this point the ventral wall of the notochordal tube fuses together with the underlying endoderm to form the notochordal plate by breaking down the two layers. Then the notochordal plate detaches completely from the endoderm and fuses its free ends together as it moves up into the mesoderm-containing space between the ectoderm and endoderm layer, changing into a solid rod called notochord (Figure 2C). Because the notochord is derived from the primitive node region and end up in the mesodermal layer it is a mesodermal derivative.
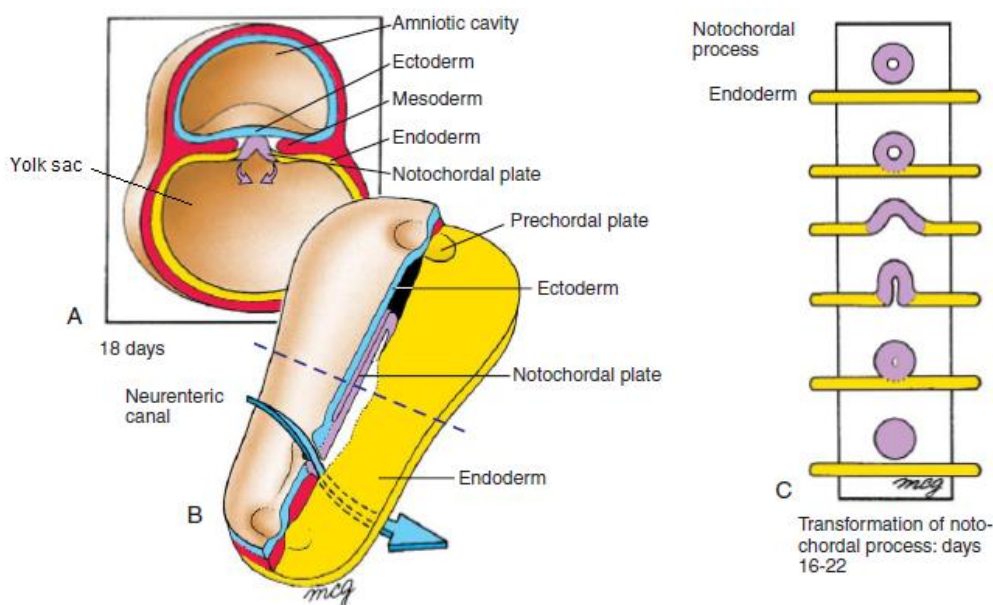
Figure 2: Notochordal process by which the hollow tube is transformed into a solid notochord (day 16-22). A: After the hollow tube structure of notochord is formed by growing cranially from the primitive node (not shown), the ventral wall of the notochordal process fuses with the underlying endoderm by breaking down the two layers, leaving behind the flattened notochordal plate (around day 18). Note that A is a transverse section of B (dotted line). B: This process commence at the caudal end of the notochordal process and proceeds cranially. During this process the Neurenteric canal forms a temporary communication between the amniotic sac and the yolk sac. The prechordal plate is important for both mesodermal and endodermal derivatives. C: The events by which the notochordal process become the notochordal plate and then the notochord: To begin with the mesoderm extent cranially from the primitive node to form a hollow tube, the tube fuses transiently with the endoderm to form notochordal plate, then the plate separates from the endoderm and forms the solid notochord. Adapted from[23].

1.2.2 Endoderm pattering and gut tube formation

After segregation from the mesoderm, the endoderm undergoes complex morphogenetic processes that form the primitive gut tube from which organ buds emerge. The primitive gut tube is a primitive precursor of both the respiratory tract and the GI-tract. At this stage the embryo is a flat trilaminar disc, however during the 3-4th week, the human embryo undergo embryonic folding were cephalocaudal and lateral folding convert the embryonic disc into a trilaminar, elongated cylinder. Cephalocaudal folding specifies the regions of the head and tail ends of the embryo, whereas the lateral folds move ventrally to assist in body wall closure. As folding occurs, the amnion and the embryonic disc grows vigorously, but not the yolk sac, leading to larger

portion of the endodermal layer is internalized into the embryonic body to form the gut tube (Figure 3A-D). Similar folds take place in mouse and chicken embryos, were a crescent-shaped fold called the anterior intestinal portal (AIP) first appears in the endoderm and moves posteriorly. Later another fold called the caudal intestinal portal (CIP) arises from the posterior part of the embryo and moves anteriorly. The two folds meet at the yolk talk which connects the embryo to the yolk sac, causing the sheet of endoderm to fold progressively into a tube[30]. As shown in different mutation studies, the body folding plays an essential role in internalizing the endoderm. For example in mouse, Sox17 has appear to be important for the body folding as well as the development of the gut tube that includes the posterior and lateral regions of the gut[31].
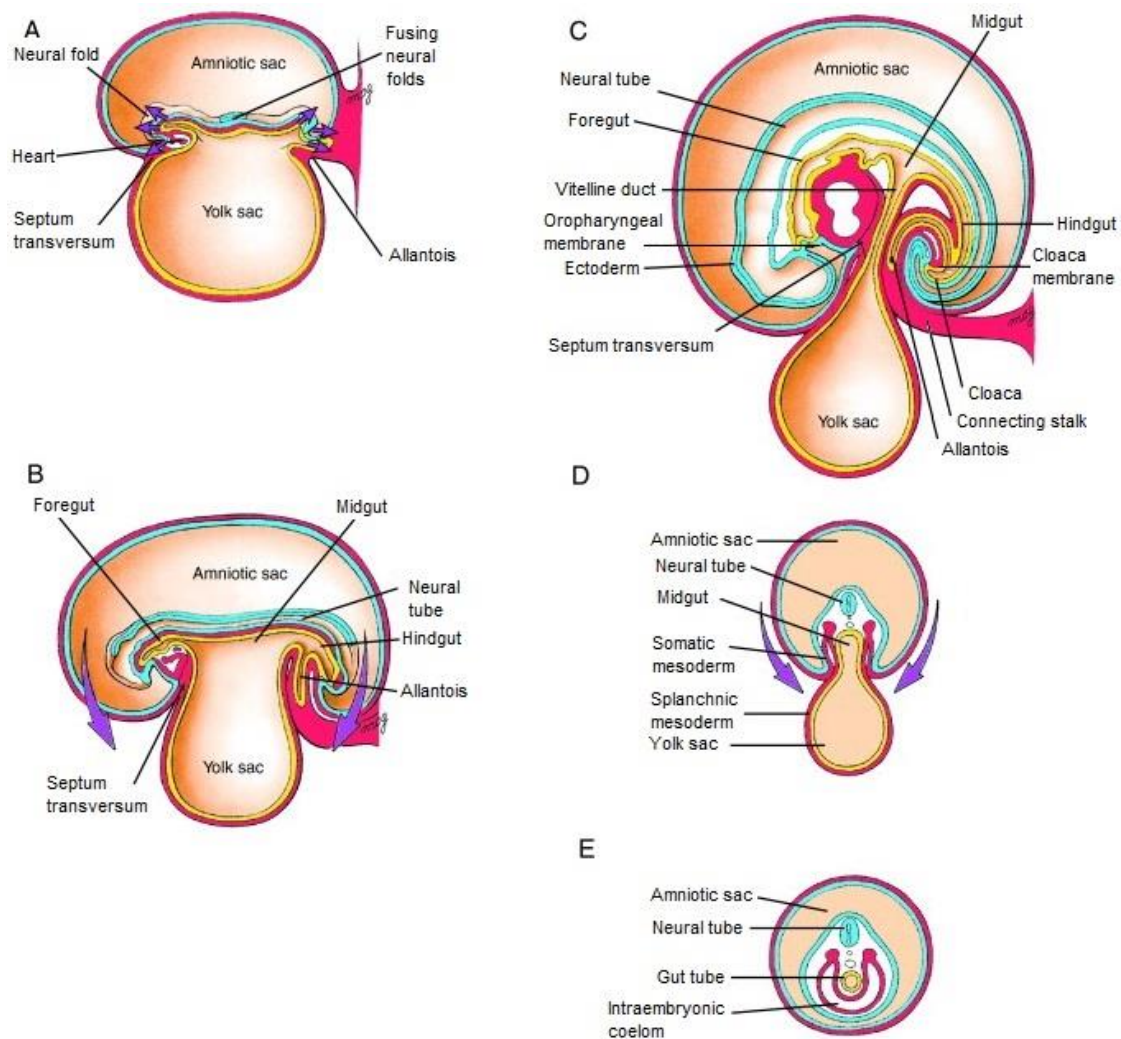
Figure 3: Cephalocaudal and lateral folding that transforms the flat trilaminar disc into an elongated cylindrical tube structure that categorizes the foregut, midgut and hindgut regions of the primitive gut tube. A: At week 3-4 the embryo is a trilaminar germ disc, however the forward growth of the neural plate (neural folds) initiates cephalocaudal and lateral folding (arrows). B-C: The cranial and caudal rim of the disc folds under the neural plate, where the cranial rim forms the ventral surface of the oropharyngeal membrane, while the caudal rim forming the ventral surface of the cloacal membrane. At the process of caudal folding, the connecting stalk and allantois combine with the yolk sac. Fusion of the ectoderm, mesoderm and endoderm from both opposite sites is prevented by the vicinity of the vitelline duct (head of the yolk sac). D: Simultaneously with the cranial-caudal body folding, the lateral edges of the embryonic disc make contact to narrow the neck part of the yolk sac. E:

6

During the fifth week, the gut tube begins to form and gradually reduction of the yolk sac neck is initiated. By the end of the 6th week the gut tube is fully formed (future foregut, midgut and hindgut) and the neck of the yolk sac has been reduced to a slim stalk called vitelline duct. Adapted from[23].

The tube is divided into three regions known as foregut, midgut and hindgut. At early stages of the gut tube lined by a single layer of a columnar endoderm and enclosed by a thin layer of splanchnic mesoderm, however as the mesoderm grows and differentiate into smooth muscle, the morphology of the gut tube alters, resulting in a clear discrimination between the three different regions. Eventually different organs emerge from specific regions as seen in Table 1.

Regions	Sub-regions	Derivatives
Foregut	Pharynx	
	Esophagus	
	Stomach	
	Superior half of duodenum	Liver, Gallbladder and common bile duct
		Pancreas (dorsal and ventral pancreatic buds)
Midgut	Inferior half of duodenum	Small intestine
	Jejunum	
	Ileum	
	Cecum	Large intestine
	Appendix	
	Ascending colon	
	Proximal 2/3 of transverse colon	
Hindgut	Distal 1/3 of transverse colon	
	Descending colon	
	Sigmoid colon	
	Rectum	Urogenital sinus, derivatives and bladder

Table 1: Schematic presentation of the different regions (foregut, midgut and hindgut), including sub-regions of the primitive gut tube and its derivatives.

In the late folding stages, the foregut and hindgut in the cephalic and caudal ends respectively are closed ends and the central midgut is still open to the yolk sac by a broad stalk called the vitelline duct. In the cephalic end of the foregut, an ectodermal-endodermal membrane called the oropharyngeal membrane is currently separating the primitive oral cavity from the gut tube. However during the fifth week,

oropharyngeal membrane ruptures and an open connection is established[32]. Similarly, the hindgut terminates at an ectodermal-endodermal membrane called cloacal membrane, which breaks down during the seventh week to establish an opening for the anal canal[33].

1.2.3   Budding organs of the main gut tube

After the formation of the gut tube, the onset of organogenesis emerges by the swelling, budding and coiling of specific regions from the main tube. In general, organogenesis begins by thickening of the epithelium, were epithelial cells either remains connected by a duct, or migrate away from the gut tube and aggregate with mesenchymal cells, as occurs in early thyroid development[34]. In these following sections however, it will be mainly focus on the intestinal and pancreatic development, because of their similarity in endocrine cell differentiation.

1.2.4   Intestine development

The GI-tract emerge along the primitive gut tube, were organs other than the esophagus, stomach, small and large intestine buds off and develop individually from the gut endoderm. The formation of the intestine takes place from the endodermal layer of both midgut and hindgut region (Table 1). A schematic overview of the small intestine development in mice can be seen in Figure 4 below.

After the primitive gut formation and before/during the initiation of villus morphogenesis, the intestinal tube consists of cells of apical and basal polarity, and a tightly packed simple epithelium called pseudostratified epithelium. These cells growth rapidly in height to thicken the epithelium[35]. Around embryonic day 14 (E14) in mice or 9 weeks in humans, the pseudostratified epithelium of the midgut and hindgut undergoes extensive reorganization to a more stratified epithelium in which apical cells are connected by junctional complexes, whereas the basally located cells are more loosely associated. At this point the stratified epithelium undergoes enormous changes, leading to the mature polarized columnar epithelial monolayer with containing villus. At E15 in mice, the secondary lumina begin to emerge at the apical surface of the stratified epithelium. The multiple secondary lumina that form are believed to be important for proper formation of villus[36]. Simultaneously to the secondary lumina, the junctional complexes are extended to neighboring cells with enlarges the size of the secondary lumina, until the secondary lumina fuses together with the primary lumen. Moreover the mesenchymal tissue under the epithelium condenses and grow towards the central lumen (invaginate) to form nascent villi. Like the epithelial reorganization the formation of the villus takes place in a proximal to distal fashion. The villi formed at this time are usually larger than mature villi, therefore several mesenchymal invaginations take place around E17 (12 weeks in humans) to separate the larger ones into smaller villi. Eventually many small villi emerge on the luminal surface of the

epithelium, each with a core lamina propria covered by single layer of columnar epithelium[37,38]. The first sign of cellular differentiation (cytodifferentiation) takes place around E17-18 at the same time of villus development and continue throughout adult life[39,40].

The formation of the villi leads to a physical separation between the epithelial cells of the lower region (known as intervilllus pockets) and the nascent villi, giving them different properties. The epithelial cells of the intervilllus pockets are proliferative cells which ultimately forms the crypts, whereas the epithelial cells of the villi are more differentiated. Crypts of Lieberkühn develops subsequently later than the villi, at around postnatal day 7 (P7) in mice by downwards invagination into the mesenchyme[41]. Notably, other vertebrates such as zebrafish do not develop crypts, but instead the stem-cells are maintained in the intervilllus pocket[42].
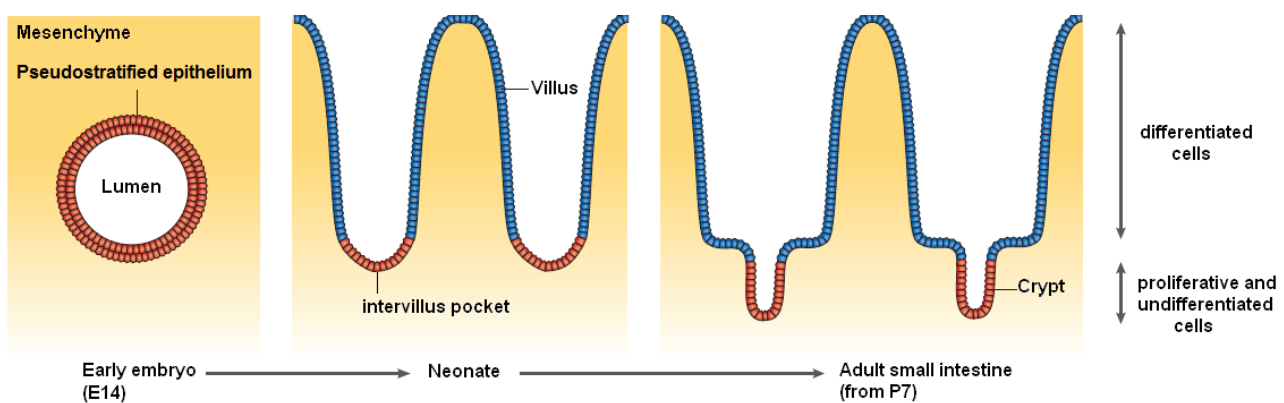
Figure 4: Morphological development of the small intestinal epithelium in mice. At early embryo the endodermal sheet at the midgut area is formed as a tube and before villus formation, the tube is lined with pseudostratified epithelium. Around embryonic day 14 (E14) the epithelium reorganize to more stratified structure, but epithelial cells are still undifferentiated and proliferate actively. At E15 villi starts to emerge due to extensive changes in both the mesenchyme and epithelium: First the mesenchyme is reshaped and forms protrusions in the gut lumen which is accompanied by the epithelium becomes monolayered and proliferation is restricted to intervilllus pockets (red cells). Only much later in the development process, around postnatal day 7 (P7), the morphology of adult small intestine is displayed, were crypts are formed as a result of invagination of the intervilllus epithelium. Adapted from[43].

Moreover, epithelial-mesenchymal interaction has been shown to be critical for modelling the intestinal epithelium during early development. Particularly expression of two ligands; Sonic hedgehog (Shh) and Indian hedgehog (Ihh) are initially found throughout the epithelium, but later becomes concentrated in the intervilllus pockets. Expression of their receptors (Ptch1 and Ptch2) and effectors (Gli1, Gli2 and Gli3) are meanwhile restricted to the underlying mesenchyme. Mice lacking either Shh or Ihh show intestinal abnormalities. Ihh mutants show reduced villi size and proliferation and differentiation in the intervilllus pockets is reduced. In contrast Shh mutants show overgrowth of duodenal villi[44]. Evidence suggest that blocking both Shh and Ihh simultaneously using a strong inhibitor, leads to complete absence of villi with the persistence of highly proliferative cells and in some regions the epithelium exhibited pseudostratified

rather than simple columnar[45]. In other words, the hedgehog family proteins are found to be important for formation of villi and the concomitant restriction of proliferation to the intervilllus pockets. Other signals identified to be important for shaping villus are the platelet-derived growth factor A (PDGFA) which is expressed in the epithelium and have a localized receptor (PDGFRA) in the mesenchyme[46]. Common for both of these signaling systems are that they depend on a molecule to convey signals from the mesenchyme back to the epithelium to control regional effects. BMP2 and BMP4 are both expressed within the intravillus mesenchyme, where they are positively regulated by hedgehog signaling[47]. These ligands act on their receptor (BMPR1A), which is expressed in the epithelium. In *Bmpr1a* knockout mice intestines, excessive amounts of crypt-like structures were observed, with overgrown stem cell population. Also nuclear β-catenin was significantly increased, which points in the direction that BMP signaling may suppress Wnt to insure a balanced control of stem cell self-renewal. On the contrary, another study did not report of β-catenin increase in *Bmpr1a* knockout mice[48]. Wnt is thought to be one of the key signals in driving proliferation of crypt progenitors in normal intestine[49,50]. Furthermore overexpression of the BMP antagonist, *noggin* showed similar numbers of crypts, which supports the notion that BMP signaling is a key factor that mediates the action of hedgehog by blocking the formation of ectopic crypts. The expression of *noggin* is normally restricted to the basement membrane adjacent to the crypt[51] where it protects the epithelium of the crypt from the action of BMP, thereby enable proliferation to continue.

1.2.5   Gastrointestinal tract

The GI-tract is essentially a muscular tube lined by mucous membrane, expanding from the mouth to anus. The mucous membrane is found to exhibit different function, depending on the containing cellular composition in different regions. Furthermore, gut is the largest hormone-producing organ in the body; about one percent of all cells within the mucosa are of endocrine cell type and they produce over 100 types of bioactive peptides with widespread functions[52,53]. This section will mainly describe the organization of the small intestine and its function. The small intestine is highly differentiated organ that accomplishes both digestive and absorptive functions with great efficiency. Concomitant with absorption of nutrients, the intestine has to provide with a kind of tight barrier or defence against harmful substances that are unavoidable ingested with the food, provide with elastic wall to respond to different luminal contents and enable peristaltic movement[54]. All these functions are reflected in the intestinal wall structure, which are composed of four structural layers: mucosa, submucosa, muscularis externa and serosa[55] as viewed in Figure 5.

Serosa
Longitudinal
smooth muscle layer
Circular
smooth muscle layer
Submucosa
Muscularis mucosa
Lamina propria
Mucosa
Continuous
epithelial sheet
Brunners
glands
Villi
Crypt of Lieberkühn
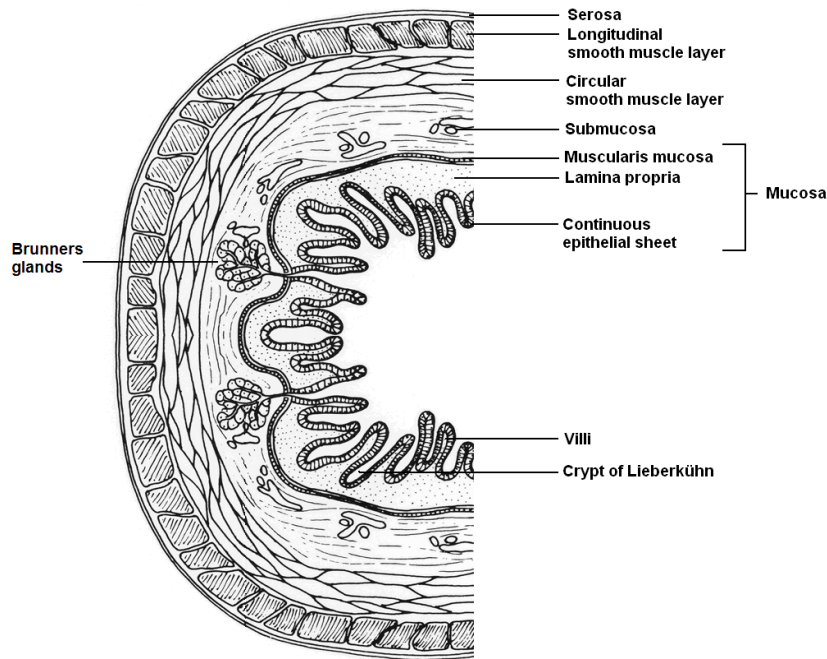
Figure 5: Illustration of the histological layers of the small intestine. The innermost section called the mucosa is divided in the epithelial sheet (consist of villus and crypts), lamina propria and muscularis mucosa. The structural integrity of the intestinal wall is provided by the submucosa layer, but it also harbors Brunner's glands (proximal duodenum only), which protects the mucosa from harmful substances. Next to the submucosa, there are layers of circular and longitudinal smooth muscles that aids absorption in the small intestine and generate peristalsis for movement of stool in the colon. Serosa is the outer layer of the intestine.

The innermost layer of the small intestine is the mucosa, which is essentially for digesting and absorptions of nutrient. The mucosa is organized in such manner to increase surface area by containing vast numbers of finger-like protrusions, called villi those projects into the luminal surface. Each villi contains a dense array of tiny hair-like structures, also known as microvilli that increases surface area, thus help absorb more nutrient. These villi structures coincide with tubular invaginations called crypts of Lieberkühn which invaginate deep into the mucosa. However the mucosa in the large intestine is simple-structured, containing only crypts. The villous projections and glandular invaginations are covered by continuous epithelial sheet. At the core of the villi a continuous connective tissue called lamina propria. It contains blood and lymph vessels, nerve fibres, fibroblasts and cells of the immune system. The outer boundary of the mucosa is the muscularis mucosa which consists of few layers of smooth muscle cells. Next to the mucosa, the submucosa layer exists. The tissue is composed of a loose connective tissue of collagen fibres that work as the skeleton of the intestine, and thus provide the structural integrity of the intestinal wall. Furthermore it supports the internal mucosa and connects it with the external muscle layers, thus allows the passage of blood vessels, lymphatic vessels and nerves to the external muscle layers[56]. In the proximal duodenum, the submucosa also contains Brunner's glands. These glands empty their content either directly to the intestinal lumen or with overlying crypts. They secrete alkaline mucus that lubricates the mucosal lining of the proximal duodenum,

11

protecting the mucosa against degradation by gastric acid, pancreatic enzymes and other active substances associated with this region[57]. External muscle layer is made of several sheets of circular and longitudinal smooth muscle, held closely together with the intrinsic afferent neurons. During digestion, the enteric nervous system becomes activated, leading to muscle constriction, also known as peristaltic reflexes, which aids the movement of food through the intestinal tract. Serosa is the outermost layer of the intestine. It consists of several layers of connective tissue that reduces frictional forces during peristalsis.

As described earlier, epithelial sheet are deposit along the crypt-villi axis, it contains two main lineages of terminally differentiated cells: the absorptive lineage and the secretory lineage. The enterocytes constitute alone the absorptive lineage, whereas enteroendocrine, mucosecreting goblet and paneth cells belong to the secretory lineage[58]. Their function is often reflected by their quantity within different segments of the intestine. For instance, enterocytes are more abundant in the small intestine, were they release enzymes such as hydrolases to aid degradation and absorption of nutrients, while increasing amounts of goblet cells are found from duodenum to the colon, helping protecting the intestinal epithelium and compaction of stool. Enteroendocrine cells represent a link between the central and enteric neuroendocrine system through the secretion of numerous hormones to regulate digestive function. For instance the control of gastric acid secretion in the gut involves endocrine hormones such as Gastrin, Histamine and Somatostatin released from enteroendocrine G cells, ECL and gastric mucosal D cells respectively[59]. Individual enteroendocrine cells are distributed throughout the mucosa surrounded by non-endocrine cells, which is not commonly found in classical endocrine glands. Paneth cells contribute to the defence against enteric pathogens with the secretion of antimicrobial agents, such as lysozyme C and α-defensins into the intestinal lumen, and for the maintenance of homeostatic relationship between host and colonized microbiota. These pyramidally shaped cells originate from the same niche of stem cells as other epithelial cell lines of the intestine[60,61].

1.2.6 Stem cell renewal of the small intestine

Intestinal stem cells or columnar cells are multi- or pluripotent which means that they are relatively undifferentiated cells with the capacity to self-renew indefinitely (clonogenic growth) and are capable to generate differentiated daughter cells in order to maintain or repair the tissue. Stem cells can be characterized by their slower cell cycle and low spontaneous apoptosis compared to other epithelial gut cells[62]. In the small intestine, it appears that a small reservoir of stem cells, are positioned near the crypt base whereas in the colon, stem cells are mostly found at the very base of the crypt[63]. Because of their different location and epithelial turnover, the stem cells in the small intestine seems to divide more rapidly than their colonic counterpart with a division approximately once per day[61].

The first evidence that all cells of the gut epithelium, arise from stem cells was demonstrated in mice small intestine. The use of ^{3}H-thymidine isotope to label a large cohort of dividing cells lead to the observation that some daughter cells appeared to escape the stem cell niche and instead migrate further up the crypt to differentiate. After post-injection with the isotope, radiolabeled cell debris were found in all cell lineages in the intestinal mucosa, indicating a common basis of origin[58]. The group of migrated daughter cells were named transit-amplifying cells which may reflect their dividing nature, during transit or migration along the crypt-villi axis. Although results also indicate that few enteroendocrine and goblet cells seems to migrate back to the crypt[64] it is generally believed that transit-amplifying cells undergo 4-5 rounds of rapid cell division, before moving out of the crypt to terminally differentiate into enterocytes, goblet cells or enteroendocrine cells[65]. These differentiated cells continue their upward migration towards the villus tip and eventually being extruded into the lumen side after 2-3 days. In contrast to other gut cells in the small intestine, Paneth cells seems not to be affected by the upward migration, but instead resides at the crypt base for 3-6 weeks before complete degeneration[66].

In the case of crypt regeneration, it is still remains to be resolved how stem cells retain homeostatic proliferation. Because transit-amplifying cells are generated from stem cells, one would expect stem cells to divide asymmetrically to produce two daughter cells with different fates: one daughter cell acquires the stem cell potential to self-renew and the other continues to divide, mature and differentiate, in other words the parent stem cell segregate cell fate determinants into only one of the two daughter cells. Because stem cell number has to remain constant over time in order to prevent formation of several type of cancers, their asymmetric division may be invariant (strictly asymmetric division) or stochastic where stem cells can have one of three divergent fates: two stem cells, one stem cell and one transit-amplifying cell or two transit-amplifying cells.

It was suggested that intestinal stem cells divide asymmetrically and only upon damage or loss they regain stemness to regenerate the crypt by symmetrical division. As proposed by Potter et al (1998) the crypt stem cells are highly compartmentalized in hierarchies, where 4-6 actual stem cells give rise to three tiers of clonogenic potential stem cells. These actual cells were located four cell positions from the crypt base in small intestine, putting stem cells above Paneth cells. Regeneration studies using low-mediate dose of radiation showed that actual stem cells were extremely prone to irradiation, which lead to the interpretation that stem cells prefer to undergo apoptosis instead of repairing the damage, even after minor DNA damage. Furthermore these studies revealed that loss of actual stem cells could be reversed by recruiting the above positioned clonogenic potential stem cells to become new actual stem cells. Thus, those cells are uncommitted and pluripotent and if necessary can acquire stem cell features to maintain the crypt[62]. However if the third tier is lost, due to excessive damage to the crypt, the remaining cells would be unable to

regenerate the stem cell population[67], indicating a gradual loss of stemness over the first two divisions. This coincides with the observation, showing unequal segregation of ^{3}H-thymidine during anaphase of intestinal stem cells lead to complete loss of parent genome after second division[68]. Still most of these experiments were based on monitoring large cohorts of cells to analyse stem cell behavior and thus not conclusively tells about the behavior of each single cell. Taken together the results indicate that the crypt contains a heterogeneous population with progenitor cells of limited stem cells potential, supported by actual stem cells following invariant-asymmetrical division.

A more recent study, use leucine-rich repeat containing G protein-coupled receptor (Lgr5) as a potential intestine stem cell marker. Lineage tracing studies using two knock-in alleles in mouse subjected to tamoxifen, confirmed the presence of all cell types in both small intestine and the colon arise from Lgr5+ cells. In contrast to the hierarchy model, the identification of Lgr5 refers to stem cells being positioned in between Paneth cells near crypt base[61]. The *Lgr5* gene was initially identified as a Wnt target gene, expressed in colon cancer[69]. Furthermore Lgr5 receptor is found to be closely related to Gonadotropin receptors such as LH and FSH receptors, which have glycoprotein ligands[70]. Like Lgr4 homolog it acts as receptor for Wnt pathway agonists called R-spondins. R-spondins are not known to initiate Wnt signals, but they potently enhance such signals[71–73].

Although the small intestine is one of the most attractive model for studying stem-cells renewal *in vivo*[74], because of its fast renewal and simple architecture of well-defined compartments. The model-systems existed until now could not predict the long-term clonogenic behavior of individual stem cells. After the characterization of stem cells as high *Lgr5* expressing cells, the authors generated a crypt-organoid containing a central lumen surrounded by villus-like epithelium and adhered crypt domains[75]. The model could develop from any Lgr5+ cell, in absence of non-epithelial cellular niche when substituted by exogenous signals. As a result of this the self-renew homeostasis of Lgr5+ stem cells must rely on individual competition for essential niche signals. In fact, *in vivo* studies in mice clearly state the close association between Paneth cells and Lgr5+ cells in the crypt, where Paneth cells provide essential niche signals for stem cell support[76]. The use of crypt-organoids in short and long term clonal tracing studies provided the first detailed evidence that homeostasis is not maintained by asymmetrical division, but is a result from natural competition between symmetrically dividing Lgr5 stem cells[77,78]. In other words the crypt drifts towards monoclonality. Equipotent stem cell population follows coincidental asymmetric division, where stem cell loss may be compensated by symmetric division of any neighboring stem cell. Taken together this recent data indicate that adult stem cells reside near the crypt base, intermingled with Paneth cells. Each stem cell retains its own stem cell potential and stem cell number remains unchanged by coincidental

division of individual stem cells. Because asymmetrical division of individual cells occurs in average, the population of stem cells are driven towards monoclonality.

1.2.7 Pancreas development from the dorsal and ventral pancreatic buds

The pancreas is a secretory organ that mainly comprises of endocrine, exocrine and ductual cell types, which collectively synthesize and secrete hormones and enzymes to maintain the body nutrient balance. Each of these distinctive cell types are derived from the endodermal layer of the duodenal region of the foregut. As for most organs in the developmental stages, the pancreas is formed by protrusions in the gut tube epithelium. These protrusions or buds are called the dorsal and ventral pancreatic buds (Figure 6A). The dorsal bud is developed close to the dorsal mesentery, whereas the ventral bud is at the ventral side close to the bile duct. However, as a result of rotation of the stomach, the duodenum become C-shape, moving the ventral bud dorsally, so it comes in close association with the dorsal pancreatic bud. Both buds subsequently proliferate and fuse together, resulting in the ventral bud forms the uncinate process at the posterior part of the head of the pancreas. The remained anterior part of the head, including the body and tail of the gland is dorsal bud derived[79]. The main pancreatic duct is also formed by the distal part of the dorsal pancreatic duct and the entire ventral pancreatic duct. Whereas the proximal part of the duct becomes a small accessory pancreatic duct (duct of Santorini). Furthermore these ducts enter the duodenum; the main pancreatic duct together with the bile duct, enters the duodenum at the site called major papilla, and the accessory pancreatic duct at the minor papilla[80] (Figure 6B). Only later in the embryo life, the islets of the Langerhans develop where endocrine cells are mainly grouped in compact spheroidal clusters in the exocrine tissue.
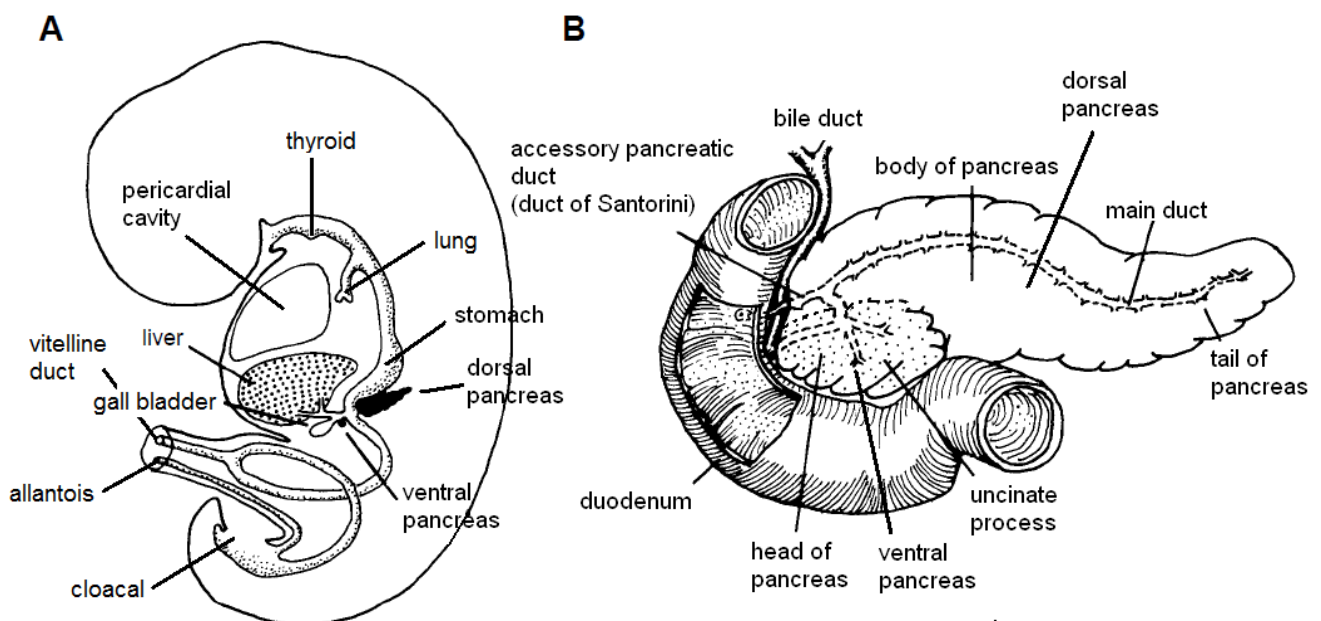
Figure 6: Schematic presentation of the pancreas in development stages and adult human pancreas. A: Showing an embryo of about 36 days, were further development from the gut epithelium gives rise to different organs, particularly the ventral and dorsal pancreatic buds. B: Showing a fully developed human pancreas in sections; at the posterior part of the 'head' the uncinate process is developed as a part of the ventral pancreas. The body and the tail of the pancreas, includes the dorsal part of the main duct and the accessory pancreatic duct or duct of Santorini. Adapted from[80].

1.3   Notch signaling pathway

Notch signaling is typically referring to as 'canonical' which describes a signal activation that relies on regulated proteolysis, as Notch is activated. The canonical Notch pathway involves activation of Notch receptor at the cell surface by DSL (Delta/Serrate/Lag-2) ligands reside on neighboring cells. To understand the ligand-receptor relationship that leads to Notch activation and transducing the extracellular signals to the nucleus, their structural composition and further processing has to be evaluated. Furthermore processing such as endocytosis, endocytic trafficking and ubiquitination have shown to help regulate the signal[81,82], however these will not be evaluated here.

In mammals, four Notch receptors has been identified (Notch1-4) and five canonical DSL ligands from two separated families called Serrate (Jagged1 and -2) and Delta (Dll1, -3 and -4). Notch receptors are type 1 single-pass transmembrane dimeric proteins positioned on the cell membrane. Although all isoforms can act on several different DSL ligands, their structural composition is very similar. Notch is composed by two domains with distinct functions: an extracellular domain (NECD) responsible for ligand binding and helps preventing ligand-independent Notch activation, and an intracellular domain (NICD) that interacts with various transcriptions factors and co-activator and repressors to mediate either positive or negative target gene expression. These domains are held non-covalently by hydrophobic regions that spans through the cellular membrane. The NECD and NICD consist of several distinct regions, important for the functional aspect of Notch, as described below. Notch ligands are also type 1 transmembrane proteins comprised of distinct motifs, including amino-terminal domain followed by DSL domain and variable numbers of epidermal growth factor (EGF)-like repeats with similar property to Notch receptors. The DSL domain is highly conserved in all DSL ligands, possibly because it's essential role in receptor binding. Unlike Dll ligands, jagged1 and -2 contain an additional cysteine-rich region between the EGF-like repeats and transmembrane (TM) domain. Following the TM domain is a relatively short intracellular (IC) region[83,84]. Interestingly, both TM and IC are shown to be important for Notch activation[85]. A full description of the different Notch domains is found below and Notch receptors and ligands of the canonical pathway are summarized in Figure 7.
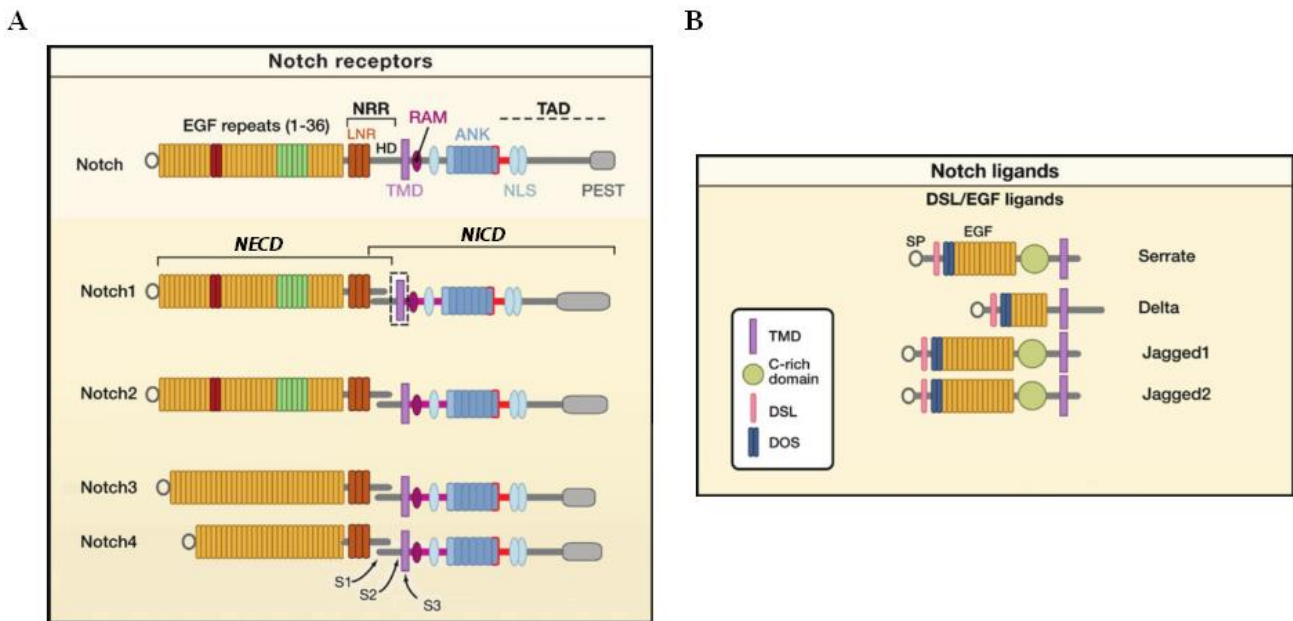
Figure 7: Domain organization of Notch receptors and ligands. A: In humans there exist four Notch receptors, Notch1-4 with very similar structure. The receptors are type 1 transmembrane proteins, containing two main domains that are separated by the transmembrane domain (TMD); the extracellular domain (NECD) and intracellular domain (NICD). NECD consist of epidermal growth factor (EGF)-like repeats, the number of repeats differ depending on the isoform. Followed by Lin12 Notch repeats (LNR) and heterodimerization domain (HD), making up the negative regulatory region (NRR). The NICD consist of RBP-Jκ association module (RAM), two nuclear localization signals (NLS), a seven ankyrin repeats (ANK) and transactivation domain (TAD) that harbors conserved proline/glutamic acid/serine/threonine rich motif (PEST). B: Classical DSL ligands are also type 1 transmembrane proteins that include five ligands of the serrate and delta family (please note that only Serrate isoforms are shown). Delta-like ligands (Dll) 1, 3 and 4 and Jagged1, -2 contain the Delta/Serrate/EGF ligands (DSL) domain, Delta and OSM-11-like proteins (DOS), EGF-like repeats and TMD. Only the jagged ligands contain the cysteine-rich domain. S1: furin-like convertase site 1, S2: metalloproteases site 2, S3: presenilin/γ-secretase site 3. Adapted from[86].

1.3.1 Notch extracellular domain mediates interaction with the ligand

Notch receptors contain variable number of EGF-like repeats, ranging between 10-36 repeats. EGF-like repeats positioned near the N-terminal part of the receptor, seems to be essential for the extracellular binding force to corresponding ligands. The EGF-like repeat 11 and 12 are reported to be sufficient for binding the ligand[87], whereas removal of the repeats to less than ten, complete abolishes the ligand-receptor interactions[86]. Furthermore some EGF-like repeats are able to non-covalently bind calcium to influence the binding affinity of the ligand. For instance the mutation of calcium-binding site in EGF-12, lead to destabilization and abolishment of Notch-1 and hDII-1 interaction, but not in EGF-11 or -13[88]. EGF-like repeats are also the site for N-linked and O-linked glycosylation. During receptor biosynthesis in the Endoplasmic Reticulum (ER) and trafficking to the surface of the cell, the enzyme *O*-fucosyl transferase catalyses, attachment of fucose to the EGF domains which are critical for the proper folding and interaction with the ligand[89,90]. EGF-like repeats are held by three cysteine-rich Lin12-Notch repeats (LNR) and a heterodimerization domain (HD). Collectively LNR and HD constitute the negative regulatory domain (NRR), containing two cleavage sites (S1 and S2).

17

Before Notch translocates towards the cell surface as its definitive form, the 300 kDa precursor protein is subjected to S1 cleavage in the *trans*-Golgi compartment by Furin-like convertase, resulting in mature heterodimer receptor. The cleaving of S1 is important for the efficient translocation of Notch to the cell membrane. Notch with mutation in S1 has shown to accumulation in both ER and Golgi compartment, simply because the precursor is too large to translocate[91]. The S2 site is cleaved by metalloproteases of the ADAM10 or TACE (TNF-α converting enzyme, also known as ADAM17) family on the cell surface that guard the initial process of receptor activation. Several experiments in context to NRR function, suggest that NRR protects the receptor against S2 cleavage during ligand absence, thus acting as a molecular activation-switch. Mutation or deletion of LNR results in gain of function phenotypes and ligand independent ADAM cleavage of S2[92,93]. However, as we shall see the S2 cleavage cannot sufficiently by itself activate the signal transduction of Notch.

1.3.2   Notch intracellular domain and sequential proteolytic processing transduce the signal

Notch receptor is normally maintained in its resting position, however interaction with its ligand, activates Notch to undergo a two-stage proteolysis also called regulated intramembrane proteolysis. Structure-study analysis shows that LNR wraps around the HD domain and thus limits the exposure of S2 site to ADAM. Only after ligand exposure, conformational changes is induced, exposing S2 site to cleavage and creates a truncated version of the ectodomain, called Notch extracellular truncation (NEXT)[94]. Immediately after, the NEXT is exposed to presenilin/γ-secretase mediated S3 cleavage that releases NICD, allowing it to translocate directly into the nucleus[95,96]. On the other hand, size increase of the extracellular domain[97] or inhibition of metalloproteases[98], decrease the progression of S3 cleavage. Taken together these results suggest that binding of ligand converts the receptor into a substrate for ADAM and γ-secretase, and S2 cleavage is necessary for S3 cleavage to progress, thereby leading to cytoplasmic release of NICD.

Although the size of NCID only constitutes a small fraction of the receptor, its structural composition seems to be essential for its action. The N-terminal region of NICD consists of an RBP-Jκ association module (RAM) domain, followed by the presence of seven ankyrin repeats (ANK). Near the C-terminal region is the nuclear localization signal (NLS) and a transactivation domain which harbors the conserved proline/glutamic acid/serine/threonine rich motif (PEST). Subsequently followed by its release, NICD is exported into the nucleus where it assembles into a complex of different protein partners, including members from the CSL protein family. CSL constitutes of a group of DNA binding proteins that contains a Rel homology domains (RHD) in both N-terminal and C-terminal and a central β-trefoil domain[99]. Particularly the identification of a CSL protein named RBP-Jκ/CBF-1 was shown to bind directly to NICD, possibly

through the interaction between RHD and the RAM region[100]. On the other hand the ANK domain interacts only weakly with RBP-Jκ[101], but proposed to implicate in the assembly of the complex[102].

Because gene repression could be disturbed by Notch activation[103], further experiments lead to the current understanding that the cellular location of NICD is crucial for the regulation of Notch target genes. In absence of NICD binding, target genes are continually repressed, because CSL proteins bind co-repressors, including SMRT/N-CoR, KyoT2 and CIR to insure a tight regulation of Notch target genes, possibly through directly blocking the DNA-binding sites or deacetylate histones to obtain compact chromatin structure[104–106].

Interestingly, the interaction of another protein in the co-repressor complex called SKIP is proposed to have dual function, because SKIP both bind to the co-repressor complex and NICD. Upon ligand binding and proteolytic liberation of NICD to the nucleus, the NICD binds to the CSL complex and competes with SMRT/N-CoR for the RBPJ-Jκ and SKIP binding sites. Eventually, the increased accumulation of NICD in the nucleus will result in displacement of SMRT/N-CoR co-repressor complex, and thus relieves the repression. In other words the exchanging partnership of RBP-Jκ and SKIP is mandatory to abolish repression of Notch target genes[107]. When the RBP-Jκ is not repressed it binds and activates Hairy and enhancer of split like (Hes) basic helix-loop-helix (bHLH) transcriptional repressors. The role of *Hes* genes are to inhibit proendocrine transcription factors, and Notch ligands to induce lateral inhibition as described later in the following chapters.

Since all canonical Notch target genes are activated by the same CSL complex[108] and the Notch response are not the same in every cell types, it is possible to imagine that tissue specific endogenous co-factors are involved in the activation of specific target genes. A protein named Mastermind-Like-1 (MAML1) showed to co-localize with NICD in the nuclear bodies, were RBPJ-Jκ also seem to be present[109].

MAML1 is human homolog to the mastermind family, originally discovered in *Drosophila Melanogaster*[110]. It acts as a co-activator, and believed to be essential for the activation of Notch target genes. Isolation of the complex, revealed that binding of NICD to CSL complex, also creates a groove which MAML helix-structure specifically recognizes[111]. However it is not unlikely that chromatin remodelling proteins also can activate the complex. For instance p300, a co-activator with acetyltransferase activity is identified *in vitro* as a direct binder to the NCID:CSL-complex[112]. In contrast other experiments indicate MAML had to be present in the complex before p300 can be recruited[113]. Yet another co-activator similar to p300, called PCAF could positively increase p300 target gene transcription[114]. Surprisingly, p300 is also able to acetylate a wide range of non-histone regulatory proteins that are known to affect protein stability, such as in tumor suppressor p53 were p300 dramatically increases p53 target genes expression[115]. Similarly to p53, the p300

binds and acetylates a proline repeat motif in MALM1 and enhances its DNA binding affinity[116]. Furthermore p300 dependent acetylation of MALM1 also could affect stability of the complex by decreasing ubiquitination and proteosomal degradation of NICD[117], suggesting that histone acetylation has a vast role in Notch-mediated gene activation[113]. Taken together, these results show that Notch has overcome both the NRR-mediated protease-resistance state, and the CSL repression in the nucleus, before it can activate signal transduction and gene expression. Furthermore the recruitment of co-activators to relief chromatin structure and induce posttranslational modification, could ensure a stable transcription activation of Notch target genes.

1.3.3 Notch generates cell-type diversity through lateral inhibition

Unlike other receptors, Notch has been reported to function both at the cell surface where it mediates lateral inhibition between adjacent cells, and in the nucleus to regulate the expression fate determined genes[118] as discussed later. Notch implication in lateral inhibition was first proposed in the differentiation of nerve cells in *D. melanogaster*[119] and relates to the assumption that no nearby cells are the same. Lateral inhibition describes cells that segregate from within a group of equipotential cells to adopt a more specialized fate, and in the same time prevents their neighboring cells from adopting the same fate over time (Figure 8). Those cells which are prevented from adopting the same fate are thus diverted to a different fate or remain undetermined.
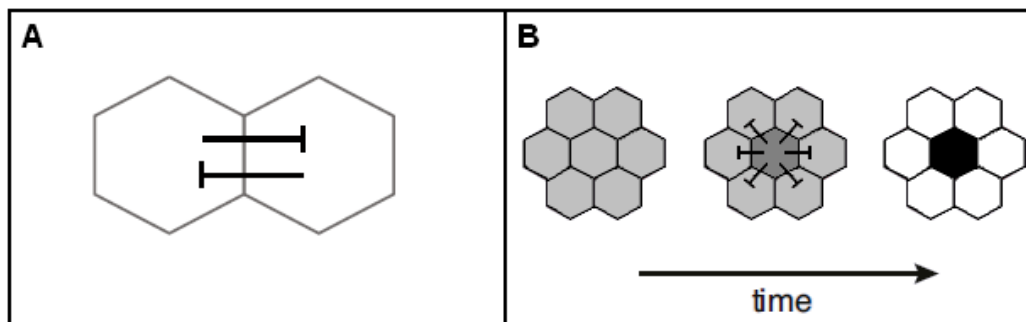
Figure 8: Illustration of lateral inhibition and its basic process in cell fate. A: Lateral inhibition, in which a cell inhibits its neighboring cell to adopt the same fate. B: A possible dynamic illustration of lateral inhibition in terms of ligand expression. To begin with, mutual inhibition exists in a group of cells which share the same 'fate potential' (light grey). However because of lateral inhibition one cell will commit to a specialized cell fate over time (dark grey/black) and inhibits the surrounding cells from adopting the same fate (light grey/white). Adapted from[118].

The way Notch exert lateral inhibition has been described during many stages of development and in many tissues, like in neurogenesis[120,121], hair-cell emergence[122] and differentiation of secretory cells of the intestine[123]. Common for these are that lateral inhibition generates a phenomena of pattern in which two different kinds of cells are mixed, called the salt-and-pepper pattern (Figure 9B). For instance in the intestine were the distribution of secretory cells is surrounded by absorptive cells. Here it will be described how lateral inhibition is thought to work in in the small intestine.

In the small intestine, enteroendocrine cell are scattered among other secretory and absorptive cells yet there has been not reported two enteroendocrine cells adjacent to each other; suggesting that the Notch signaling pathway decide cell fate through lateral inhibition. When Notch function is lost, excessive enteroendocrine cells are made and these cells are clustered next to each other[40], suggesting that Notch is involved in endocrine development in a mechanism resembling the lateral inhibition utilized in neuronal differentiation. Interestingly, gastroenteropancreatic neuroendocrine tumors (GEP-NETs) are made up of clusters of endocrine cells.

So how is Notch suggested to control, which cells differentiate and which not? In the crypt of small intestine a population stem cells proliferate and continually give rise to a mixture of terminally differentiated cell types. At early differentiating phase, these crypt cells initiate expression of Notch and its ligands on their cell surface and initiate cell-to-cell interactions by sending and receiving Notch signals[39,40]. This mutual bi-directional Notch signaling have two objectives; First the activation of Notch inhibit cellular differentiation in cells, thereby maintaining dividing precursor cells and enabling the inhibited cells to adopt different fate at later stages, depending on transcription factors expressed (Figure 10). Second, Notch activation also down-regulates expression of Notch ligands, such as Dll ligands in neuronal development[124], thereby making cells committed to differentiation, express Notch ligands and become 'sender' cells, while neighboring 'receiver' cells do mostly not express Notch ligands and therefore inhibited. As a consequence, cells with initially higher expression of Notch ligands, compared to surrounding cells, will outmatch nearby cells by decreasing their ligand expression through Notch activation and thus amplify its own differentiation. In other words, the small initial difference between cells is amplified through a positive feedback loop, which ultimately leads to two mutually exclusive fates (Figure 9A). This feedback is obtained only when cells express both Notch receptors and ligands; each cell performs lateral inhibition and when ligand expression is inhibited by Notch signaling. Thus, if cells fail to activate Notch signaling, for example in RBP-Jκ deficient mice, the result is more cells adapting that specialized cell fate, while excessive Notch signaling prevents the differentiation of these cells.
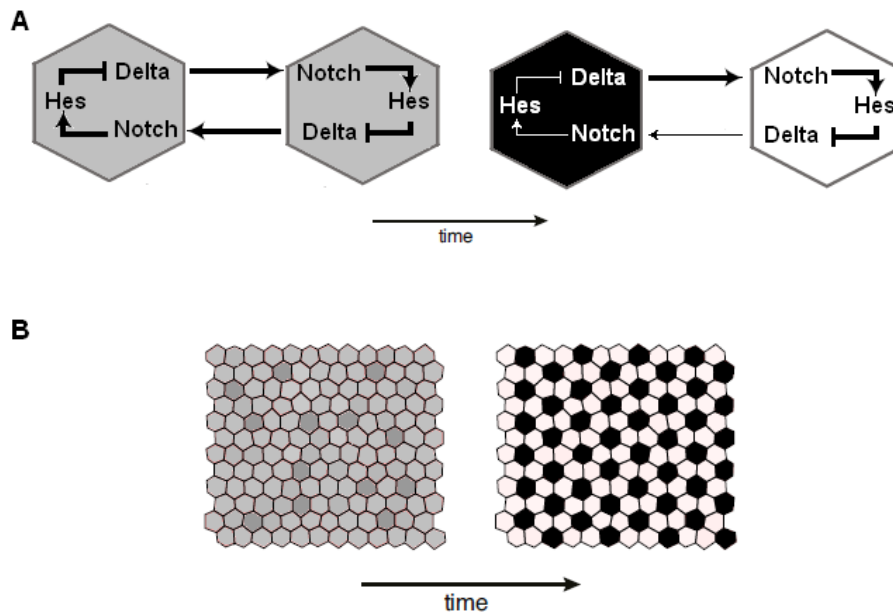
Figure 9: Illustration of Notch mediated lateral inhibition through positive feedback loop and "salt-and-pepper" pattern.
A: To begin with two interacting cells are equivalent, were each cell expressing comparable levels of Notch receptors and ligands. Thus each cell possesses equivalent signal sending. However, over time small difference in some aspects of the signaling arises between the two cells. This is due to a positive feedback loop that amplifies the small initial difference. The feedback loop lies within the Notch signaling, were Notch activate Hairy and enhancer of split like (Hes) genes in order to down-regulate ligand expression. Thus Notch receptor and ligand expression are responsible to these changes by amplification mechanism that ultimately drives two cells to adopt distinct roles as either 'sender' cells (high ligand, low Notch) or 'receiver' cells (low ligand, high Notch). B: Lateral inhibition acting on tissues with equivalent precursor cells leads to a 'salt-and-pepper' pattern of two kinds of cells.

The standard lateral inhibition model in the small intestine thus predicts that cells committed to secretory cell differentiation (that escapes Notch activation) should strongly express one or more Notch ligands, while those cells that are committed to the absorptive enterocyte fate (subjected to Notch activation) should not. By studying the most strongly expressed Notch ligands; Dll1 and Dll4 in the small intestine, using Dll1$^{lacZ/+}$ heterozygote mice as model system and the use of corresponding markers of goblet and enteroendocrine cell, it was shown that only cells committed to secretory fate undergoes a phase of strong Dll1 and Dll4 expression at some point of their development. Furthermore, Dll1 conditional knock-out mice, expressing Cre recombinase in the intestine in response to β-naphthoflavone, confirmed that Dll1 is a regulator of cell fate choice by showing increased number of goblet and enteroendocrine cells, compared to the control without Cre recombinase[125]. When β-naphthoflavone was injected in these mice, leading to loss Dll1 expression the lateral inhibition was abolished. In other words, cells committed to secretory fate can no longer inhibit nearby cell to commit different cell fate in the crypt (by activating Notch on their cell surface), thereby more terminally differentiated cell types of secretory fate emerge.

Subsequently after some progenitor cells begin to express high Dll1 (low Notch activation) and commit themselves to secretory fate, several studies suggests that these cells stop dividing almost after their commitment, leading to a single secretory cell, but not a clone of many secretory cells. As shown in

Stamataki et al. (2011), Dll1$^{lacZ/+}$ heterozygote mice were used to track cells of secretory fate followed by injection of 5-ethynyl-2'-deoxyuridine (EdU) to detect DNA synthesis in cells *in vivo*[126]. The result showed almost all secretory cells (93%) being EdU negative[125], suggesting a very small fraction of cells are found in S-phase and therefore in dividing phase, while most secretory cells are withdrawal from the cell cycle. This coincide with the results demonstrated in knock-out mice of both Notch1 and Notch2 in the intestine where cells affected cease to divide by increase their expression of two cyclin-dependent kinase inhibitors; p27^{kip1} and p57^{kip2} [127].

Taken together these results suggest that lateral inhibition in the small intestine is essential for generating divergent cell fate, depending on cells individual expression of *Dll1* and *Dll4*. Progenitor cells in the crypt that are committed to differentiation use Notch cell to cell interactions to activate Notch receptor in nearby progenitor cells. Cells affected by Notch activation down-regulate Dll1 and Dll4 on the cell surface, making Notch receptors on nearby cells less susceptible for activation. In time, these cells continue to decrease Dll1 and Dll4 as a result of decreased Notch activation and increased *Dll1* and *Dll4* expression on nearby cells. Ultimately, the pattern of salt-and-pepper is generated were most cells exert high Notch activation but absent *Dll1* and *Dll4* expression, while fewer cells have absent Notch activation but high *Dll1* and *Dll4* expression. At this point progenitor cells stops proliferating and initiate differentiation as these cells migrate along the villus were they are terminally differentiated to either absorptive enterocytes and secretory cells (goblet, enteroendocrine or Paneth cells) respectively.

1.4 Endocrine differentiation

1.4.1 Transcription factors regulate cytodifferentiation of the small intestine

As daughter stem cells, initiates their outward migration from the crypt base towards the villi, these undifferentiated cells begins to differentiate as a direct cause of different stimuli expressed from both the mesodermal tissue and cell to cell contact. In this chapter Notch involvement will be described during enteroendocrine differentiation. As earlier encountered, Notch and its ligands are transmembrane proteins used for cell to cell communication, only when close contact between cells are favorable. In mice, Notch pathway components are found to be expressed in the epithelium of crypts in adult intestine (P25) but in most cases not in the villi, suggesting that Notch signals are mainly exchanged between cells in the crypts. Notably, these components are already expressed prior to intestinal epithelium morphogenesis and cytodifferentiation (around E13), but found to be restricted to the mesenchyme and in few individual cells of the premature intestinal epithelium[39].

In order to investigate how Notch pathway influence differentiation of intestinal epithelial cells, several Notch components has been deleted or mutated in vertebrate species. Partially inactivation of Notch pathway components by deletion of *Hes1* in mice or nonsense mutation in the Notch ligand DeltaD (correspond to mammalian Dll4) in zebrafish results in excessive numbers of goblet cells and the presence of enteroendocrine cells, which suggest that progenitor cells escaping Notch activation become secretory[40,128]. Similar but more prominent phenotype is observed after using γ-secretase inhibitors to prevent release of NICD[129]. Interestingly, the deletion of *Hes* genes upstream target, RBP-Jκ induces almost all transit-amplifying cells into post-mitotic goblet cells. Thus compared to Hes1 inactivation, the result suggests that different *Hes* genes, other than Hes1 are inactivated in order to lead epithelial cells to secretory fate[130]. Beside Hes1, Hes3 and Hes5 are found to be expressed in the intestine. Hes1 is thought to be the main target of Notch signaling, however results show that when Hes1 is inactivated the related genes Hes3 and Hes5 are up-regulated[40], suggesting that Hes3 and Hes5 compensate for Hes1 deficiency. Indeed it is the case, in adult mice intestine the absence of Hes1, Hes3 and Hes5 continued to display increased goblet and enteroendocrine cells, however in mice only deficient to Hes1 these phenotypes were not observed during adulthood[131].

In a similar way as the pancreas cytodifferentiation, Hes1 also negatively regulates bHLH transcription factors. Deletions of Hes1, showed elevate expression of Math1, NeuroD, Dll1 and Dll3 in the small intestine, whereas Math1 was not up-regulated in the large intestine. Math1 is first activated in the immature crypt and villi during intestinal development. In mice Math1 seems to be required for secretory cell lineage commitment, since loss of Math1 leads to completely absences of all three secretory cells. Furthermore Math1 null mice, showed completely loss of *NeuroD* expression[132], suggesting that Math1 act upstream to NeuroD.

Interestingly, expression of *NeuroD* seems not to be required for daughter cells commitment to enteroendocrine differentiation, but instead is required for specific enteroendocrine cell types. NeuroD is found to be important for regulation of *Secretin* gene[133] and *CCK* gene expression in the intestine[134]. Failure in the development of both secretin and CCK-expressing cells are found in NeuroD deficient mice, whereas other enteroendocrine cells, such as Serotonin expressing cells that do not express NeuroD are still found in small intestine[135], indicating that absence of NeuroD leads to an abnormal enteroendocrine differentiation.

Mature enteroendocrine cells arise from proliferative progenitor cells of the crypt, expressing neurogenin-3 (ngn3)[136,137]. In mice, ngn3-expressing cells are first found in scattered cells within the gut endoderm at early stage (E12.5). These cells proceed to express NeuroD, which is detected in the intestinal epithelium only later, from E14.5. In adult intestine, ngn3-expressing cells are detected in the crypt, but not the villi as NeuroD-expressing cells are, which further suggest that NeuroD is expressed only at later differentiation

stages. In absence of ngn3 in mice, no development of enteroendocrine cells are found, however goblet cells and enterocytes are still present[138]. In addition cell lineage tracing studies, using transgenic mice expressing Cre recombinase, under control of ngn3 showed that all enteroendocrine cells, expressing CgA are descendants of undifferentiated progenitor cells expressing ngn3. Interestingly, these results also showed that some descendants of *ngn3* expressing cells adopts secretory non-endocrine fate[137], suggesting that immature secretory cells have to express sufficient levels of ngn3, before endocrine differentiation is initiated. Interestingly, evidence also suggests that Wnt pathway is not only controlling proliferation, but also implicated in controlling differentiation. Inhibition of Wnt signaling by disruption of the downstream target Tcf4 resulted in absence of terminally differentiated enteroendocrine cells, but absorptive enterocytes remained partly unaffected[139]. Similarly, blocking the Wnt pathway by overexpression of *DKK1* (a potent and specific inhibitor) showed that enterocytes differentiate normally, but all secretory cells are absent from effected areas of the small intestine[140]. Both these results suggest that Wnt is required for making cells competent for secretory cell fate. Another experiment where Wnt was overactivated by loss of *Apc*, the differentiation of enterocytes, goblet and enteroendocrine cells were disturbed leading to reduced number of terminally differentiated cells. However overproduction of Paneth cell precursors was seen, suggesting that Wnt may disrupt differentiation in all cell types other than Paneth cell lineage[141,142]. This coincides with the fact that Paneth cells reside in the crypt base, where Wnt protein is plentiful. All other terminally differentiated intestinal cell types maintain their differentiation outside the crypt, where Wnt is not active.

Taken together, the results suggest that Math1, ngn3 and NeuroD are proendocrine factors and these are ultimately regulated by Notch pathway. Activation of Notch inhibits Math1 through Hes homologs, which is required for secretory fate of progenitor crypt cells. Therefore secretory differentiation is reduced in favour for absorptive differentiation. In contrast when Notch is absent, Math1 is up-regulated and direct progenitor cells to secretory lineage, where ngn3 specifically direct differentiation to enteroendocrine cell lines. Ngn3 may also induce termination differentiation of enteroendocrine cells, other than NeuroD expressing cells (secretin and CCK cells) in the small intestine. The enteroendocrine differentiation is summarized in Figure 10 below.
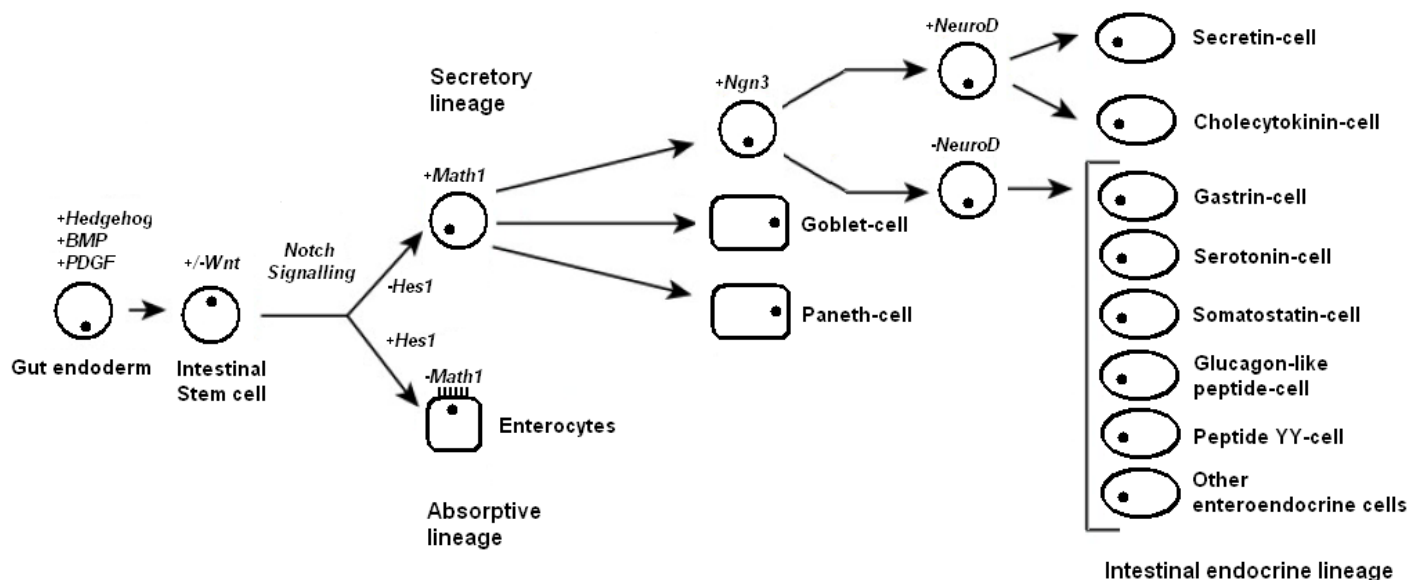
Figure 10: Illustration of the different transcription factors known to be expressed during cytodifferentiation of enteroendocrine cells of the small intestine (showed as a cascade). The gut endoderm is subjected to various stimuli before it develop into stratified cuboidal epithelium with villi and intervilllus pockets. For instance Hedgehog, BMP and PDGF are epithelial-mesenchyme signals that are important for the basic tissue architecture of the small intestine. When intervilllus pockets/crypts develop, they harbor a stem cell population, which are mostly at proliferative state. Proliferation is mainly controlled by the canonical Wnt pathway. At the point of differentiation, daughter cells are subjected to Notch stimuli in the crypt, which drive the differentiation into either absorptive or secretory lineage. Depending on if Hairy and enhancer of split like *(Hes)1* is up-regulated or down regulated, progenitor cells at early stage are specified into enterocytes, goblet, Paneth or enteroendocrine cells. As for enteroendocrine lineage, Notch has to be shut down first in order to increase the secretory specific transcription factor called Math1. Second neurogenin-3 *(ngn3)* expression has to be increased to specify enteroendocrine differentiation, whereas *NeuroD* are more specific to which enteroendocrine cell types.

1.4.2 Transcription factors regulate cytodifferentiation of the pancreas

Several studies suggest that Pdx1, a homeodomain transcription factor is implicated in early pancreatic development and is later restricted to mature β-cells[143,144]. In Pdx1-deficient mice initial stages of bud formation occurs, however the subsequent growth and branching of buds are impaired. The pancreatic mesenchyme develops normally, suggesting that absence of PDX1 make the epithelium unable to respond to mesenchymal signals that normally induces growth and differentiation. Furthermore, early Insulin and Glucagon cells are still developed when PDX1 is lost, suggesting that PDX1 is not required for differentiation, but may serve as early marker of the pluripotent cell population of the epithelium[145].

During the growth and differentiation of the pancreas, the endodermal tissue relies on current interactions with the mesoderm tissue. Specifically, the mesodermal derived mesenchymal tissue that surrounds the dorsal pancreatic bud expresses the Insulin gene enhancer protein-1, Isl1 and is not found in ventral mesenchymal tissue. Isl1 is shown to be important for development of the dorsal bud, since Isl1 knockout mouse fail to develop the dorsal mesenchymal tissue and exocrine differentiation is impaired in the dorsal pancreas. Furthermore the dorsal epithelium expression of PDX1 is reduced, compared to wild-type[146].

26

FGF10 is also found to be expressed in the dorsal and ventral mesenchymal tissue and may be required for proper proliferation and differentiation of progenitor cells in early and later stages. When FGF10 expression is persistent in the embryonic pancreas, progenitor cells shows sustaining proliferation at the expense of differentiation. Evidence suggests that persistent expression of FGF10, affects Notch signaling by maintaining lateral inhibition on proendocrine factors and thus impair tissue differentiation[147].

Notch signaling is believed to play an important role in mediating cytodifferentiation of the pancreas (Figure 11). From the four mammalian Notch factors known, only three, Notch1, Notch2 and Notch3 are found during pancreatic and intestine development[148]. Loss of function studies specifically targeting various components of the Notch at early development of the pancreas in mouse, all show accelerated differentiation of progenitor cells into endocrine cells, at the expense of proliferation, eventually leading to pancreatic hypoplasia[149,150]. For example, Dll1 mutant mice showed increased number of ngn3+ cells in E9.5 and reduced bud size with marked number of differentiated endocrine cells, expressing NeuroD/Beta2 in E10.5. These results indicate also that increased Notch expression during the early stages prevents premature differentiation of endocrine cells. One of the known downstream targets of Notch signaling is the, Hes1 which encodes a bHLH transcriptional repressor that can counteract bHLH transcription factors[40,151]. Hes1 is suggested to work in similar manner as during neurogenesis were it works as a negative regulator of neural differentiation[152]. During development of the pancreas, Hes1 down-regulates a bHLH transcription factor called ngn3, a member of neurogenin/neuroD family. Ngn3 is found to be transiently expressed in a subset of pancreatic cells at the time of budding and is found to be one of the key initiators of endocrine differentiation[148]. Target disruption of the *ngn3* gene shown to completely abolish differentiation of all endocrine lineages, but differentiation of the exocrine cell lineage remains unaffected, suggesting that ngn3 is only specific for endocrine cells of the pancreas[144]. Ectopic expression of ngn3 in chick is shown to be sufficient to induce the formation of Glucagon and Somatostatin cells[153]. In addition loss of function studies, suggest that ngn3 act upstream of NeuroD in a ngn3-NeuroD cascade[148,154]. Taken together, ngn3 is a proendocrine transcription factor, that in absence of Notch signaling and thus induction of Hes1 is sufficient to induce cytodifferentiation of the pancreatic epithelium, whereas progenitor cells where ngn3 is repressed by Notch are committed to exocrine lineage.

Interestingly, ngn3 seems preferentially to commit cells for endocrine lineage other than Insulin producing β-cells (mostly α-cells), suggesting other key components may be involved in β-cell specification. Nkx2.2 is found co-localized in Insulin and Glucagon producing cells, but not in δ-cells and seems to be required for the final β-cell differentiation stage in the islets. In absence of Nkx2.2, β-cells develop prematurely and do not express Insulin[155]. Furthermore another member of the NK2 homeobox transcription factor family, Nkx6.1 is found to be similar expressed as Nkx2.2 however it appear not to have a vast role in

differentiation of β-cells, but rather required for maintaining and expanding the β-cell population. Nkx6.1 mutant embryos showed normal initial development of β-cells, however at later stages mutant embryos fail to expand their β-cell population[156]. Pax4 is believed to act downstream of NeuroD/Beta2 and to be involved in early development and islet cell differentiation[157]. Pax4 knockout mouse reveal complete lack of both β- and δ-cells, but Glucagon producing α-cells are increased, which suggest that Pax4 is essential for early β- and δ-cell development and acts upstream of Nkx2.2 and Nkx6.1[158].
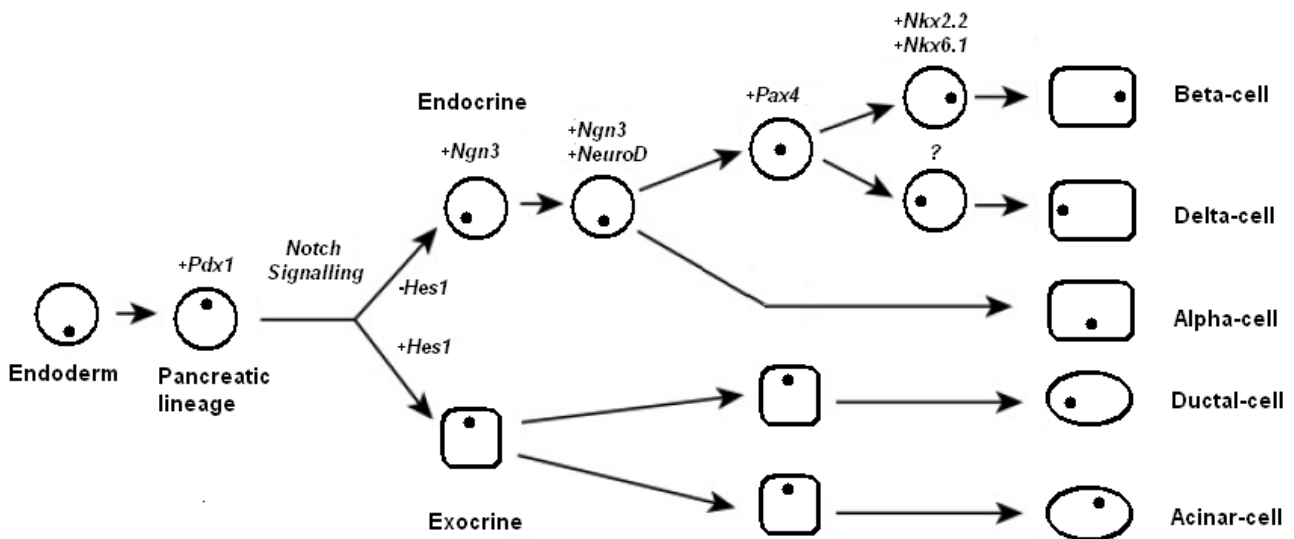
Figure 11: Illustration of the different transcription factors known to be expressed during cytodifferentiation of the pancreatic endocrine cell lineage (showed as a cascade). The pancreatic endoderm is subjected to various stimuli, including the Notch signaling which is normally increased initially to prevent premature endocrine cells and pancreatic hypoplasia. Depending on if Hairy and enhancer of split like *(Hes)1* is upregulated or down regulated, progenitor cells at early stage are specified in the endocrine or exocrine lineage. As for endocrine lineage, Notch has to be shut down in order to increase neurogenin-3/NeuroD **(**ngn3/NeuroD) expression and depending Pax4 activation the cell can be directed into the three major endocrine cell types (pancreatic polypeptide cells are not shown).

1.5   MicroRNA biology

1.5.1   The biogenesis of miRNAs

MicroRNAs or miRNAs are short, single stranded non-coding RNA molecules of 20-23 nucleotides that regulate gene expression by inhibiting translation of messengerRNA (mRNA) with complimentary sequence. These are transcribed from regions localized between genes or inside genes known as intergenic or intragenic regions respectively[159]. The miRNA biogenesis comprises by miRNA transcription and several coordinated processes that involve subsequent processing of the primary miRNA transcripts (pri-miRNA) and maturation of the miRNA which can be viewed in Figure 12.

Initially, miRNA genes are transcribed into pri-miRNAs by either RNA polymerase II or III[160,161]. Many of these pri-miRNAs are capped, polyadenylated transcripts and are usually several kilobases long with hairpin loop structure at the upper part. Subsequently the nuclear-located pri-miRNA is cleaved by the nuclear microprocessor complex formed by the RNase III enzyme Drosha and the co-factor DiGeorge critical region 8 (DGCR8) to release a precursor of miRNA (pre-miRNA)[162,163], while the cleaved off flanking fragment is degraded in the nucleus. Following nuclear processing, the pre-miRNA is exported into the cytoplasm by the Exportin5/Ran-GTP complex[164,165]. The complex does not recognize pre-miRNAs by its sequence or the loop structure, but more generally on the defined length of the double-stranded stem and the 3' overhangs structure[166]. When exportin5 is depleted from cells, the pre-miRNA and mature miRNA form is reduced in the cytoplasm. Notably, pre-miRNA does not accumulate in the nucleus[167], suggesting that exportin5 also protect the pre-miRNAs against nuclear digestion. Gel retardation assay showed that exportin5 binds directly to pre-RNA in a Ran-GTP-dependent manner and had a much higher affinity for pre-miRNA than tRNA[168,169], suggesting that pre-miRNA are the main cargo of exportin5.

In the cytoplasm, the pre-miRNA is further processed into the mature miRNA where it is incorporated into the RNA-induced silencing complex (RISC) and guided to its target mRNA. Collectively, the cytoplasmic processing and RISC assembly are known as the RISC loading complex (RLC). RLC is a multiprotein complex consisting of Dicer, TRBP, PACT, RISC and Ago2 which are described below. To begin with the pre-miRNA is processed by the cytoplasmic RNase III Dicer, generating a roughly 22 nucleotide miRNA duplex with two nucleotides protruding as overhangs at each 3'end. The miRNA duplex contains both a strand that is complimentary to the target (guide strand) and a complimentary strand to the functional guide strand (passenger strand). This cleavage is shown to be essential for miRNA processing as knockdown or knockout of Dicer results in accumulation of pre-miRNAs whereas mature miRNAs is diminished[170,171]. Furthermore Dicer is highly conserved among eukaryotic species, such as animals and plants. It contains a

putative helicase domain, DUF283 domain, Piwi-Argonaute-Zwelle (PAZ) domain, two tandem RNase III domains and a dsRNA-binding domain[172]. The PAZ domain have shown to specifically recognize dsRNA ends containing the 3' overhang[173,174], such as those products from Drosha cleavage. Dicer associates with several other proteins that are found to regulate its activity. TRBP and PACT are shown not to be essential for the Dicer-mediated cleavage, but is important for a proper cleavage as TRBP stabilizes Dicer[175]. Depletion of either Dicer or TRBP resulted in decrease levels of mature miRNA, which was reflected by destabilization of both proteins[176,177]. Dicer is also regulated by its own product, as in let-7 which target *Dicer* mRNA, creating a negative feedback loop[178]. Other proteins that are known to exert regulatory functions are the argonaute family proteins, preferentially Ago2. Before Dicer-mediated cleavage, pre-miRNAs that display high degree of complementary along hairpin undergo an additional endonucleolytic cleavage step: the slicer activity of Ago2 cleaves 3'arm of the hairpin on the passenger strand, thus generating a nicked hairpin called ac-pre-miRNA. The cleavage of 3'arm is suggested to contribute to future strand selection or participate in miRNA maturation after Dicer processing[179]. Furthermore Ago2 has been identified in association with RISC to help cleaving the target mRNA[180,181].

After Dicer-mediated cleavage, Dicer and other associated proteins are dissociated from the miRNA duplex and the active RISC that preforms the gene silencing is formed by separation of the miRNA duplex, into the guide strand. In order to do so, a helicases associated with RISC unwinds the miRNA duplex and the passenger strand is degraded. Several helicases has been identified to associate with RISC[182,183]. For instance the helicase p68 in mouse is found to unwind let-7 miRNA duplex[184]. Interestingly, the selection of the guide strand into the RISC is thought to depend on thermodynamic stability of the base pairs at the two ends of the duplex. In the duplex, guide stands have less stable base pair at the 5'end compared to passenger strands, and therefore selected and loaded into RISC. The assembly of RISC is ATP-dependent which precedes target recognition[185,186].

The retained ssRNA strand (miRNA in its mature form) is loaded into RISC and acts as a guide by targeting this complex to a complementary mRNA. The miRNA-RISC complex interacts with the mRNA target through sequence complementation, typically within the 3'-untranslated region (3'UTR). The complimentary mRNA is then inactivated by cleavage or translational interference, depending on the extent of base pairing between the miRNA and its mRNA target[187].
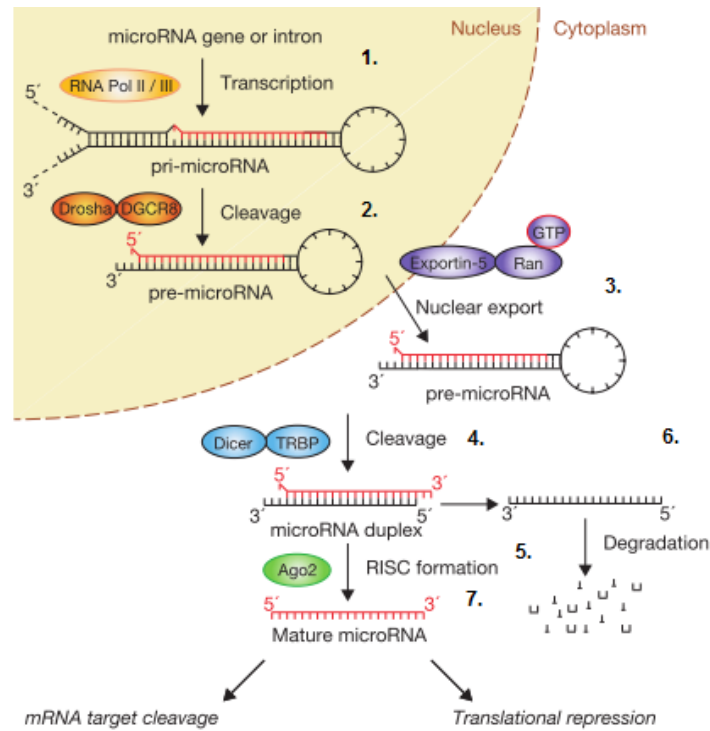
Figure 12: The pathway of miRNA processing. 1: Initially primary miRNA transcripts (pri-miRNA) are produced by RNA polymerase II or III from genes or introns in the nucleus. As these pri-miRNAs are several kilobases long they need to be reduced in length before nuclear export can be made of precursor miRNA (pre-miRNA). Therefore, 2: pri-miRNA is further processed by the RNase III enzyme Drosha and DGCR8 and 3: pre-miRNA is exported to the cytoplasm by Exportin5/Ran-GTP complex. In the cytoplasm, 4: Dicer with TRBP co-factor, unwinds and cleaves the pre-miRNA so only the miRNA duplex is retained, followed by separation of the guide strand (mature miRNA) and passenger strand, 5: the guide strand is incorporated into the RISC-Ago2 complex and 6: passenger strand is degraded. 7: RISC containing mature miRNA guides miRNA to its complementary target mRNA and depending on the complementarity it either cleaves the target mRNA, partially mediated by Ago2 or repress translation of the mRNA target. Note that all processes contain the mature miRNA sequence (red) and these steps are necessary to uncover the mature sequence and its function. Adapted from[188].

Gastroenteropancreatic neuroendocrine tumors

1.5.2 Introduction to gastroenteropancreatic neuroendocrine tumors

The origin of GEP-NETs appears to be caused by malignant transformation of neuroendocrine-committed cells or adult neuroendocrine cells of the GI-tract (carcinoids) and pancreas (pancreatic islet tumors). As demonstrated in earlier studies of transgenic mice expressing a potent oncogene, endocrine cells were able to transform into heritable neuroendocrine tumors (NETs)[189,190]. In some incidence, this transformation is based on genetic alternations of the *MEN1* gene however in most tumors, the pathogenesis are currently unknown. Although GEP-NETs represent a rarer form of tumors than adenocarcinomas, their heterogeneity and site of origin, including molecular markers, render it a rather complex disease. These tumors can either be termed functioning or non-functioning (NF) depending on clinical findings. Functioning tumors usually secretes one or more peptide hormone, resulting in the production of symptoms or syndrome, due to hormone excess in the blood, while the 'non-functioning' produce and secrete peptide hormones, but may not result in hormone excess and a recognizable syndrome. For example, patients with functioning tumors such as gastrinoma, insulinoma or VIPoma may produce symptoms attributable to hormone excess, such as gastric ulceration, hypoglycaemia or profuse watery diarrhea respectively. Furthermore, tumors are presented as well-differentiated or poorly differentiated, depending on their histological features. Well-differentiated tumors are often slow-growing with low mitotic and proliferative status and they express intensely the markers of neuroendocrine differentiation, in particular CgA. Conversely poorly differentiated tumors are characterized by high mitotic index and proliferative status with abundant necrosis. They often express cytosolic neuroendocrine markers together with Synaptophysin, but CgA is rarely found in these tumors[191].

At onset most GEP-NETs display well-differentiated phenotype, with intact hormone capacity, but because most tumors are NF, they often represent malignant behavior, with tumor mass-related symptoms and distant metastasis at time of diagnosis[192,193]. GEP-NETs follow a similar progression path as for other tumors with development of hyperplasia, dysplasia, neoplasia and metastasis. However unlike the majority of tumors, progression through these stages is slow[194]. As tumors become less differentiated, they also develop the potential to secrete other peptides which may result in a syndrome other than the initially presenting syndrome.

Over the past few decades a general steady increase in GEP-NET incidence has been reported. Based on the US Surveillance Epidemiology and End Results (SEER) database, incidence for all GEP-NETs from 1973-2007 increased from 1 case per 100.000 to 3.65[195,196]. Interestingly more than half of all NETs registered, were GEP-NETs (61%) showing highest frequency in the distal part of the GI-tract including rectum, small

intestine and colon. Similarly in England, the incidence of gastrointestinal NETs increased from 0.31-1.33 in almost the same period of time[197].

1.5.3   Classification of neuroendocrine tumors in general

NETs were first described as 'carcinoids' by Obendorfer at the beginning of the twentieth century. These types of tumors were described as benign tumors relative to other 'classical' carcinomas[198]. The endocrine character of these tumors became evident later in 1914, where the origin of carcinoids were described from ECL cells of the GI-tract[199] and much later the monoamine neurotransmitter, Serotonin was successfully isolated from a carcinoid tumor[200]. Furthermore, symptoms, like flushing and diarrhea were reported in patients with carcinoids as a result of excessive hormone secretion[201]. This phenomenal was referred to as the carcinoid syndrome (CS). The fundamental understanding of NETs as carcinoids, arising from enterochromaffin (EC) cells lead to the presumption that, the term 'carcinoid' could be established for most endocrine tumors in the gut[202]. The classification divided carcinoids into foregut (lung, stomach, duodenum, upper jejunum, and pancreas), midgut (lower jejunum, ileum, appendix, and cecum) and hindgut (colon and rectum), based on the tumor embryonic origin and known histological features, without taking into account the heterogeneity and differentiation stage of the tumor and therefore was proven unfit for clinical trials. For instance, patients with carcinoid arise from type A atrophic gastritis cannot be compared with Gastrin producing carcinoids of the duodenal, since both types are morphology, biological and functionally different[203]. In 1980 the World Health Organization (WHO) classification was introduced to distinguish gastrointestinal NETs from other unspecified tumors[204] and in recent years the histological classification have been repeatedly revised. The most recent published by WHO in 2010 was established upon proposal from the European Neuroendocrine Tumor Society (ENETS) and others[205,206] to revise the previous 2000/2004 classification. The 2000/2004 classification was mainly based upon three groups that separate neuroendocrine neoplasm in well- and poorly differentiated, depending on specific neuroendocrine markers. Moreover the term carcinoid was used for well differentiated neoplasm, whereas 'carcinomas' was used when overt malignancy was proven (metastasis- or invasion capacity)[207]. As a result of this, poorly differentiated neoplasms, judged from their condition were designated carcinoma almost conclusively. An increase in incidence of digestive NETs in that period, possibly due to better preventive gastroenterology awareness and various prognosis studies[208], augmented the pressure in finding a more precise and comparable classification[209]. The WHO classification 2010 tries to resolve some of the issues by implementing the term neuroendocrine tumor or neoplasm in replacement of the word carcinoid. Moreover introducing a grading system to refine tumor differentiation and to standardize diagnosis, which otherwise seem controversial due to the fact that some well-differentiated tumors exhibit malignant behavior[210]. The grading scheme is based on proliferation rate and is composed of three grades (G1, G2 and G3), defining the

basis of tumor morphological criteria and help classify tumors in five different classes (Table 2). The proliferation rate is assessed as the number of mitosis per unit area of tumor or percentage of MIB-1 immunolabeling of neoplastic cells, in the area with strongest nuclear labeling (hot spots). The latter is used to determine the Ki67 index, although it has some limitations[211] and should be used with other prognosticators to avoid misclassification[212]. For mitotic count, the grading requires at least 50 high power fields (HPF) and MIB-1 percentage is calculated from hot spot areas of 500-2000 cells. To improve prognostic strength, grading is combined with a site-specific TNM (tumor, node, metastasis) staging system[213], but is evaluated separately to allow classification of tumors in more advanced disease stage.

Definition	Grade	Mitotic count (10 HPF)	Ki67 index (%)	Malignancy (expected)
NET	G1	<2	≤2	+
NET	G2	2-20	3-20	++
NEC	G3	>20	>20	+++
MANEC	mr	mr	mr	variable
Hyperplasia/dysplasia	na	na	na	na

Table 2: The WHO 2010 grading rules and projected malignancy for neuroendocrine tumors. NET: neuroendocrine tumor, NEC: neuroendocrine carcinoma, MANEC: mixed adeno-neuroendocrine carcinoma, HPF: high power fields, mr: missing recommendation from current WHO 2010, na: not applicable. Adapted from[214].

1.5.4   Clinical presentation of carcinoids and associated syndromes

Carcinoids account for 55% of all NETs. The tumor is derived from neoplastic proliferation of EC or Kulchitsky cells found in any organ derived from the primitive endoderm, but predominantly in the GI-tract, urogenital tracts and bronchial epithelium. The most common site for carcinoids is the small intestine, appendix and rectum[215] as described below.

In the small intestine, the majority of the cases are found in the distal ileum, while less commonly in the jejunum and rarely in the duodenum. These tumors arise in the crypts of the small intestine in people of 40-60 years of age, where it grow as submucosal nodules and therefore can be detected early by enteroclysis. However the diagnosis is usually not made, until the patient undergo exploratory surgery or during routine endoscopy, due to small intestinal carcinoids are mostly asymptotic. Tumors larger than 2 cm are more likely to present symptoms and metastasize[216,217]. Symptoms are often non-specific, such as abdominal pain, diarrhea and bowel obstruction. The latter can be caused by primary tumors growth, but more frequently as a

result of an extensive mesenteric reaction-fibrosis, leading to bulking of the intestine[218]. The overall 5 year survival of jejunoileal carcinoids is reported to be 47-65%[219].

Appendiceal carcinoids, occurs at earlier age than carcinoids of the small intestine and occur more frequently in women. This type of carcinoid is thought to arise from subepithelial endocrine cells located in the lamina propria and submucosa of the appendix wall[220]. As for small intestinal carcinoids, most patients are asymptomatic, but some may present with pain in the right lower abdomen or right testis[221]. The majority are located at the tip of the appendix and therefore do not lead to luminal obstruction by tumor growth as in small intestinal carcinoids[222]. Tumor size is one of the best predictors of prognosis; particularly over 95% of the appendiceal carcinoids with size less than 2 cm, rarely show any progression to metastatic disease and thus can be cured by appendectomy. In contrast about 30% of the patients with larger tumors present metastases at time of diagnosis[217,221]. The 5 year survival is 94% for patients with local disease, 85% for patients with regional metastases and 34% for patients with distant metastases[223,224].

Rectal carcinoids are the third most common carcinoid of the GI-tract and are typically encountered in patients of 50-60 years of age incidentally, during routine sigmoidoscopy and colonoscopy screenings. Therefore it is not surprising that incidence of rectal carcinoids has been increased in the last 35 years[225], where black and Asian populations appear to be over-represented[196]. The prevalence of rectal carcinoids in adults undergoing screening endoscopy has been reported to be 0.05-0.07%[226,227]. They are usually presented as small, non-functioning tumors with a size less than 1 cm and rarely present any distant metastases at time of diagnosis. However, tumors larger than 2 cm have been reported to metastasize in 60-80% of the cases[228,229], suggesting tumor size to be an important prognostic factor. Others are infiltration of muscularis propria and atypical histology[230,231]. Small tumors with no sign of infiltration or invasion can be managed by local excision preformed either endoscopically or surgically after preforming endoscopic ultrasound. If there is evidence of spread to regional lymph nodes, lymph node dissection has to be considered[232,233]. Local resection of larger tumors with hepatic or lymph node metastases is also considered to provide symptomatic relief and prevent bleeding and obstruction[234], however it does not improve the survival of the patient. Instead most patients undergo a major surgery called total mesorectal excision to improve survivability[235]. The 5 year survival is over 80% for local disease, 44% for regional metastases and 20% for patients with distant metastases[196].

The most prominent secretory products of carcinoids are the storage and secretion of amines, kallikrein and prostaglandins, where Serotonin (5-HT) is their main characteristic in relation to producing syndromes. 5-HT is synthesized from tryptophan through its precursor, 5-hydroxytryptophan (5-HTP) and subsequently metabolised to 5-hydroxyindoleacetate (5-HIAA), which is excreted in the urine. In normal subjects, approximately 99% of tryptophan is used for the production of nicotinic acid (niacin), whereas only 1% or

less is used for 5-HT synthesis[236]. In patients with carcinoids there is found a higher production of 5-HT and eventually increased 5-HIAA excretion. Normally the higher 5-HT amount produced, do not cause any sighs of systematic symptoms, since 5-HT and other products are efficiently metabolized by the liver. However if liver metastasis are present or primary lesions in the bronchus or ovaries are found, the features of CS become more evident[237]. Interestingly, there is a significant variation in secretory factors of carcinoids, depending on anatomic site of origin. Carcinoids of the foregut (bronchi, stomach, pancreas, gall bladder, jejunum, duodenum), produce low amounts of 5-HT, because they lack the enzyme that converts 5-HTP to 5-HT and produce therefore 5-HTP and histamine instead of 5-HT[238]. Similarly hindgut carcinoids (left colon, rectum) cannot convert tryptophan to 5-HT and therefore rarely cause CS[239,240]. However, midgut carcinoids (ileum, appendix, right colon) tend to produce large amounts of 5-HT and other vasoactive compounds.

1.5.5   The carcinoid syndrome

CS is found in less than 10% of all patients with carcinoid tumors and is characterized by symptoms involving several organs, including the skin, gastrointestinal, respiratory and cardiovascular system. Most commonly flushing, diarrhea and abdominal pain is present and less commonly; wheezing and pellagra[241,242]. It is a directly result of the synergistic interaction between 5-HT metabolites and other factors such as kinins, kallikrein and prostaglandin, released by the tumor into the circulation.

The CS is subdivided into typical and atypical syndrome: the typical syndrome account for most patients with CS and most common symptoms are flushing, diarrhoea, cardiac fibrosis, wheezing, dyspnoea and pellagra. The flush is of sudden-onset in patients with CS, and usually manifest in a pink-red color involving the face and upper trunk with a lasting of only few minutes. The diarrhea usually occurs in the small intestine and colon as a result to secretory and gastrointestinal motor abnormalities, accompanied by abdominal cramping. If diarrhea remains untreated it may manifest into gut lymphangiectasia and bacterial overgrowth. The flush and diarrhea seems to relate directly to the 5-HT, tachykinins, histamine, substance P and prostaglandin in the circulation, typically released by midgut carcinoids[238]. In contrast to the common CS, atypical syndrome occurs only in 5% of the cases. It consists of a prolonged flush with purplish of color and tends to last for hours, leaving telangiectasia (dilated blood vessels) and hypertrophy of the skin. Furthermore other features, including headache and lacrimation may also occur. This type of flush is not triggered by alcohol or tyramine-containing foods as the typical flush. The atypical syndrome is believed to be caused by excessive 5-HTP and histamine into the circulation as a result of foregut carcinoids[243]. In patients with foregut or midgut carcinoids, the CS can sometimes lead to carcinoid crisis, which is a life-threatening complication of CS. Beside flushing and wheezing, patients with carcinoid crisis develop

hypotension, tachycardia arrhythmias and central nervous system dysfunction. Although it is a rare event, it may occur during tumor manipulation and percutaneous fine needle biopsy, but also spontaneously[244].

1.5.6   Clinical presentation of functional pancreatic neuroendocrine tumors

Insulinomas are the most common islet cell tumor (55% of the cases) and are typically small, solitary and benign functioning tumors that are present with hypoglycaemic episodes. Insulinoma has been reported to occur in people of different ages, however most people are at 30-60 years of age at the time of diagnosis[245]. Approximately 10% are displaying either multiple or malignant behavior, and 4-6% are associated with MEN1[245,246]; these tumors are usually multiple and have a higher risk of malignancy[247]. Thus if multiple nodules are found at time of diagnosis, MEN1 should also be considered. Almost all insulinomas are located within the pancreas, while less than 5% has been described to be located ectopically, in the lung, duodenum, ileum, cervix and ovary[248,249]. Insulinoma is characterized by its hypersecretion of Insulin, resulting in common symptoms of neuroglycopenia, such as headaches, lethargy, dizziness and amnesia in patients. Furthermore due to elevated levels of Insulin, symptoms related to increase catecholamine release has been reported including sweating, weakness, hunger, and nausea, however these may not always be present[250]. Another notable manifestation of insulinoma is weight gain, as patients eats more frequently to avoid symptoms[251]. Sporadic malignant insulinoma are usually not multiple, but the tumor is larger compared to the benign form. Histologically speaking, these tumors are often difficult to distinguish from the others, and therefore in most cases metastasis has to be present, before diagnosis can be made[252].

Gastrinomas, after insulinomas are the second most frequent pancreatic neuroendocrine tumor (PNET), which is found in about 36% of all patients. Gastrinoma is typically present in late adulthood at ages between 40 and 50, but is rarely found in children[253,254]. The tumors are characterized by inappropriate section of Gastrin which is known to cause Zollinger-Ellison syndrome (ZES), characterized by gastric acid hypersecretion, peptic ulceration and occasionally diarrhoea. In about 75% of the cases, ZES occurs as a consequence of the disease (known as sporadic ZES), while in the remaining cases, as part of MEN1 syndrome[255,256]. Sporadic gastrinomas are more frequently found in the duodenum than the pancreas. Duodenal gastrinomas are very small (<1 cm) and mostly located in the submucosa of the proximal duodenum. In contrast, pancreatic gastrinomas appear to be larger than their duodenal counterparts, with a diameter of 2-3 cm and in most cases found in the head of the pancreas[257]. The region that encompasses the proximal duodenum and head of the pancreas is known as the 'gastrinoma triangle'. Other rare sites of primary gastrinoma have been reported in the liver, bile duct, ovary, heart, pyloric canal, jejunum, and omentum[258,259]. Despite the small size of duodenal gastrinomas, lymph node metastases are already present in 60-80% of the patients at the time of diagnosis. In about 10% of patients liver metastases are present,

however this only occur in the very late disease course[260]. The majority of PNETs in MEN1 patients are functional gastrinomas (>50%), these gastrinomas are almost exclusively present in the duodenum and are often multiple with multifocal Gastrin cell hyperplasia. In the few known MEN1 associated pancreatic gastrinomas, the pancreas in these patients usually contains micro and macro tumors with almost no Gastrin production[261,262].

Other functional tumors such as glucagonoma, VIPoma and somatostatinoma are only present in rare cases. Glucagonomas are slow-growing tumors arising from α-cells of the pancreatic islets, which is commonly associated with the glucagonoma syndromes as a result of excessive amount of Glucagon secretion. Most glucagonomas are found to be sporadic by nature, but between 5 and 17% are associated with MEN1[263]. These functionally active glucagonoma are large tumors (>6 cm) and normally found in the tail of the pancreas. Although glucagonoma are extremely rare, most tumors express highly malignant behavior, where approximately 60-70% of the sporadic tumors have hepatic metastases at time of diagnosis[264–266]. People with present glucagonoma have been reported to be between 19 and 84 of age; however higher incidences are present between 40 and 60 of age[263]. One of the most presenting features of the syndrome is necrolytic migratory erythema (NME) which occur about 70% of all patients with glucagonoma. This type of rash starts usually at the perineum or groin and migrates to the distal extremities, such as the trunk and legs. The cause of the skin rash remains unknown, but surgery or somatostatin-analogs treatment have shown to clear the skin disorder[267]. Other symptoms caused by hyperglucagonemia is weight loss, mild glucose intolerance, anemia, depression, diarrhea and development of deep vein thrombosis[268,269]. Furthermore secondary endocrine syndromes have been associated with glucagonoma due to other peptides are secreted. Beside high Glucagon levels, some patients (20-40%) also have raised fasting Gastrin and vasoactive intestinal polypeptide (VIP) levels, leading to ZES and watery diarrhea respectively[270].

Severe watery diarrhea is a universal symptom of the Verner-Morrison syndrome or Watery Diarrhea, Hypokalemia, Achlorhydria syndrome (WDHA), reported in VIP secreting tumors or VIPomas. VIPomas have also been reported to produce several other peptides, including pancreatic polypeptide (PP) and Gastrin[271]. Because vast amounts of watery stool are produced, these patients often suffer from severe fluid and electrolyte loss (mainly potassium and bicarbonate), causing dehydration, severe hypokalemia, hypochlorhydria or achlorhydria and hyperchloremic acidosis, with subsequent cramps in the limbs leading to tetany and cardiac alterations[272]. As for other functional tumors, most VIPomas are sporadic and approximately 90% of the primary tumors originate from the pancreas (mostly the pancreatic tail), the remaining tumors originate from the nervous system and very few have been reported in the liver[273]. VIPomas of neuronal origin are mostly found in children as ganglioneuromas and ganglioneuroblastomas[274].

The primary tumor is usually large (4-5 cm) and approximately 50% of the pancreatic VIPomas have developed metastases at the time of diagnosis. The mean age of patients when diagnosed is 50-60 years[275].

Another rare form of tumor are somatostatinomas, they are classified by predominantly or exclusively presence of Somatostatin producing D cells. These cells are normally distributed in tissues of the pancreas, GI-tract and the central nervous system[276]. Therefore it is not surprising that somatostatinomas are found in both pancreas and the small intestine, mainly the duodenum. The pancreatic somatostatinomas are usually larger (>2 cm) than their duodenal counterparts. These tumors seems to have different malignancy depending on the location; in one study a higher malignancy is reported in pancreatic somatostatinoma than the duodenum[277]. Another larger study with 173 patients reports of no significant difference in malignancy between these two groups[278]. Somatostatinoma are found to be sporadic in most cases, only few patients have somatostatinoma in association with MEN1 (5-10%). As a part of the functional tumors, somatostatinoma over secrets Somatostatin that has an inhibitory secretory function of both exocrine and endocrine character, including the motor function of the stomach and gallbladder, these multisecretory insufficiency and gastrointestinal symptoms are collectively called somatostatinoma syndrome or inhibitory syndrome[279]. This syndrome includes upper abdominal pain, diarrhoea, maldigestion of food (suppression of exocrine function of pancreas), cholelithiasis (suppression of CCK release and gallbladder contractility), weight loss and hyperglycemia as frequent manifestations[280]. In contrast to other functional PNETs, the complete syndrome is not diverse in patients with somatostatinoma, however most patients still remained symptomatic, displaying hyperglycemia and cholelithiasis[281]. In another case study there has been reported of hypoglycemia in somatostatinoma patients due to the multi-inhibitory function of Somatostatin. Hypoglycemia occurs when the inhibitory effect of Somatostatin on growth hormone and Glucagon is superior to that of Insulin. Another thing that may reinforce hypoglycemia is malabsorption of carbohydrate due to pancreatic exocrine deficiency. These patients are often misdiagnosed with insulinoma, because clinicians fail to test for plasma Somatostatin[282].

1.5.7   Clinical presentation of non-functional pancreatic neuroendocrine tumors

NF PNETs represents about 30-50% of all pancreatic NETs and in contrary to other functional tumors, these tumors are not associated with clinical syndromes caused by hormone hypersecretion. However these tumors may show positive for immunohistochemical markers, such as Insulin, Glucagon, Somatostatin and PP[243]. In the initial phase of the tumor, no symptoms are presented and are thus found only by accident when diagnostic imaging is used for other reasons. Most NF PNETs are first discovered at advanced disease stage, when metastases or symptoms caused by tumor growth/spread, such as back pain, vague abdominal pain, weight loss or jaundice are present. Patients with NF PNET are mostly in their fifth decade at time of

diagnosis, the tumor found is solitary, large (>3 cm) and commonly located in the head of the pancreas, but also other areas of the pancreas. At the time of diagnosis over 60% of all NF PNET patients are presented with liver metastases[283]. In contrast to the highly malignant sporadic counterpart, the MEN1 associated NF PNET demonstrate a more benign course. It appear in about 20% of all MEN1 patient, however the true incidence is unknown. Patients with NF PNET in MEN1 are often diagnosed earlier than its sporadic counterpart and at the time of diagnosis only 9-19% and 14-33% of the patients have liver and lymph node metastases respectively. These tumors are also smaller (<3 cm), multiple with micro and macro adenomas and appear to exhibit indolent growth with average doubling time of diameter at 5-10 years. The overall 5 years survival rate for NF PNET in MEN1 patients is similar to patients with gastrinomas, which is about 80%[284,285]. The clinical silence of these tumors may be related to the production of hormones is inactivated or still intact but not metabolically active due to co-secretion of peptide inhibitors, peripheral receptors are down-regulated on tumor surface or simply because substances secreted are not associated with any specific symptoms (PP, Neuron-Specific Enolase (NSE) or chromogranins)[286].

1.5.8 General diagnosis of gastroenteropancreatic tumors

Diagnosis of GEP-NETs relies not only on the clinical presentation and pathological features of the relevant tumor, but also on biochemical markers that can be measured in the serum or plasma of affected subjects. Some NETs produce and secrete a multitude of peptide hormones and amines, which some can cause specific clinical syndromes as mentioned earlier. The tumors that are known to produce a clinical syndrome are in most cases due to vast secretion of one specific hormone, which can be used as indicative marker of a specific tumor type. These are described in diagnosis of functional tumors. Furthermore some markers are produced and secreted or co-secreted with other peptides/amines in a broad spectrum of GEP-NETs, but not necessarily produce any syndrome; these remain non-specific but sensitive. As described earlier, chromogranins are glycoproteins that are ubiquitously present in neuroendocrine tissues. In most NETs CgA is more abundant and thus better circulating tumor marker than CgB. The serum levels of CgA in GEP-NETs, ranges from slightly elevated (~70 ng/ml) to extreme levels (>9000 ng/ml) and has a sensitivity[1] at 60-80%[192,237,287]. The tumor marker has been shown to depend on the localization and type of the tumor, notably CgA was increased most frequently in patients with gastrinomas (100%), carcinoid tumors (89%) and non-functioning tumors (89%), while rarely present in insulinoma[288], but also which type of assay used.

---

[1] The term sensitivity is a statistical measurement that measures the proportion of positive findings in actual disease, which are the percentage of patients with the disease that are currently identified as having the condition[521,522]. In other words if the sensitivity is low there is a higher rate of false-negative patients (people that are sick but are termed to be healthy) in the amount of patients studied.

Currently, two different methods for measuring CgA are used on routine basis, immunoradiometric assay (IRMA) and enzyme-linked immunosorbent assay (ELISA). One study reports on the sensitivity and specificity[2] of CgA in NET patients by the two different methods, showing a sensitivity of 77 and 84%, and specificity 71 and 85% for IRMA and ELISA respectively[289]. Moreover the study showed that metastatic patients had higher CgA levels compared to patients without metastases, showing that CgA was able to discriminate between patients with or without metastasis. However this also depends on the type of assay and cut-off values used. Other studies have showed that the level of CgA correlates with tumor mass and the malignant nature of the tumor[288,290]. The currently used serum/plasma assays are for intact CgA protein or its cleavage products found to be released by specific NETs[291], but these assays also have their drawbacks, since elevation of CgA is also seen in patients with renal failure, proton pump inhibitor (PPI) treatment and chronic atrophic gastritis[192]. Although CgB immunoassays are less sensitive than CgA, the circulating CgB levels have been shown to be unaffected by these clinical parameters. Therefore commercial kits are available today that combines CgA and CgB to reduce the possibility of false-positive diagnosis[292]. Other non-specific markers available are PP and NSE; however these are not radically used in the clinic. PP in diagnostic use has low sensitivity but higher specificity when compared with healthy subjects. But when PP is combined with CgA, the sensitivity increases compared to either of the makers alone[293]. In contrast NSE shows high sensitivity but rather low specificity and thus has a little diagnostic value[294].

Furthermore topographic diagnosis is helpful in localization of different GEP-NETs in order to make tissue diagnosis by biopsies, which is crucial for later management. The localization procedures used to identify both primary and metastatic tumors falls into three major categories: cross-sectional imaging, functional imaging and endoscopic approaches. Cross-sectional imaging constitutes mainly of contrast-enhanced computed tomography (CT) and magnetic resonance imaging (MRI) both provide efficient visualization of primary tumor and metastatic lesions. The general detection frequency of CT or MRI is estimated to be between 22-45%, but small tumors are often difficult to detect using standard imaging. Therefore CT scan of the chest is often followed by somatostatin receptor scintigraphy-single photon emission computed tomography (SRS-SPECT) and triphasic CT for more accurate detection and localization of the tumor[295]. In detection of small pancreatic tumors such as insulinomas, the combined approach using CT and ultrasonography has been suggested to increase overall sensitivity[296].

---

[2] The term specificity is a measurement of the percentage of healthy subjects that are correctly identified not having the actual condition[521,522]. In other words if the specificity is low there is a high rate of false-positive patients (people that are healthy but are termed to be sick). in the amount of patients studied.

Functional imaging includes SRS, *meta*-iodobenzylguanidine (MIBG) and positron emission tomography (PET). SRS is a method to localize and imaging tumors by using the advantage of somatostatin receptors are expressed on tumors. High affinity somatostatin receptors have been identified many cells of neuroendocrine origin, including tumors, such as PNETs and carcinoids. Because Somatostatin has a short half-life, radioactivity labeled somatostatin-analogs, such as octreotide and lanreotide are used, these bind with high affinity to receptor subtype 2 and 5 so that radionuclide complex gets trapped within the lysosome of the tumor, after receptor induced internalization[297]. The most commonly used radioligand for SRS is [111In]DTPA-octreotide (OctreoScan), and SPECT is usually performed for increasing the sensitivity for detecting tissue that are somatostatin receptor positive and gives a better anatomical delineation. The majority of GEP-NETs can be visualized using OctreoScan and therefore SRS remains the golden standard for functional imaging of GEP-NETs[298,299]. In patients with carcinoids and gastrinomas, the tumors were identified in 58-90% of the cases. Moreover the patients with malignant gastrinoma with spread to the liver was detected in 92% of the cases[300,301]. In contrast to other functional PNETs, is insulinoma difficult to detect using OctreoScan alone, about 50% of all insulinomas are discovered[302,303]. Others have reported only 14% detection rate using SRS[304] or failing to detect any insulinoma patient[305]. These studies however did only use few insulinoma positive patients and therefore the real sensitivity may be higher.

In patients where OctreoScan fails to reveal the primary tumor and endoscopy of the upper and lower GI-tract is not closer to reach any diagnosis, a triple phase CT of the thorax and abdomen is frequently used for localize potential lung carcinoids[306]. For detecting secondary tumors in the bone and liver the SRS is the treatment of choice, considering its sensitivity at 65-94%[307–309]. This applies also for the detection of secondary tumors of insulinomas as it is thought that SRS have a better sensitivity in locating the metastases than the primary tumor. The use of SRS to visualize tumors have also its drawbacks that includes false-positive results of the location of NETs or metastases, occur when radioisotopes accumulates in the accessory spleen, gallbladder and patients with renal cyst. Other conditions are pneumonitis, respiratory infections and cerebrovascular accidents. Furthermore treatment with unlabeled octreotide or the production of Somatostatin by the tumor itself, may lead to lower accumulation of the radioligand in the tumor. This is due to occupancy, competition with or down-regulation of the receptor by unlabeled ligand[310]. The presence of different subtype receptors with different binding efficiency to the radiolabeled ligand have also to be taken into consideration. For instance in insulinoma the expression of more than one receptor subtypes, with different affinities makes the tumor difficult to localize when using radiolabeled octreotides[311,312]. Moreover octreotide binds preferentially to somatostatin receptor subtype 2, found in high quantities in other tumors than most PNETs[313] and therefore the diagnosis of PNETs should not be made by SRS alone. MIBG scintigraphy is another method for visualizing tumors, as the compound is concentrated in neuroendocrine cells. This method has been shown to be excellent in imaging neural crest tumors, such as

phaeochromocytomas and neuroblastomas, however MIBG used for detection of carcinoids and PNETs have also been done. The cellular uptake of ^{123}I-MIBG or ^{131}I-MIBG is mediated by the same mechanism as noradrenalin and therefore do not depend on somatostatin receptor viability. Because of SRS and MIBG have different mechanism for cellular detection; the MIBG is used in the clinic as an alternative for SRS or as a secondary approach[314]. MIBG is thought to have a lower sensitivity compared to SRS, demonstrating overall sensitivity at 50-52%, with a higher detection rate for foregut carcinoids when compared with other sites[315,316].

The use of PET combined with a radiolabeled fluorodeoxyglucose (FDG) is the most widely used method for detecting cancer in general. FDG is an analogue of glucose that is actively taken up and accumulates in cancer because of tumors high rate of glucose uptake compared to normal cells[317]. The current clinical application of ^{18}F-FDG PET imaging is for diagnosis, staging and monitoring recurrence of different types of cancers, including lung, colorectal and lymphoma[318], however to date the ^{18}F-FDG PET has never been used on routine basis for imaging of NETs. Few studies have implicated the use of ^{18}F-FDG PET to imaging NETs, but the sensitivity was low compared to other functional imaging methods[319,320]. This may be due to NETs are generally slow growing tumors and have low metabolic activity, leading to decrease uptake of FDG and thus low sensitivity. Another study also showed the ^{18}F-FDG PET sensitivity in correlation of the Ki67 index; GEP-NETs with a proliferative index that exceeds 15%, tends to show a higher sensitivity (92%) compared with NETs with lower Ki67 index[315], indicating that ^{18}F-FDG PET can be used complementary to other functional imaging methods for poorly differentiated GEP-NETs. The presence of somatostatin receptors on NETs has also been exploited in PNET with the use of ^{68}Ga-DOTA-DPhe[1]Tyr[3]-octreotate (DOTATATE) which is a somatostatin receptor 2 analog. Currently, ^{68}Ga-DOTATATE is replacing traditional SRS, because of its clinical application and higher sensitivity and specificity towards NETs[321,322]. As in case of detecting high grade tumors, the use of ^{18}F-FDG to supplement ^{68}Ga-DOTATATE PET can be beneficial, since high grade tumors may express low amounts of somatostatin receptor, but have high metabolism[323].

Endoscopic approaches, includes endoscopic ultrasonography (EUS) that is a direct way to identify lesions, such as carcinoids in the lung and GI-tract. The method combines endoscopy with ultrasound, which allows high-resolution imaging of structures as small as 3 mm in diameter. EUS is especially used in the clinic to identifying insulinomas and gastrinomas, located mostly in the pancreas, and has an accuracy of nearly 100%[324,325]. These tumors tend not to be easily visualized using CT or MRI and therefore these methods should be used to exclude the possibility of metastases[326,327]. Furthermore EUS is used in the clinic to locate multiple intrapancreatic tumors that are frequently found in MEN1 patients. One of the main advantages with this technic is that it can localize tumors that are very small (≥0.5 cm) and can be used to obtain tissue

biopsies by using fine needle aspiration. The use of tissue sampling alone can therefore help to distinct pancreatic adenocarcinoma from a NETs[328,329]. Even though EUS allows detail visualization of the pancreas and almost all parts of the gastric and duodenal wall, tumors located outside the pancreas (mostly carcinoids and MEN1 associated gastrinomas) are difficult to detect and special endoscopic expertise is necessary to locate very small tumors[306,330].

1.5.9 Diagnosis of functional and non-functional pancreatic neuroendocrine tumors

Insulinomas produces hypoglycemia in the presence of normal or increased Insulin levels. The initial diagnostic approaches for insulinomas are based on the demonstrating Whipple's criteria that are reliable in establish hyperinsulinemia in patients after several hours of fast. The criteria includes that the patient have symptoms of hypoglycemia at the time of low glucose levels, a plasma glucose less than 45–50 mg/dl and relief of symptoms after glucose intake[331]. Thus the purpose of the fast is in relation to the diagnosis of insulinoma is to document hypoglycemia and to associate hypoglycemia with inappropriate Insulin levels and C-peptide concentrations ($\geq$200 pmol/L). C-peptide is a protein that connects Insulin A and B chain together in Proinsulin, when Insulin is made C-peptide is released. The measure of C-peptide is based on the findings that hypoglycemia induced by exogenous Insulin levels fails to suppress C-peptide concentration in insulinoma patients[332]. In other words exogenous Insulin administration in healthy subjects will suppress normal Insulin production in β-cells, leading to low or absent C-peptide concentration, while in insulinoma the C-peptide remains high due to persistent Insulin production from the tumor. Another study showed that the most specific criterion for diagnosis of insulinoma was to combine increased Proinsulin levels, but not Insulin with fasting glucose levels below 45 mg/dl[333].

Patients with classical gastrinoma have symptoms of hypersecretion of gastric acid, these patients are therefore diagnosed using a biochemical testing, demonstrating elevation of fasting serum Gastrin (FSG) (>150 pg/ml) and increased gastric acid secretion. In case of patients that receiving gastric acid suppressive medicine, like H_2-antagonist and PPIs, FSG can be raised and therefore should be discontinued in at least seven days prior to testing[334]. The criteria for raised gastric acid secretion is determined by having a basal acid output over 15 mEq/h or pH of less than two in not operated patients, and basal gastric volume higher than 160 ml/h[335]. Because FSG is also raised in other diseases, such as *Helicobacter pylori* infection, chronic atrophic gastritis, gastric cancers and gastric outlet obstruction[336–339], these have to be excluded before diagnosis of gastrinoma can be made. If FSG or acid secretory studies fail to diagnose patients with a clinical suspicion of gastrinoma, Secretin is injected intravenously or calcium is infused and subsequently FSG is measured. In secretin test, a FSG higher than 100 pg/ml, or 395 pg/ml in calcium test, confirms diagnosis of gastrinoma with presence of ZES. Calcium test is normally preserved as a secondary test in case

of negative secretin test[340,341], although both provocative test shows very high efficiency. By using secretin test 96% of ZES patients are diagnosed with gastrinoma, while 80% with calcium test[342].

In glucagonoma skin lesions are often important for diagnosis, specifically NME which occur in most glucagonoma patients[343]. One problem with presenting symptoms, such as in NME may be that it occurs at some point during clinical illness, but not necessarily at the initial stages of the tumor. This may delay the diagnosis after initial presentation. Therefore the diagnosis of glucagonoma is done by the presence of elevated serum Glucagon levels using IRMA and presence of characteristic clinical features, also histological finding of a NET is important. Normal the immunoreative Glucagon level is <150 pg/ml, but the level in patients with glucagonoma has been found to be in average 1400 pg/ml, however the Glucagon levels can vary, some patients with glucagonoma have been shown to have as low as 84 pg/ml[268]. Because secondary hormones are secreted by glucagonomas these can also be examined, for diagnostic purposes. Histological findings of the tumor itself are usually not important for diagnosis, however positive staining for intracytoplasmic Glucagon and other secondary hormones can be useful for confirmation[344]. As for other functional tumors (except insulinoma) glucagonoma express somatostatin receptors in 80% of the cases, and thus SRS or ^{68}Ga-DOTATAE PET may be helpful in localization of the tumor[345].

The diagnosis of VIPoma requires the presence of watery diarrhoea, elevated fasting VIP levels and the presence of NET. In VIPoma, the watery stool is usually more than three litres per day, if volume less than 700 ml/day is observed under no symptomatic treatment; the diagnosis of VIPoma can be excluded. The stools are characterized by their incohesive structure which remain odourless and tea-colored[346]. This diagnosis approach can be assisted by measurement of fasting plasma VIP levels, which has to be more than 3-10 times above normal[271,347], a different study reports of plasma VIP levels have to be >5 pmol/l for VIPoma to the present[348]. For somatostatinoma diagnosis is established by demonstrating elevated fasting serum Somatostatin and pathological examination. However the test for Somatostatin in serum levels is often ignored, because of unspecific symptoms related to somatostatinoma. Therefore a suspicion for somatostatinoma can be assisted by SRS and FDG-PET imaging to successfully detect and localize the tumor[349,350]. Moreover histological examination of tumor tissue with presence of intense positive immunochemical staining of Somatostatin is important for accurate diagnosis. Somatostatinoma show positive for Synaptophysin and in some cases positive for Insulin, Gastrin, Glucagon and VIP has been found[351,352].

Most NF PNETs (60-85%) are first diagnosed at advance stage of the disease, others are found by coincidence due to patients complaining about unspecific abdominal symptoms, found at surgery or other reasons. Immunohistochemically, NF PNET cannot be differentiated from other functional tumors, due to the fact that most tumors still have immunoreactivity for Insulin, Glucagon, PP and other peptides. Almost

all patients have elevated CgA and therefore serum CgA is measured in these patients, others have also elevated PP or human chorionic gonadotropins (hCG) such as hCGα and hCGβ, which can be used for general diagnosis[353]. At late stages, when tumor mass symptoms are present or metastases, EUS/fine needle aspiration usually carried out for localization and confirming NF PNET[354]. However early detection and diagnosis remains the key to improve prognosis for these patients. The use of EUS for detecting MEN1 associated NF PNETs may have a good use in the clinics, since EUS are able to detect the tumors at diameters 0.4-1.1 cm with high accuracy (55-82%) in asymptotic patients[355,356]. The next section will discuss the treatments available for PNETs as summarized in Table 4, Appendix.

1.5.10   Treatment and management of functional and non-functional tumors

In case of insulinomas are localized in the pancreas, surgical intervention is often considered as the first line of treatment to cure these patients, although other techniques for the management of insulinomas exists, such as treatment with octreotide, embolization, radiofrequency ablation (RFA) and EUS-guided alcohol ablation[357–359]. Depending on the features of the tumor mass, such as the type, size and location, the use of atypical resection (includes enucleation, partial or middle pancreatectomy) is considered as a safe strategy to preserve the pancreas parenchyma and reducing the risk of late exocrine and endocrine insufficiency. The cure rate for benign insulinoma is 75-98% after surgery with a 10 years survival rate of 98%[360]. If tumor localization is unsuccessful at surgery, the following action should be carefully evaluated to be certain of diagnosis and in general not undergo blind resection[361,362]. After tumor resection the Insulin levels are expected to decrease and glucose to be normalized, however if it is not the case or patients made unfit for surgery, a single dose of octreotide daily can be used to relief hypoglycemia[363,364].

In patients with malignant insulinoma, the hypoglycemic event is often more radical and control of hypoglycemia is difficult. Diazoxide is frequently used, combined with octreotide or lanreotide for effective Insulin and Proinsulin suppression. During later stages of the disease increasing dosages may be needed. Other medical treatment considered is beta-blockers and diphenylhydantoin to decrease Insulin levels[365,366]. Different therapies have been used for managing sporadic malignant insulinoma, including aggressive surgical resection such as and liver and extended pancreatic resection, chemoembolization, liver transplantation or RFA of the liver in attempted to improve patients survival[367–369], however the prognosis of these patients is still relatively poor. Furthermore malignant insulinoma has been shown to respond poorly to conventional chemotherapy. The mean survival period for malignant insulinoma is two years[252].

While insulinoma appear to be more curable by surgery, gastrinomas can be harder to intercept especially because most of them that occur in the duodenum are small. If the gastrinoma can be removed by surgery, the patients should undergo surgical exploration to locate lesions. However the surgical approach used to

detect these tumors is controversial. It is therefore recommended that combination of extensive palpitation of all suspected areas, intraoperative ultrasound, endoscopic transillumination and duodenotomy should be included before resection can occur. The latter is shown to be essential for discovering duodenal gastrinomas as they are frequently small and not always detected by other intraoperative localization methods[370,371]. Prior to surgery the syndrome has to be controlled in order to avoid complications. Currently medical treatment with H$_2$-receptor antagonists and PPIs is used to control gastric acid hypersecretion in patients, whereas total gastrectomy or antisecretory surgery is only rarely required[372,373]. After surgical resection it is recommended to follow-up on patients with at least two FSG and secretin tests, before antisecretory drugs are restarted. The best approach to determine if surgery has been successful and to insure no recurrence is to make FSG and secretin test, three and six months postoperatively and yearly thereafter[374]. In patients with gastrinoma associated MEN1 or malignant sporadic gastrinomas, with no opportunity of surgical resection, octreotide is the treatment of choice to prolong survival, mainly because of its low side effects compared to conventional chemotherapy[375].

Medical management of tumor syndromes in glucagonoma, VIPoma and somatostatinoma are directed in controlling the syndrome before actual treatment is considered. The ideal and curable treatment for glucagonoma is by surgical resection of the tumor before metastases can occur, however at time of diagnosis most glucagonomas express malignant behavior and therefore cannot be removed completely[263]. Nevertheless incomplete resection of the tumor should be considered, as tumors are slow growing and debulking will lead to reduced plasma Glucagon levels and rapid alleviate clinical manifestation. Furthermore blood transfusion, parenteral amino acids and administration of zinc with somatostatin-analogs can relieve anemia, hypo-aminoacidemia and NME in some patients[268,269]. Another study report of parenteral amino acids and fatty acids to be ineffective against NME[376]. Anti-coagulants, such as warfarin or heparin is commonly need for prevent deep venous thromboembolic events and mild glucose intolerance, which often precedes NME, is managed with the use of hypoglycemic agents and Insulin after an oral glucose tolerance test. However after surgical intervention most patients have markedly improved glucose intolerance, and neurological manifestations after surgical treatment are often insignificant, weight gain in patients are also to be observed[377,378]. These patients Glucagon levels should be regularly monitored and any sustain increase should be result in instant reinvestigation. Several chemotherapeutic drugs have been used to improve syndrome condition, including streptozotocin and fluorouracil, however these have only been proven efficient in some patients with glucagonoma[270,379]. Dacarbazine has also been considered in glucagonomas as it showed promising results by improving the syndrome[380], but somatostatin-analogs is still considered as the drug of choice. New biological treatments to increase survival rate of patients such as sunitinib, bevacizumab (angiogenesis inhibitors) and everolimus (mTOR inhibitor), have been investigated for glucagonoma, but also other functional tumors[381–383]. Despite the high rate of malignancy and presence

of metastases, the 10 year survival rate for glucagonoma is 51.6% with- and 64.3% without metastases, which is considerably lower than patients with gastrinoma[266].

In VIPoma, the patient needs to be corrected for their metabolic abnormalities, before the treatment with somatostatin-analogs may be used. VIPoma patients are initially treated for correction of electrolyte and volume derangements, which requires intensive intravenous supplement of fluid and careful correction of acid-base and electrolyte abnormalities[384]. However in some cases the diarrhea can be very difficult to control, and therefore octreotide is administrated to reduce tumoral VIP secretion and control the secretory diarrhea[385,386]. Somatostatin-analogs are commonly used in patients to control symptoms and stabilize the patient before surgery. Because about 50% of the tumors are indolent in nature, patients with VIPoma have good prospection for a possible cure if the diagnosis is made early. In patients with VIPoma accompanied by liver metastases, lobectomy (lobe removal) of the liver is available, otherwise patients with local lesions, embolization therapy of the hepatic artery or liver transplantation is an option. Embolization is also used in patients with intense symptoms that attain no benefits in surgical or medical remission of symptoms[387,388]. For patients that cannot benefit from surgery due to the advanced disease stage, prolonged treatment with the chemotherapeutic agents streptozocin and doxorubicin or sunitinib showed to reduce tumor bulk and increase survival of these patients[389,390].

Treatment options for somatostatinomas are often surgical resection, depending on the stage and location of the tumor. Because most pancreatic somatostatinoma are located in the head of the pancreas, pancreaticoduodenectomy (Whipple procedure) is the treatment of choice. Today Whipple procedure involves resection of the lymph nodes, beside resection of pancreas head, duodenum, bile duct and gallbladder[391]. Tumor located in the body or tail of the pancreas, left-sided pancreas resection is often considered. In duodenal somatostatinomas, tumors located in the ampulla are removed by papillectomy or the Whipple procedure, while tumors located at the duodenum, duodenectomy is used[392]. At surgery most somatostatinomas have already metastasized to the liver and lymph nodes, therefore tumor debulking, octreotide treatment, chemotherapy and chemoembolization of the primary tumor and/or hepatic metastases can be used to control the clinical symptoms[349,351]. Patients without metastatic disease the mean 5 year survival rate is 100 or 60% if metastases are present[278].

As for other functional PNETs, surgical resection of NF PNETs is the treatment of choice, although there is considerable debate about the procedures. In recent years, the number of incidentally discovered NF PET has increased due to the fact that a more widespread use of cross-sectional imaging techniques. Given that the earlier detected tumors are small (≤ 2 cm), most tumors are possibly benign or intermediate-risk tumors and therefore can be surgically removed[393]. The treatment of choice for small NF PET has been standard pancreatic resection, however this type of surgery are often associated with high risk of post-operative

complications. Therefore Parenchyma-preserving resections have been proposed for management of small NF PET, which have the advantage of lowering the risk of endocrine and exocrine sufficiency[394]. Larger tumors (>2 cm) are often in the advanced disease stage and metastases can be present; therefore more aggressive resection is needed. Furthermore treatment with somatostatin-analogs have shown to be effective if the SRS scan is positive and if there is evidence of tumor progression or high Ki67 index[395].

Because most GEP-NETs express somatostatin receptors and can be treated with radiolabeled somatostatin-analogs; the use of peptide receptor radionuclide therapy (PRRT) with radiolabeled somatostatin-analogues plays an increasing role in treatment of patients with an inoperable or metastasized GEP-NET[396,397]. Next generation somatostatin-analogs used for PRRT are currently on phase trial, but they have shown to be effective in increasing the survival of patients. These analogs consist of modified somatostatin-analog, Tyr^3-octreotide and a different chelator, DOTA instead of DTPA with gives a more stable binding to the β-emitting radionuclide ^{90}Yttrium (^{90}Y). Recently, long-term treatment with ^{90}Y-DOTA-Tyr3-octreotide or ^{90}Y-DOTA-TOC has been reported to increase the overall survival in NET patients were high tumoral uptake on SRS was associated with longer median survival, such as in NF PNETs and small intestine carcinoids where median survival were about 60 and 55 months, respectively[398]. Another recent study uses ^{177}Lu-DOTA-TOC for treatment against advanced small intestine carcinoids in a small group of patients with an overall survival of 61 months, however the partial response was low, about 13%[399]. Interestingly, experiments in rats suggested that the anti-tumoral effect of ^{90}Y-DOTA-TOC is better in larger tumors, and ^{177}Lu-DOTA-TOC better in smaller tumors, whereas a combination showed to give the most effective response[400].

1.6   Notch and miRNA in neuroendocrine tumors

1.6.1   Notch signaling pathway in neuroendocrine tumors and other tumors

In addition to Notch roles during tissue development is Notch also a contributory factor to development of many cancers. The first link between Notch signaling and cancer was found in patients with T-cell lymphoblastic leukemia (T-ALL), where a chromosomal translocation was identified. This translocation resulted in constitutive expression of Notch through a truncated Notch1 receptor[401]. Subsequently, it was shown that most cases of constitutive expression of Notch were caused by *Notch* mutation in the PEST and HD domains, leading to constitutive activation and prolonged half-life of the NICD respectively[402,403]. These observation lead to the identification that several human cancers had increased expression of Notch receptors and their ligands, including colorectal cancer, pancreatic adenocarcinoma, renal cell carcinoma, prostate cancer and breast cancer[404–406]. Interestingly, in both renal and breast cancers the expression of Notch components is associated with poor prognosis[407,408]. Although it appears that Notch have oncogenic and growth promoting roles, the results are more complex in tumorigenesis, as Notch is also involved in tumor suppression in some types of cancers. The first clues came from studies in the skin where loss of *Notch1* leads to the development of spontaneous basal cell carcinoma[409]. In mice Notch1 activation is thought to induce differentiation of keratinocytes, accompanied by cell cycle arrest through expression of the cell cycle regulator p21$^{\text{WAF1/Cip1}}$ [410,411]. Notch involvement in cell cycle arrest has also been studied in other cancers. In the neuroendocrine phenotypic small cell lung cancer (SCLC), Notch receptors are rarely expressed and overexpression of *Notch1* lead to cell cycle arrest, involving Notch mediated induction of the cyclin-dependent inhibitors p21$^{\text{WAF1/Cip1}}$ and p27$^{\text{kip1}}$ [412]. A similar result is found in lung human adenocarcinoma cell lines where overexpression of the activated Notch1 induces growth inhibition and cell cycle arrest[413]. In contrast to SCLC, Notch1 is highly expressed in pancreatic cancer and prevents cell cycle arrest by down-regulating p21$^{\text{WAF1/Cip1}}$ and p27$^{\text{kip1}}$.

Several components of Notch has been identified to be frequently overexpressed in colorectal cancer *in vivo* compared to the normal expression in crypt cells, including *Notch1*, *Jagged1/2* and *Hes1* [414]. Interestingly, mice heterozygote for loss of *Apc* allele combined with NICD overexpression displayed earlier tumor appearances with additional tumors and worse survival compared to the mice carried only mutant *Apc*[415], suggesting that aberrant Notch activation have a strong impact on the initial phases of tumor development by inducing hyperplastic conditions in these cells. Conversely, when *Hes1* is lost in mice carried mutant *Apc*, the proliferation was reduced and increased differentiation of secretory cells was displayed in tumor regions[131] suggesting that Hes1 is important in maintaining the high proliferative state in these tumors. In fact Hes1 expression is directly regulated by Notch and Wnt/β-catenin signaling in colorectal cancer[416],

which explains why the loss of Hes1 leads to decrease proliferation in *Apc* mutant mice. Interestingly, *Jagged1* expression seems to be induced in colorectal cancer as a result of increased nuclear β-catenin, while Jagged1 is dispensable for homeostasis of normal crypt cells of the small intestine[417], suggesting Jagged1 to be a tumor specific therapeutic target.

The transforming ability of Notch may be mediated through activation of Ras signaling pathways[418]. Results from breast cancer cell lines with oncogenic *Ras* demonstrate that increased expression in Notch help drive transformation and tumorigenesis of these cells[419], suggesting that Ras and Notch may act together to induce transformation in breast cancer. Another study, suggest that simultaneous activation of Ras and Hedgehog drives transformation and early tumorigenesis in pancreatic cancers with Notch as a downstream contributing factor[420]. Notch implication in tumor development has also been suggested to crosstalk with other pathways, including the TGFβ signaling pathway. Beside the role in gut endoderm development, TGFβ plays an important role in controlling tumor development, which is in most cases by exerting a tumor suppressive role through Smad-dependent transcription of genes, important for cell cycle arrest. Smad proteins exert their activity through p300 binding[421]. Deregulation of Notch1 in tumors is thought to repress TGFβ signaling by expression of c-Myc, which have shown to rend epithelial cells resistant to growth inhibitory signals[422] or the NICD directly binds to p300 to prevent smads-p300 interaction[423].

Moreover, activation of Notch in tumors has also found to exert anti-apoptotic effect. Treatment with γ-secretase inhibitor or using siRNA to inhibit Notch1 expression in pancreatic cancer showed to induce apoptosis by decreasing the expression of anti-apoptotic proteins, Bcl-2 and Bcl-xL through the interaction with NF-κB[406], suggesting that high Notch expression in pancreatic cancer prevent apoptosis by maintaining the expression of Bcl-2 proteins. The Notch-dependent activation of Bcl-2 proteins is thought to be at least partly mediated through the activation of the canonical pathway involving RBP-Jκ[424]. Another pathway that was linked to the anti-apoptotic effect of Notch1 is the PI3K-PKB/Akt pathway[425]. In the context of NF-κB pathway, a positive feedback loop involving Jagged1-mediated activation of NF-κB and NF-κB induced transcription of Jagged1[426,427] may further enhance the protective role of Notch in tumors.

The role of Notch in NETs appears to be acting as a tumor suppressor by inhibiting growth and inducing apoptosis, rather than promoting growth of these tumors. Recent studies demonstrate that Notch1 signaling is minimal or absent in most NETs. In human carcinoid cell line BON1, Notch isoforms are only vaguely expressed, and overexpression of Notch1 resulted in suppression of growth and dramatically reduction of endocrine differentiation markers (CgA, Serotonin Synaptophysin) and secretory granules. The growth inhibitory effect appears to be related to Hes1 dependent reduce of achaete-scute homologue-1 (hASCL1) expression[428,429]. hASCL1 or Mash1 belongs to the bHLH transcription factor family and has been found to play a pivotal role in the development and differentiation of pulmonary neuroendocrine cells in the lung[430],

but have not been analyzed in great detail in gut endocrine cell differentiation. Nevertheless, high levels of hASCL1 have been reported in different types of NETs, including medullary thyroid cancer, carcinoids and NE-related cancers, such as SCLC and prostate cancer, but hASCL1 is not present in non-NE tumors, such as papillary thyroid cancer[431–433]. Constitutive expression of hASCL1 have shown to promote airway epithelial dysplasia in transgenic mice [434] and depletion of hASCL1 in SCLC cell line by antisense oligonucleotide resulted in decrease expression of NE markers[430], further suggest that hASCL1 is important for tumorigenesis, but also in maintaining tumor NE differentiation in lung. The mechanism that underline the growth inhibitory effect, was demonstrated using a histone deacetylase inhibitor called valproic acid (VPA) as Notch activator. VPA treatment of H727 and BON1 carcinoid cell lines showed a reduce growth and change in NE phenotype by repressing hASCL1 transcription and inducing $p21^{WAF1/Cip1}$ [435]. In a different study, VPA treatment showed to inhibit cell growth in medullary thyroid cancer cells by increase active caspase3 and caspase9[436], however the involvement of hASCL1 in inducing apoptosis remains to be determined.

Other studies demonstrate hASCL1 activation induce endocrine differentiation markers, but also repressing putative tumor suppressors. Inhibition of hASCL1 transcription levels by using siRNA show to increase *DKK1* in BON1 cell line[437], suggesting high *hASCL1* expression in tumors escape proliferation inhibition by down-regulating *DKK1*. Regulation of *DKK1* expression is mediated by histone deacetylation and repressive lysine 27 trimethylation in the promoter region of *DKK1*. Similar result was found in SCLC where the protein is found to inactivate *DKK1* and *DKK3*, and down-regulation of other proteins related to cell adhesion, such as E-cadherin and integrin β1[438]. This is supported by the observation that Notch1 is completely absent in highly proliferative PNETs, but not in all of the benign types[439]. The use of hASCL1 as a marker for poorly differentiated NETs has also been proposed as these tumors have significantly higher hASCL1 expression, than carcinoids or adenocarcinomas. However hASCL1 was not associated with an decrease in survival in these tumors[440,441]. Taken together these results suggest that constitutive expression of hASCL1 due to absent Notch signaling is important for maintaining growth and differential phenotype of NETs. On the other hand exogenous Notch activation down-regulates NE markers and represses growth of these tumors, by decreasing hASCL1. The mechanism hASCL1 represses growth may occur by down-regulating *p21^{WAF1/Cip1}* and *DKK1/DKK3* expression. Other genes, such as *E-cadherin* and *integrin β1*, important for cell adhesion are also been down-regulated.

1.6.2 MicroRNA linked to the pathology in neuroendocrine tumors

In general, malignant transformation of cells is caused by the accumulation of genomic alternations which inactivate tumor suppressors and activate proto-oncogenes[442]. Because miRNAs targets mRNA and negatively regulate their stability and translational efficiency it is not surprising that miRNA is dysregulated in a many forms of cancers. Examination of tumor-specific miRNA expression profiles has revealed that indeed it is the case, that miRNAs are found differentially expressed in cancers, such as B cell chronic lymphocytic leukemia, breast cancers and prostate cancer[443–445]. The first clues that these molecules play a role in cancer pathogenesis came from model systems such as *Caenorhabditis elegans* and *D. melanogaster* were miRNAs demonstrate a contribution to the regulation of differentiation, proliferation and apoptosis[446–448]. Increase understanding of the causative role of specific miRNAs in tumorigenesis; suggest that miRNA contains either tumor suppressor or oncogene functions. Examples of miRNA that have tumor suppressor activity are miR-143 and let-7. miR-143 is down-regulated in colorectal cancer and increased expression of miR-143 showed to inhibit growth in these tumors[449,450]. Similarly, diminished levels of let-7 cause tumor cells in breast cancer to maintain proliferation and inhibit differentiation, while forced let-7 expression interferes with both tumor initiation and tumor self-renewal[451].

In contrast to other tumor types, the information regarding miRNA expression pattern in GEP-NETs is limited. Nevertheless relative recent studies provide evidence that miRNA is dysregulated in carcinoids and PNETs. One study identified five miRNAs to be down-regulated in metastatic compared to primary ileal carcinoids. The most significant down-regulated miRNA in that study was miR-133a, where the decreasing levels of miR-133a was associated with development and progression from primary to metastatic ileal carcinoid tumors[452]. Another study showed using Affymetrix miRNA array that nine miRNA were significantly dysregulated in well-differentiated small intestinal carcinoids; where five (miR-96, miR-182, miR-183, miR-196a-5p and miR-200a) were upregulated during tumor progression, while four (miR-31, miR-129-5p, miR-133a and miR-215) were significantly down-regulated[453]. A small profile study of a single case of colonic carcinoid by using Illumina sequencing technology demonstrated a total of 38 miRNAs were significantly dysregulated compared to normal mucosa[454], including miR-7-5p as one of the most upregulated.

As for carcinoids, several studies have tried to elucidate the miRNA profile in PNETs. A comparison study between the expression profile of PNETs and normal human islet samples identified miR-142-3p, miR-142-5p, miR-155, miR-146a and miR-483 as upregulated. The latter miRNA was suggested to be important for the hyperproliferative stage during tumorigenesis, but not in metastases progression[455]. Another study investigated the circulating miRNA serum profile on a relative large cohort of patients with pancreatic adenocarcinoma, PNETs, chronic pancreatitis and healthy control subjects. The results showed that

preferable miR-1290 was down-regulated in sera and had the highest diagnostic performance in discriminating PNETs from adenocarcinoma. Other significantly down-regulated miRs in sera of PNETs patients were miR-584, miR-1285, miR-550 and miR-1825[456].

A larger study investigated the global miRNA expression pattern in PNETs, pancreatic acinar carcinoma and normal pancreas using class comparison analysis. The analysis identified several miRNAs to be differentially expressed; 87 and eight miRNAs were upregulated and down-regulated respectively in PNETs, when compared to normal pancreas. Moreover only 10 miRNAs (miR-125a, miR-99a, miR-99b, miR-125b-1, miR-342, miR-130a, miR-100, miR-132, miR-129-2 and miR-125b-2) were differentially expressed (upregulated) between PNETs and pancreatic acinar carcinomas, suggesting that these miRNAs may be important for pancreatic endocrine differentiation or endocrine tumorigenesis. Among the PNETs, miR-21 overexpression was associated with high proliferation index and the presence of liver metastasis, miR-204 showed to be specific for well-differentiated insulinomas[457].

1.6.3   MicroRNA-375 and microRNA-7-5p

MiR-375 was first discovered in mouse pancreas and is believed to be an islet-specific target and influence endocrine maintenance. The inhibition of endogenous miR-375 expression by siRNA target of miR-375 decrease Insulin secretion of endocrine cells in response to glucose stimulus. Similarly, overexpression of miR-375 decreased Insulin secretion, demonstrating miR-375 has to be fine balanced in order to maintain Insulin homeostasis[458]. Several human cancers such as gastric, liver, carcinoma it appears that miR-375 is frequently down-regulated, and forced miR-375 expression has growth suppressive effect on these tumors. In gastric carcinomas, miR-375 overexpression significantly inhibited proliferation in gastric carcinoma cell lines, but also suppressed xenograft tumor formation *in vivo*, apparently through target mediated repression of JAK2[459]. miR-375 inhibits cell invasion and also proliferation in hepatocellular carcinoma cell lines[460]. In contrast, *in vitro* studies of lung tumors that exhibit characteristically neuroendocrine features and *in vivo* studies of insulinoma and NF PNET have shown to have miR-375 upregulated[457]. The miR-375 promoter is known to contain conserved E-boxes, which are binding sites for transcription factors, including the bHLH family proteins[461]. For instance, chromatin immunoprecipitation experiments have shown that NeuroD interacts with conserved sequences both upstream and downstream the miR-375 promoter in the pancreas[462]. Therefore it is not surprising that miR-375 promoter has been identified as a target of hASCL; co-transfection of luciferase reporter construct containing a highly conserved miR-375 promoter and hASCL expressing vector showed a marked transactivation of the reporter by hASCL[463,464]. The same study also revealed that increase expression of miR-375 by pre-miR-375 transfection also lead to gradual induction of

NE-related genes, suggesting that miR-375 independently induce NE phenotype. These results are in good agreement with hASCL role in regulating lung neuroendocrine cell differentiation[430].

miR-7-5p is also expressed in the endocrine pancreas[465], as well as in several types of cancers. miR-7-5p is thought to play a role in β-cell differentiation, as inhibition of miR-7-5p in developing mouse pancreas, resulted in reduction of the Insulin content in the pancreas and lower number of Insulin-producing cells[466]. In colorectal cancer, miR-7-5p is found to be down-regulated and when ectopically expressed, it exerts tumor suppressor activity possibly by direct targeting the oncogenic protein YY1[467] and Pax6[468]. Deregulation of *YY1* and *Pax6* expression has been reported in several other types of cancers, including breast and prostate cancer[468–470]. In contrast miRNA profiling revealed that miR-7-5p is overexpressed in SCLC when compared to normal lung tissue[471]. The role of miR-7-5p in other NETs is currently unknown.

2 Aim of the thesis

The aim of this thesis was:

1. To characterize differences in miRNA expression between GEP-NETs and the surrounding normal tissue.
2. From this list of differentially expressed miRNA choose one or two miRNAs that previously had been associated with endocrine cell biology and
   a. Validate the expression pattern
   b. Characterize cellular expression by *in situ* hybridization
   c. Examine how they affect the growth of carcinoid cell lines *in vitro* by using xCELLigence system
   d. Identify which pathways are regulated by the miRNAs
   e. Identify and validate potential target mRNA

The following chapters will concern my scientific work while being at the Department of Centre for Genomic Medicine. A full description of the methods I have used for my experiments is found in the section methods, followed the results, discussion and conclusion of my experiments.

3 Methods

In this section there is a short introduction to the methods used, followed by a description of the materials, chemicals, instruments and software used to conduct the various experiments. The experiments were conducted to examine the possible effect of miR-375 and miR-7-5p on endocrine cell differentiation in tumors and addressing their presence in normal and tumors tissue.

3.1 Affymetrix-array

The miRNA microarray profiling was performed using Affymetrix GeneChip 4.0 miRNA Array (Affymetrix, Santa Clara, USA) according to manufactures instruction. Briefly, 1 μg of total RNA was labeled by polyA polymerase followed by ligation of the biotinylated signal molecule to the target RNA sample using the Genisphere FlashTag HSR Kit (Genisphere, Hatfield, PA). The polyA tail reaction at the 3'end is necessary for proper ligation of the biotinylated signal molecule. The high sensitivity of FlashTag HSR Kit is due to a branched structure of single and double stranded DNA called 3DNA® dendrimer, which is conjugated with biotin. To confirm that the FlashTag HSR Kit has performed appropriately, the Enzyme-linked oligosorbent assay (ELOSA) was performed, through the hybridization of biotin-labeled RNA Spike control oligos to complementary ELOSA spotting oligos. After FlashTag ligation, the respective miRNAs were hybridized to the Affymetrix miRNA array at 48 °C as recommended. Standard Affymetrix array cassette washing, staining and scanning was performed using Post-Hybridization Kit (Cat no. 900720) and GeneChip Scanner 3000. Staining was done using Streptavidin conjugated with Phycoerythrin to detect biotin labeled RNA after washing steps (Figure 24, Appendix). The results were extracted using the Affymetrix Command Console Software and raw data was analyzed in Qlucore Omics Explore v. 3.1. The data were normalized by using the qspline method[472] and two group comparison t-test was done.

3.2 Cell lines

Using cell line model systems for NETs poses several challenges, mostly because the number of cell lines is limited and it is often difficult to get access to them[215]. I therefore ended up using two cell lines: NCI-H727 and CNDT2 which are described below. NCI-H727 is a human lung carcinoid cell line, derived from a 65 years old Caucasian female and is the best differentiated available bronchial carcinoid cell line. The expression of Notch is minimal in this cell line, but high expression of hASCL1 is found[428,432]. NCI-H727 express easily detectable levels of p53 mRNA compared to normal lung and is able to secrete parathyroid hormone-like protein, which is calcium-stimulated through a protein-kinase C pathway[473]. Furthermore, cells are able to synthesize neuromedin B, but not the Gastrin-releasing peptide[474]. The NCI-H727 is also found to express EGF receptors, since cell growth is inhibited by EGF monoclonal antibodies. As for several

other types of cancers, the PI3K-PKB/Akt signaling pathway is found upregulated in NCI-H727, promoting growth, survival and chemotherapy resistance[475]. CNDT2 is a human midgut carcinoid cell line that was first isolated from a liver metastasis, of a patient with primary ileal carcinoid. However, it is still on debate if the cell line is of neuroendocrine origin, since the short tandem repeat genotype data of CNDT2 were unable to match the carcinoid tumor tissue and loss of hASCL1 gene expression, which is usually expressed in all NET cell lines[476]. Furthermore the presence of neuroendocrine secretory granules showed not to contain the CgA, even though NSE and Synaptophysin are found in this cell line[477,478]. CNDT2 showed also to express various tyrosine-kinase receptors and somatostatin receptors, which is normally found in malignant midgut carcinoids *in vivo*[479].

The human pulmonary carcinoid cell line NCI-H727 cells were cultured in RPMI 1640 Glutamax (Life Technologies) containing 10% FBP, 100 U/ml Penicillin (Life Technologies) and 100 µg/ml Streptomycin (Life Technologies), 1 mM Sodium Pyruvate (Life Technologies) and kept at 37 °C in 10% CO_2. CNDT2 was a kind gift from Lee Ellis, the cells were maintained in DMEM/F12 including 15 mM HEPES supplemented with 10% FBS, 100 U/ml Penicillin (Life Technologies) and 100µg/ml Streptomycin (Life Technologies), 1 mM Sodium Pyruvate (Life Technologies), 1x MEM NEAA, 2 mM L-Glutamine, 1x MEM Vitamins Solution, 10 nM NGF and kept at 37 °C in 5% CO_2.

3.3 RNA extraction

Total RNA was extracted using TRIzol® Reagent (Cat. no. 15596-026, Life Technologies) according to the manufactures specifications. Importantly, the extraction was performed on ice during all steps to minimize RNA degradation. In brief, samples were first homogenized at room temperature (RT) using Trizol reagent and the aqueous phase (containing the RNA) was removed and put into a new tube. After the phase separation step RNA was precipitated using Isopropanol, centrifuged and supernatant was removed. Then the pellet was briefly washed with 70% Ethanol and centrifuged at 7500 rpm for five minutes. Supernatant is removed again and pellet containing RNA is dried and then suspended in RNase-free water. The RNA concentration was measured on the Nanodrop (Thermo Scientific, WI, USA) and the integrity determined using the Agilent 2100 Bioanalyzer (Agilent Technologies, Santa Clara, CA). RNA was stored in -80 °C until use.

3.4 TaqMan microRNA assay

3.4.1 Complementary DNA synthesis

Reverse transcription reactions are performed using the TaqMan® MicroRNA Reverse Transcription Kit (Cat. no. 4366596, Applied Biosystems). All subsequently steps were performed on ice. For primers I used

hsa-miR-375 (Part no. 4373027), hsa-miR-7-5p (Part no. 4395425), hsa-miR-191 (Part no. 4395410), RNU44 (Part no. 4373384) and RNU48 (Part no. 4373383), a multiplex reverse transcriptase reaction was performed with up to five primers in one reaction using 1 µl of each primer, 100 ng of RNA and a respectively lesser volume of water. The protocol was as follows; 0.15 µl 100 mM dNTPs (with dTTP), 1 µl 50 U/µl MultiScribe Reverse Transcriptase, 1.5 µl 10x Reverse Transcription Buffer, 0.19 µl 20 U/µl RNase Inhibitor, 4.16 µl Nuclease-Free Water, 3 µl 5x Primer and 5 µl RNA sample, adding to a total of 15 µl per reaction. The reverse transcription reaction was run on a Thermocycler (Eppendorf, Hamburg, Germany) with one cycle for 30 min at 16 ^{o}C, 30 min at 42 ^{o}C and 5 min at 85 ^{o}C. TaqMan® MicroRNA Reverse Transcription is described in Figure 25, Appendix.

3.4.2   Quantitative PCR amplification

The PCR application, quantitative PCR (qPCR) is method used to identify initial concentrations of DNA or cDNA template. Although there are different forms of strategies in doing so, I used TaqMan assay to quantify the cDNA in the samples. It relies on specific hybridization probes and is simple, reliable and direct method to detect fluorescence in real-time as the PCR proceeds. The probes consist of an oligonucleotide labeled with fluorescent reporter at one end of the molecule (5'end) and quencher at the other end (3'end). During PCR, the oligonucleotide probe binds specifically to the complimentary sequence in the annealing step, between the forward and reverse primer. When the probe is intact, the proximity of the reporter to the quencher, results in suppression of reporter fluorescence signal. As the *Taq* polymerase extent from the primer in the direction of the probe, its 5'exonuclease activity degrades the hybridization probe, thus releases the reporter from the quencher, increasing the fluorescence signal (Figure 26, Appendix). The increase fluorescence signal happens only if the target sequence is complimentary to the probe and increases in direct proportion to the number of starting molecules.

The reverse transcription reaction product was diluted a minimum of 1:15 and a master mix was prepared using the TaqMan universal PCR Master Mix, No AmpErase UNG (Cat. no. 4324020, Applied Biosystems). The general protocol is as follows, 1 µl 20x Primer, 10 µl 2x TaqMan Universal PCR Master Mix, 7.67 µl Nuclease-Free Water and 1.33 µl cDNA of a total of 20 µl per reaction with three PCR replicates per reverse transcriptase reaction. The miRNA expression was assessed using ABI PRISM 7900 HT Sequence Detection System (Applied Biosystems, Carlsbad, CA) with 40 cycles of amplification.

The fluorescent signal accumulated during positive qPCR reaction is expressed by a cycle threshold (Ct) value. This value is defined as the number of cycles required for the fluorescent signal cross a given threshold, thus it is a relative measure of the concentration of target in the PCR reaction. The threshold is defined by the background fluorescence and its value is set to exceed background levels. Furthermore the Ct

value is inversely proportional to the amount of nucleic acid in the sample; thus low Ct value at ≤29 indicate a strong positive reaction of abundant target nucleic acid, while a Ct value of 30-37 and 38-40 represent a positive and 'weak positive' reaction, respectively. Data used in determination of hsa-miR-375 and hsa-miR-7-5p expression were normalized using two reference miRNAs; RNU44 and RNU48 (Life Technologies) to determine the expression in different cell lines (Figure 18), and RNU44 and miR-191 were used in Laser capture microdissection (LCM) (Figure 16 and Figure 17). Relative expression was calculated using the 2^{-dCt} equation.

3.5 Cell line transfection

For NCI-H727 and CNDT2, 1.000.000 cells/ml and 500.000 cells/ml were seeded in 6 cm petri dishes, one for each transfection, respectively. For each petri dish, 282.5 µl Opti-MEM (Life Technologies) with 5 µl 25 µM precursor hsa-miR-375, hsa-miR-7-5p (Cat. no. AM17100, Ambion) or All-stars negative control siRNA (Cat. no. SI03650318, Qiagen) is added, giving a final concentration of 50 nM in 3 ml, and vortexed. Then 10 µl Turbofect Transfection Reagent (Cat. no. R0531, Life Technologies) was added, vortexed and left to incubate for 20 minutes at RT. In the meantime 2.5 ml of fresh complete medium was added to each petri dish and the transfection mix is added drop-wise to cells, followed by mixing the complete medium with transfection mix by carefully tipping the petri dishes. For growth analysis, cells were harvested 24 hours after transfection and 40.000 NCI-H727 or 15.000 CNDT2 cells were seeded to each well of the 16 well E-plate in triplicates. Proliferation was measured by xCELLigence RTCA System (Roche). For western blot analysis, plates are harvested after 6, 24, 48 and 72 hours, after transfection with hsa-miR-375 LNA Inhibitor (Product no. 410232-00, Exiqon), hsa-miR-7-5p LNA Inhibitor (Product no. 4101452-00, Exiqon) or siGLO (Cat. no. D-001600-01-20, Thermo Scientific Dharmacon). This was done in duplicates. For protein purification and RNA-isolation, using RNA/DNA/Protein Purification Kit (Cat no. 24000, Norgen Biotek) by following manufactures instructions.

Notably, Turbofect or Lipofectamine 2000 transfection reagents are liposomes, which are synthetic analogues of the phospholipid bilayer. These cationic lipids are amphiphilic molecules that have a positive charged polar head group linked to an apolar hydrophobic domain, generally comprising by two alkyl chains. The electrostatic interactions between the positive charges of the cationic head groups and the negative charged phosphates of the RNA/DNA backbone are the main forces that allow RNA/DNA to spontaneous associate with the cationic lipids[480]. Thus in the presence of free RNA or DNA under aqueous conditions, the lipids encapsulate the nucleic acids to create a spheroid liposome. The lipid-mediated gene delivery or lipofection are based on the similarity in structure of the liposome and the phospholipid bilayer of the membrane. Under specific conditions, the complex containing liposome and nucleic acids emerges with the cell membrane and taken up by endocytosis and subsequently the nucleic acid is released into the

cytoplasm. Although Lipofectamine 2000 is considered to be toxic at high concentrations, I have obtain successfully transfection of HEK293, using lower amount of the reagent (see section 3.10) than the recommended amount in manufacture protocol. However the transfection efficiency was not assessed directly by using a reporter vector or siRNA as in Turbofect (Figure 19).

3.6   Western blot

Samples were run in 2 x SDS PAGE Loading Buffer (100 mM Tris-HCl pH 6.8, 4% w/v SDS, 0.2% w/v Bromophenol Blue, 20% w/v Glycerol and 200 mM DTT). After transfection, lysed cells were loaded on a 4-20% PAGE® Duramide^{TM} Precast Gel (Cambrex, Denmark). Proteins were transferred, using iBlot® Gel Transfer Stacks Mini (8 cm x 8 cm) with a pre-activated PVDF transfer membrane. Each Transfer Stack contains a copper coated electrode with appropriate amount of cathode or anode buffers. Blotting was performed using the iBlot™ Gel Transfer Device (Cat no. IB1001), by first placing the pre-run gel on the PVDF Anode Stack, then a pre-soaked iBlot™ Filter Paper was placed on the gel and finally the cathode stack on top. The transfer is carried out for 7 minutes at 20 Volts current, according to manufacture instructions. Membrane containing transferred proteins from the gel was blocked in PBS with 3% Skimmed Non-Fat milk Powder (Cat no 1.15363.0500, Merck) with agitation for 1.5 hours, followed by washing with washing buffer (400 ml of 50 mM Tris-HCl pH 9.0, 500 mM NaCl, 0.1%   5x Tween 20 (Cat. no. LAB98620.5000, Bie & Berntsen) for a total of 30 minutes (changing washing buffer every five minutes). After washing steps the membrane is now ready to incubate in blocking buffer containing primary antibodies. The membrane was incubation overnight with agitation at 4 °C. The following day blocking buffer containing primary antibodies was collected and incubated in -20 °C for next use. Membrane is washed in washing buffer as mentioned above, and incubated with blocking buffer containing secondary antibodies for one hour at RT with agitation. Then membrane was washed again and Supersignal Substrate (Product no. 34080, Pierce) was added drop wise on the membrane, followed by two minutes incubation at RT. The luminescent signal present on the membrane was captured by a Fuji Film Las1000 Luminescent Image Analyser Model LAS1000plus IDX2 using the Image Reader LAS1000 Pro v.2.5 was used to visualize luminescent signal present on the membrane. The Image Gauge v.4.0 Software was used quantify the bands and display the results. The area from the measured region was subtracted from the background and a ratio between the controls and samples with hsa-miR-375 LNA inhibitor or hsa-miR-7-5p LNA inhibitor was calculated.

Molecular weight markers used for western blot were Biotinylated Protein Ladder (Cat. no. 7727, Cell Signaling Technology) and Spectra Multicolour Broad Range Protein Ladder (Product no. 26623, Thermo Scientific).

Antibodies used for detection of the RBP-Jκ protein and controls with dilutions were:

Polyclonal Rabbit Anti-Human RBPJK (Cat. no. ab25949, Abcam) 1:1000

Polyclonal Rabbit Anti-Human GAPDH (Cat. no. sc-25778, Santa Cruz) 1:2000

Polyclonal Rabbit Anti-Acetyl-Histone H3 (Cat. no. 06-599, Millipore) 1:2000

Secondary antibodies used for western blot analysis were:

Goat Polyclonal Anti-Rabbit IgG (Cat. no. ab6721, Abcam) 1:1000

HRP-Conjugated Anti-Biotin (Cat. no. 7075S, Cell signaling) 1:2000

3.7   The xCELLigence system

The xCELLigence system is a system that allows dynamic monitoring of cellular phenotypic changes in real-time using impedance as readout. Furthermore assessment of short or long-term cell response can be done without labeling and microscopy. The system measures electrical impedance across interdigitated gold micro-electrodes, intergraded on the bottom of well-designed plates (E-plates). The more cells are attached on the electrodes, the larger is the increase in electrode impedance. However factors, other than cell number affects the impedance, such as interaction strength with the electrodes, cell viability, adhesion degree and cell morphology. Therefore electrode impedance, which is displayed as a cell-index (CI) value, reflects the biological condition of monitored cells. The CI value is a relative and dimensionless value; due to it represent the impedance change divided by the background value. Because these number of factors can change the CI value, the application of this system is widespread, like monitoring cell proliferation before and after treatment, cytotoxicity of cells and apoptosis[481,482].

In our experiment, cell growth of NCI-H727 and CNDT2 was monitored after 24 hours post-transfection with precursors of hsa-miR-375, hsa-miR-7-5p or All-stars Negative Control siRNA. E-plates containing 100 µl complete medium in each well were first mounted into the device station, placed inside a humidified incubator at 37 °C to measure the background value. The cells were counted and seeded giving a total of 200 µl cell suspension in each well, followed by 30 min incubation at RT. After cells were allowed to settle at the well bottom, the plates with cells were mounted back to the device station and the program was started. To begin with cell adhesion was monitored in 15 min interval for 6 hours, then proliferation was measured every 30 minutes for 100 hours. In case of CNDT2 cell lines, proliferation was measured for 50 hours, due

to the CI value decreased after 50 hours of monitoring. The mean CI value was calculated and normalized at 5 hours using RTCA v.1.2 Software.

3.8   Global analysis of miRNA target genes

3.8.1   Evaluation of global down-regulation of microRNA-375 target genes

The global changes in gene expression were evaluated by using NCI-H727 cell line transfected with miR-375 or siGLO siRNA as a negative control. After 24 hours post-transfection the total RNA was extracted and the mRNA microarray analysis, HG-U133 Plus 2.0 Human (Affymetrix, Santa Clara, USA) was performed. The microarray expression data was analyzed using the affy package in Bioconductor[483]. Probe set signal intensities were extracted, summarized and quantile normalized[484] using Bioconductor RMA package. Differential expression was determined per probe set using a t-test. The probe sets were then mapped into Ensembl Transcripts v. 49 using mappings provided at BioMart. Probe sets that mapped to two different Ensembl genes were discarded.

Subsequently after analysis of possible mRNA targets down-regulated by miR-375, the mRNA targets were characterised by scanning the 3'UTR of the transcripts for matching 6mer, 7mer and 8mer miRNA seed sites. Transcripts with 3'UTR sequences shorter than 50 nucleotides were discarded. Global evaluation of mRNA target genes, down-regulated after miRNA transfection was tested using the null hypothesis were the expression change distribution of miRNA targets having a 7mer target site was equal to the distribution of 6mer target sites using the non-parametric Wilcoxon rank-sum test.

3.8.2   Statistical assessment of 3'UTR unbiased word analysis

Assessment of word occurrence in 3'UTR and change in gene expression after miR-375 transfection was done using a previously published non-parametric statistical framework for scoring and ranking of oligonucleotide words, based on their overrepresentation in a ranked list of sequences[485,486]. For given sequence and word, I estimated a p-value and sorted them from the lowest value.

3.8.3   Gene set enrichment analysis

To examine if the differentially expressed genes after miR-375 transfection were enriched in specific GO and KEGG terms, I performed a regulator pathway annotation based upon the p-values of pathways collected from the KEGG database (http://www.genome.jp/kegg/). The p-values below 0.05 were checked for enrichment using the *GOstats* Bioconductor package.

3.9   Cloning

3.9.1   Preparation of insert using primers for RBP-Jκ 3'UTR fragment

RBP-Jκ 3'UTR luciferase reporter plasmids were constructed by first amplifying RBP-Jκ 3'UTR fragments for miR-375 and miR-7-5p, from human genomic DNA using primers with restriction sites and TATA sequence incorporated. The predicted RBP-Jκ 3'UTR site with potential binding sites for miR-375 and miR-7-5p were found, using the http://targetscan.org website. The predicted sequence alignment is shown in Figure 22A. For miR-375, primers used were 5'-TATAacgcgtCAAGGATGGTCAGGCTTGGA-3' (MluI restriction site in low-case letters) as forward primer, and 5'-TATAactagtCAAAAACCCCGTTGTCTCCC-3' (SpeI restriction site in low-case letter) as reverse primer (TAG Copenhagen A/S, Copenhagen, Denmark). For miR-7-5p, primers used were 5'- TATAacgcgtTGTGGCTGGAATACAAGTTGA-3' (MluI restriction site in low-case letter) as forward primer, and 5'- TATAactagtTATTGCAGGCAAGGCAGAGG-3' (SpeI restriction site in low-case letters) as reverse primer (TAG Copenhagen A/S, Copenhagen, Denmark). Primers were pre-designed, using Primer-BLAST (NCBI) with a distance of 100 nucleotide from 7mer target site, that include a TATA sequence, to generate a 423 or 443 nucleotide fragments, containing a potential miR-375 or miR-7-5p binding site respectively. The 7mer target sequence for miR-375 is GAACAAA and TCTTCCA for miR-7-5p, positioned 334-340 and 562-568 of the 3'UTR site respectively.

Safe-lock Eppendorf tubes (0.5 ml) was prepared with 48.5 µl Reaction mix (1x HF reaction buffer, 0.5 µM Primers, 0.2 mM dNTPs, 0.02U/µl Phusion hot start II High-Fidelity DNA polymerase, Thermo Scientific) in nuclease-free water and added 1.5 µl of 100 ng/µl template DNA. The thermal cycle programme, run on a Thermocycler (Eppendorf, Hamburg, Germany) consisted of one cycle initial denaturation step at 95 °C for 30 seconds, followed by 35 cycles of denaturation: 95 °C for 5 seconds, annealing: 65 °C for 30 seconds, extension: 72 °C for 30 seconds and left to incubate at 72 °C for 3 minutes during final extension. Amplified PCR fragments were then column purified using GenCatch Advanced PCR Extraction Kit (Cat no. 23-60250, Epoc Life Science), according to manufactures instructions. To make sure that 3'UTR fragment contains 7mer site for miR-375 or miR-7-5p, the amplified PCR product was cloned into topoisomerase containing vector (pCR™-4-TOPO®) for later sequence analysis, using TOPO® TA Cloning® Kit (Cat no. 450030, Life Technologies). The TOPO® cloning reaction was then transformed into TOP10 cells, followed by Maxi preparation.

After verifying that pCR™-4-TOPO® contained the 3'UTR fragment with 7mer site, the recombinant pCR™-4-TOPO® was subjected to *MluI/SpeI* double digestion, then loaded into 1% Agarose gel and purified using GenCatch Advanced Gel Extraction Kit (Epoch Life Science, Missouri City, Texas),

according to manufactures instructions. To insure high restriction activity of both enzymes, 10x NEBuffer 2 (50 mM NaCl, 10 mM Tris-HCl, 10 mM MgCl₂, 1 mM DTT) together with 10x BSA was used in 20 µl restriction digest mix, followed by overnight incubation at 37 °C. Luciferase reporter plasmid with a multiple cloning site (MCS), were also subjected to restriction digest. The region between 495 and 525 was removed through *MluI/SpeI* double digestion (Figure 13) and purified from 1% Agarose gel as mentioned above. DNA concentration of both fragment and plasmid were measured on Nanodrop and digested 3'UTR fragment and luciferase report plasmid were then prepared in the molar ratio 3:1 and ligated with T4 DNA ligase (Cat. no. 15224-017, Invitrogen) at 16 °C overnight. Please note that results obtained by Agarose gel electrophoresis are found in Figure 29, Appendix.
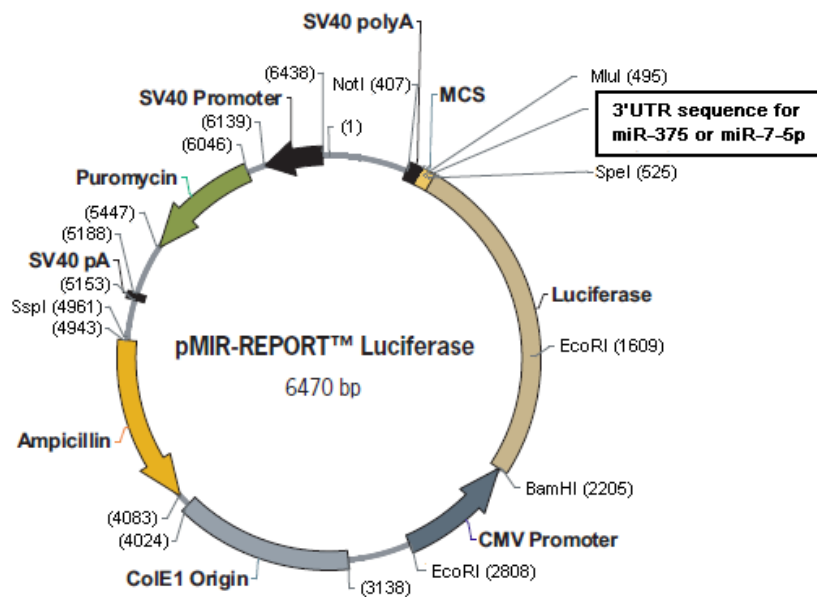
Figure 13: pMIR-REPORT luciferase reporter plasmid and the location of cloned 3'UTR fragment. By inserting predicted miRNA target sequence (3'UTR sequence, containing wild-type or mutated 7mer target site) in the multiple cloning site (MCS), pMIR-REPORT luciferase miRNA expression reporter vector can be used to conduct accurate and quantitative measurement of miRNA function. The 3'UTR sequence is inserted downstream to the firefly luciferase reporter gene under the control of CMV promoter/termination system. By cloning of 3'UTR sequence using MluI and SpeI restriction recognition (recognizing nucleotide sequence; ACGCGT/TGCGCA and ACTAGT/TGATCA, respectively) in both the insert and vector MCS, followed by ligation - the luciferase reporter construct is subjected to regulation that mimics the miRNA target. pMIR-REPORT luciferase reporter plasmid contains the CMV promoter: 2210-2813, firefly luciferase: 540-2210, MCS: 467-539 containing restriction sites (for simplification only MluI and SpeI are shown), SV40 Poly(A): 404-467, SV40 Promoter: 6139-6438, Puromycin: 5447-6046, SV40 pA signal: 5153-5188, Ampicillin: 4083-4943 and CoIE1 Origin: 3138-4024.

3.9.2   Transformation of recombinant pMIR-REPORT in One Shot® TOP10 cells

For each transformation mixture, a vial of 50 µl TOP10 chemically competent *E. coli* were taken out from -80 °C and thawed on ice. From each ligation mix, 2 µl were mixed carefully into the vial of competent cells and incubated on ice for 30 minutes. As a positive control, 10 pg pUC19 was added in a separate vial, to verify transformation efficiency of competent cells (only done once). Transformation was carried out by

heat-shock, cells to increase uptake of product vector at 42 °C for exactly 30 seconds and placed on ice in 2 minutes. To obtain maximal transformation efficiency, 250 µl of S.O.C Medium (Cat. no 15544-034, Invitrogen) was added to each tube and left to shake horizontally at 37 °C for 1 hour at 200 rpm in a shacking incubator. Transformed cells were then plated out in 20 µl/100 µl and 1:10 pUC19 of transformed cells were plated 25 µl/100 µl on preheated LB agar plates, containing 100 µg/ml Ampicillin, incubated for 14-16 hours at 37 °C. The reason for ampicillin was added to the growth medium, was to avoid contamination and/or cells that did not successfully uptake the pMIR-REPORT construct, containing ampicillin resistance gene (Figure 13).

3.9.3 Isolation of recombinant plasmid using minipreparation and colony-PCR

Screening TOP10 cells for the presence of 3'UTR luciferase reporter plasmids were done by isolating single colonies approximately 1 mm in diameter with a toothpick, then transferred to a 0.5 ml Eppendorf PCR tubes as template DNA, and 12 ml tubes containing LB medium and 100 µg/ml Ampicillin. Tubes containing LB and isolated colonies incubated overnight at 37 °C with 160 rpm shacking. PCR tubes with colonies were mixed with 50 µl PCR reaction mix and amplified, according to the method previously described in the PCR section, then loaded into a 1% Agarose gel to determine colonies with recombinant plasmids. Colonies containing recombinant plasmids were purified with Sigma GenElute™ Five-Minute Plasmid Miniprep Kit, according to the manufactures instructions and eluted with nuclease-free water. To verify if the 3'UTR fragment is correctly inserted, sequencing of purified DNA was performed. Plasmid DNA was stored at -20 °C until use.

3.9.4 Sequencing of plasmids

Cycle sequencing was performed first by preparing a total master mix volume of 20 µl in a Safe-lock Eppendorf tubes (0.5 ml), containing BigDye®, 5x Sequencing Buffer (Cat. no. 4305603, Applied Biosystems), template DNA and nuclease-free water with 3.2 pmol forward primer or reverse primer. The thermal cycle programme, run on a Thermocycler (Eppendorf, Hamburg, Germany) consisted of one cycle initial denaturation step at 94 °C for 4 minutes, followed by 35 cycles of denaturation: 96 °C for 30 seconds, annealing: 50 °C for 15 seconds, extension and final extension: 60 °C for 4 minutes and left to incubate at 4 °C overnight. The extension products were left on ice and purified by first adding 2 µl 3 M NaAc and 58 µl ice cold 96% Ethanol for precipitation and incubated in -80 °C for 30 minutes, following 1400 rpm centrifugation at 4 °C for 30 minutes. Supernatant in tubes were carefully removed without disturbing the pellet and 100 µl ice cold 70% Ethanol were added, followed by second spin in 10 minutes. Supernatant was removed again and tubes with remained pellet were dried in a Savant DNA 110 Speedvac

(Farmingdale, NY, USA), and stored at -20 °C until sequencing was made. The reaction was analyzed in ABI PRISM® 377 DNA Sequencers (Applied Biosystems).

3.9.5   Site directed mutagenesis

Site directed mutagenesis *in vitro* is a method to introduce point mutations and delete or insert of single or multiple nucleotides into a double-stranded plasmid. This method does not require specialized vectors, unique restriction sites or multiple transformations, but only a plasmid with an insert of interest as template and two synthetic primers containing the desired mutation. The primers complimentary to the template strand can hybridize to the gene of interest and then the primer is extended using DNA polymerase, which copies the rest of the plasmid[487]. Thus the incorporation of primers generates a mutated plasmid containing staggered nicks next to the template plasmid. While most plasmids isolated from *E. coli* stains (dam+) are methylated[488], the newly generated mutate plasmid is not, and thus parental plasmid can be removed by treatment with DpnI. The DpnI endonuclease recognizes specific sequence (5'-Gm6ATC-3') of methylated and hemimethylated DNA located on the parental DNA template, and digestion leads to its removal. The remained plasmid with desired mutation can then be transformed directly into super competent cells, which repair the nicks of mutated plasmid.

Mutagenic primers were designed from the 3'UTR fragment sequence to contain four point mutations in miR-375 or miR-7-5p target sites (Figure 22A). Primers used for the miR-375 mutant plasmid were 5'-TTAGATTTGTGTCTTCTAGTAACATCAACTTGTATTCCAGCCACATTATTTACTTCTTGCCCA-3' (sense) and 5'-TGGGCAAGAAGTAAATAATGTGGCTGGAATACAAGTTGATGTTACTAGAAGAC-ACAAATCTAA-3' (antisense) and primers for mutant miR-7-5p plasmid were 5'- CCTTAGACCAAA-AAAAAAAAAACCACCTAGAGTATGATAGATTAAACAAGGATGGTCAGGCTTG-3' (sense) and 5'-CAAGCCTGACCATCCTTGTTTAATCTATCATACTCTAGGTGGTTTTTTTTTTTTGGTCTAAGG-3' (antisense).

Mutant plasmid was prepared using Phusion PCR-reaction. For PCR reaction, 2 µl of each Mutagenic Primer (TAG Copenhagen A/S, Copenhagen, Denmark) were added to a 46 µl reaction mix (1x HF reaction buffer, 3% DMSO, 60 ng 3'UTR luciferase reporter plasmid, 0.2 mM dNTP mix, 0.06 U/µl Phusion Hot Start II High-Fidelity DNA polymerase) in nuclease-free water. Each reaction was done in duplicates with a negative control, without template DNA. The thermal cycle program, consisted of one cycle initial denaturation step at 98 °C for 30 seconds, followed by 35 cycles of denaturation: 98 °C for 15 seconds, annealing: 65 °C for 30 seconds, extension: 72 °C for 2 minutes and incubated at 72 °C for 5 minutes during final extension. Amplified PCR fragments were then incubated at 37 °C with 1 µl 10 U/µl DpnI (Cat. no. ER1705, Life Technologies) overnight to remove methylated template DNA (parental DNA template),

followed by run on 1% Agarose gel with a negative control (DpnI untreated). Samples containing mutant plasmid were then transformed into One Shot® TOP10 cells, followed by minipreparation and sequencing.

3.10 Luciferase assay

Luciferase assay is a genetic reporter system that is mostly used to study eukaryotic gene expression and cellular physiology, including study of miRNA function, receptor activity, mRNA processing, protein folding and denaturation. Firefly and Renilla luciferase are evolutionary distinct with different structure and substrate, which make it possible to discriminate between their respective bioluminescence (Figure 14). Firefly luciferase is a 61 kDa monomeric protein that does not require post-translational processing for activating, hence its function as generic reporter, take place immediately upon translation. The photon emission is achieved through oxidation of beetle luciferin in a reaction that requires ATP, Mg^{2+} and oxygen. Renilla luciferase is a 36 kDa monomeric protein and like firefly luciferase it does not require post-translational processing. Its luminescent reaction is catalyzed by Renilla luciferase by using coelenterazine and oxygen.
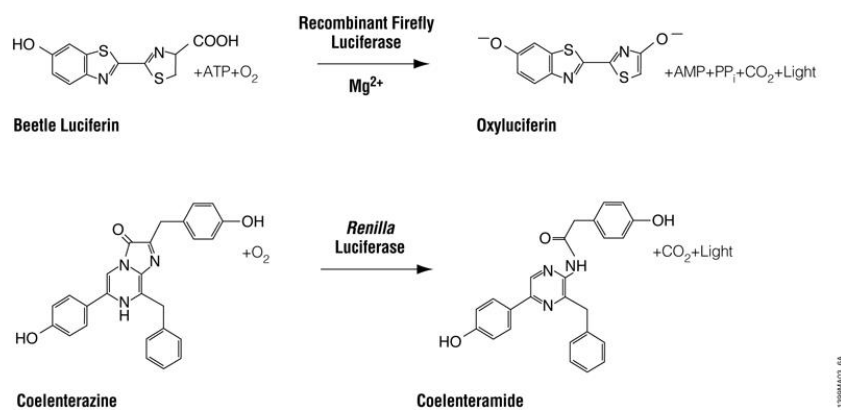
Figure 14: Bioluminescent reactions, catalyzed by firefly and Renilla luciferase. Emission of light is achieved by oxidation; Firefly luciferase enzyme, that catalyse the conversion of luciferin, ATP and oxygen to oxyluciferin, AMP, PP and CO_2. Similar to Firefly luciferase, the Renilla luciferase enzyme catalyses Coelenterazine and oxygen to CO_2 and Coelenteramide.

In this assay, I used dual-luciferase reporter assay system which allows simultaneous expression and measurement of two individual reporter enzymes within a single system. Given that the Firefly luciferase is extremely sensitive and by-products is often generated, which strongly inhibits the bioluminescence reaction. A more stable luminescence is insured by incorporation of coenzyme A (not shown in Figure 14) which produce a much less powerful inhibitor, thus induces both the stabilization and yields a significantly higher light emission[489]. The Firefly luciferase is measured first by adding Luciferase assay reagent II (LARII) to generate the luminescent signal. Then after quantifying the firefly luminescence, the reaction is

quenched simultaneous with the Renilla luciferase reaction is initiated, by adding Stop & Glo® reagent to the same well, producing a relatively stable signal from Renilla luciferase[490].

HEK293 cells were seeded in a 24-well plate with 14.000 cells/well and allowed adhering overnight to reach 70-90% confluence, before transfection. For each well, transfection mix was prepared by first mixing 100 ng pMIR-REPORT construct with wild-type or mutated sites, 6.25 ng Renilla, 1 µl 25 µM pre-miR (hsa-miR-375, hsa-miR-7-5p or AllStars negative control siRNA) giving a final concentration of 50 nM in 500 µl. miR-375 or miR-7-5p LNA inhibitors were also used, to reverse the inhibitory effect on the luciferase reporter gene. After vortex, the mixture consisting of plasmids and pre-miR were combined with Opti-MEM contained 1.5 µl Lipofectamine 2000 (Cat. no. 11668-027, Life Technology), giving a transfection mix a total volume of 100 µl. The complete transfection mix was vortexed and left to incubate for 20 minutes at RT. In the meantime old medium is removed and 400 µl fresh medium was added (DMEM glucose 4.5 g/l, 10% FBS, 1% P/S) to each well. Transfection mix is added drop-wise to cells, followed by mixing the complete medium with transfection mix by carefully tipping the petri dishes. After 24 hours incubation in 37 °C with 5% CO_2, cells were carefully washed in PBS and lysed in 120 µl 1x Passive Lysis Buffer (Cat. no. E1945, Promega) followed by 30 min vortex. The lysis buffer is transferred from the 24-well plate to 1.5 ml tubes, one for each well and centrifuged for 10 minutes. From each tube, 30µl supernatant is transferred to white 96 well plates (3 wells for each tube), and signal from the plasmid constructs are measured and analyzed by using Dual-Luciferase Reporter Assay System (Cat. no. E1910, Promega) and the Glomax 96 Micro Plate Luminometer (Promega, Madison, USA), according to the manufacturer's specifications.

For calculation and normalization of Firefly luciferase, I first subtract background measurements from Firefly and Renilla measurement. Because neither of these enzymes is endogenously expressed in mammalian cells, the background luminescence is either from the luminometer or the luminescent substrate. Next, the ratio between the luciferase luminescence and Renilla luminescence was calculated for the AllStars negative control siRNA and the other pre-miRs and LNAs with either wild-type or mutated pMIR-REPORT construct. To calculate the relative ratio, the ratio of each well was hold against the average Luciferase/Renilla ratio of the respective control group. Normalization of the ratios permits comparison of ratios between plates in the same experiment. For statistical analysis the standard deviation of each group was calculated and unpaired t-test was performed.

3.11 *In-situ* hybridization

In situ hybridization (ISH) is a technique that allows precise location of a specific segment (RNA or DNA sequences) within a histological section. The basic concept of ISH is that nucleic acids are preserved adequately within the histological specimen and can be detected through the use of complimentary strands

of nucleic acid to which a reporter molecule is attached. Thus the visualization of reporter molecule allows the localization of the specific RNA or DNA sequence in a heterogeneous cell population in a tissue sample. In this assay, I use a Double (5' and 3') digoxigenin (DIG)-labeled miRCURY LNA miRNA detection probes, which provide a great sensitivity and specificity to detect miRNA in Formalin-fixed and paraffin-embedded (FFPE) tissue sections. In order to the complementary strand can bind to miRNA in cells, the tissue or cell membrane of cells has to be 'opened' by treating samples with Proteinase K. Subsequently, the hybridization step allows the complimentary RNA (also called riboprobe) to hybridize to the target miRNA sequence at elevated temperatures and excessive probe is washed away. Then alkaline phosphatase (AP) conjugated anti-DIG antibodies are added, which recognize and bind to the DIG-labeled probe. Finally, the addition of AP-substrate creates blue precipitation where the probe is located for visualization. As background stain, I used a nuclear counter stain, called Nuclear Fast Red™ which gives a red precipitation. This allows not only a histological distinguishes of cells (type of cells, location of neoplasm etc.), but also detection of a specific miRNA in target cell.
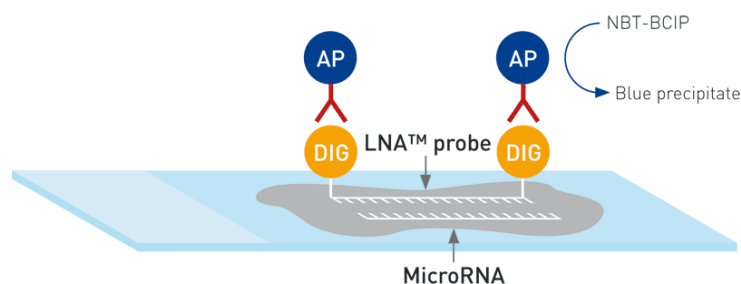
Figure 15: Basic principles of DIG-labeled miRCURY LNA miRNA detection probes used in this experiment (Exiqon). After Proteinase K treatment of sections, the cellular tissue is 'opened' and thus susceptible to the intake of complementary DIG-labeled miRNA probes which hybridize to the specific target miRNA at elevated temperature. To allow probes to be detected, treatment with anti-DIG antibody, followed by addition of its substrate creates blue precipitation which can be visualized in any microscope.

FFPE tissue samples of GEP-NETs were obtained from the Department of Pathology (Rigshospitalet, Copenhagen, Denmark) and 5 µm thick tissue sections were cut under RNAse free conditions and placed on slides. Then slides left to incubate for 45 minutes at 60 °C to make the tissue stick to the slide, followed by deparaffinizing and rehydration steps. To avoid the complete dry-out of sections, slides were placed in PBS until ready for treatment with 300 µl Proteinase K, 5 µg/ml in Proteinase K-buffer (5 mM Tris-HCl, pH 7.4, 1 mM EDTA, 1 mM NaCl) at 37 °C for 8 min in a Dako Hybridizer (Dako hybridization, Glostrup, Denmark). After denaturation, the sections rinsed twice in PBS, dehydrated and left to air-dry for 15 minutes to allow hybridization.

35 µl hybridization mix was added, containing 40 nM double-DIG-labeled miR-375 LNA, miR-7-5p LNA or scramble LNA detection probe (Exiqon, Vedbaek, Denmark) and 0.25 mM Levamisole in 1 x ISH buffer, hybridized at 53 or 52 °C respectively for 2 hours in the Dako hybridizer (Dako hybridization, Glostrup, Denmark). After hybridization, the slides were washed in pre-heated water bath at same temperature as hybridization; once with 5x Saline-sodium citrate (SSC), twice in 1x SSC, and twice in 0.2x SSC after which the slides are placed in 0.2x SSC at RT and transferred to PBS. In humidifying chamber, sections were left to incubate for 15 minutes at RT with 300 µL blocking solution (PBS-T with 2% sheep serum and 30% BSA) and then treated with AP conjugated Anti-DIG Antibody (Roche, Basel, Switzerland) diluted 1:800 in Dilution solution containing 2% Sheep serum, incubated 60 min at RT, followed by wash in PBS-T containing 0.1% Tween 20. Fresh AP-substrate, NBT/BCIP tablet dissolved in 5 ml Mili-Q water, 0.2 mM Levamisole was prepared, and added to each slide, before slides were incubated at RT overnight, protected from light in the humidifying chamber.

The next day, slides were incubated twice in 5 minutes, with KTBT (50 mM Tris-HCl, 150 mM NaCl, 10 mM KCl) buffer to stop staining reaction and washed twice in Mili-Q water. Then 200 µL Nuclear Fast Red™ (Sigma-Aldrich, Denmark) was applied as a nuclear counter stain for 20 seconds and slides were washed in running tap-water for about 10 minutes, followed by dehydration. Finally slides were mounted, using Eukitt™ Mounting Medium (Sigma-Aldrich, Denmark) and coverslips were immediately placed on each slide for microscopy.

To validate the specificity of the miR-375 and miR-7-5p expression, the miRs expression in samples were compared to a non-specific sequence (scrambled) miR, which gives no expression, to exclude non-specific binding of the anti-DIG antibody. In Figure 28, appendix the scramble miR expression is shown relative to miR-375 and miR-7-5p in insulinoma.

4 Results

4.1 Affymetrix microRNA of carcinoid tissue

It has previously been shown that miRNAs are involved in cellular proliferation, differentiation, apoptosis and can function as oncogenes or tumor suppressors. However, only few studies have examined microRNAs in NETs[452,453,457]. I therefore examined the differential expression of all mature miRNA sequences released in miRBase, using the latest Affymetrix miRNA 4.0 on five matching carcinoids and four normal tissues. The expression profile of miRNAs for all tumor samples was normalized to normal tissue expression profile. Only human miRNA was included in the analysis. For the up-regulated miRNAs, miRNA exhibiting a 5-fold or greater change of expression, compared to normal tissue were chosen. For down-regulated miRNAs the cut off value was set to be 2-fold. Furthermore, all miRNAs chosen should have a p-value <0.01. The result of our analysis (Table 3, Appendix) contained 26 up-regulated and 12 down-regulated miRNAs. I next asked if any of the aberrantly expressed miRNAs previously had been associated with endocrine cells. Previously, miR-7-5p has been identified as a major islet miRNA, which is predominantly expressed in endocrine cells of developing pancreas. Furthermore miR-375 was also expressed in islet cells, but with a significantly lower expression than miR-7-5p[465,491]. Therefore both of these miRNAs were chosen for further investigation.

4.2 MicroRNA-375 and microRNA-7-5p located in carcinoid tissue are upregulated in carcinoids

To validate the array results, that miR-375 or miR-7-5p are upregulated in NETs, LCM in human carcinoid tumors were performed followed by real-time RT-PCR. Carcinoids from five different patients were micro dissected, together with corresponded normal mucosa (Figure 16K) and Taq-Man RT-PCR analysis was performed. As shown in Figure 16J, there was a significant up-regulation of miR-375 in the enriched carcinoid tissue compared to normal mucosa, when samples were normalized with RNU44 and miR-191. Taq-Man RT-PCR analysis of miR-7-5p was not measured, because of insufficient time. Next, I analyzed both miRs expression in carcinoid tumor tissue by *in situ* hybridization using anti-miR-375 and anti-miR-7-5p LNA probes. For positive expression of tumor tissues and endocrine cells, I used CgA immunohistochemical staining. Both miR-375 and miR-7-5p expression was observed in high number of carcinoid tumor cells as shown in Figure 16B, E and H, and C, F and I, respectively. Moreover *in situ* hybridization on carcinoid tissue blocks also reveal endocrine cell specific expression of miR-375 and miR-7-5p in normal tissue of the intestine (indicated by arrows) as compared to CgA immunohistochemical

stained tissue. The expression levels of miR-7-5p appeared to be slightly lower, as judged by the intensity of the hybridization signal of carcinoid tumor tissue.
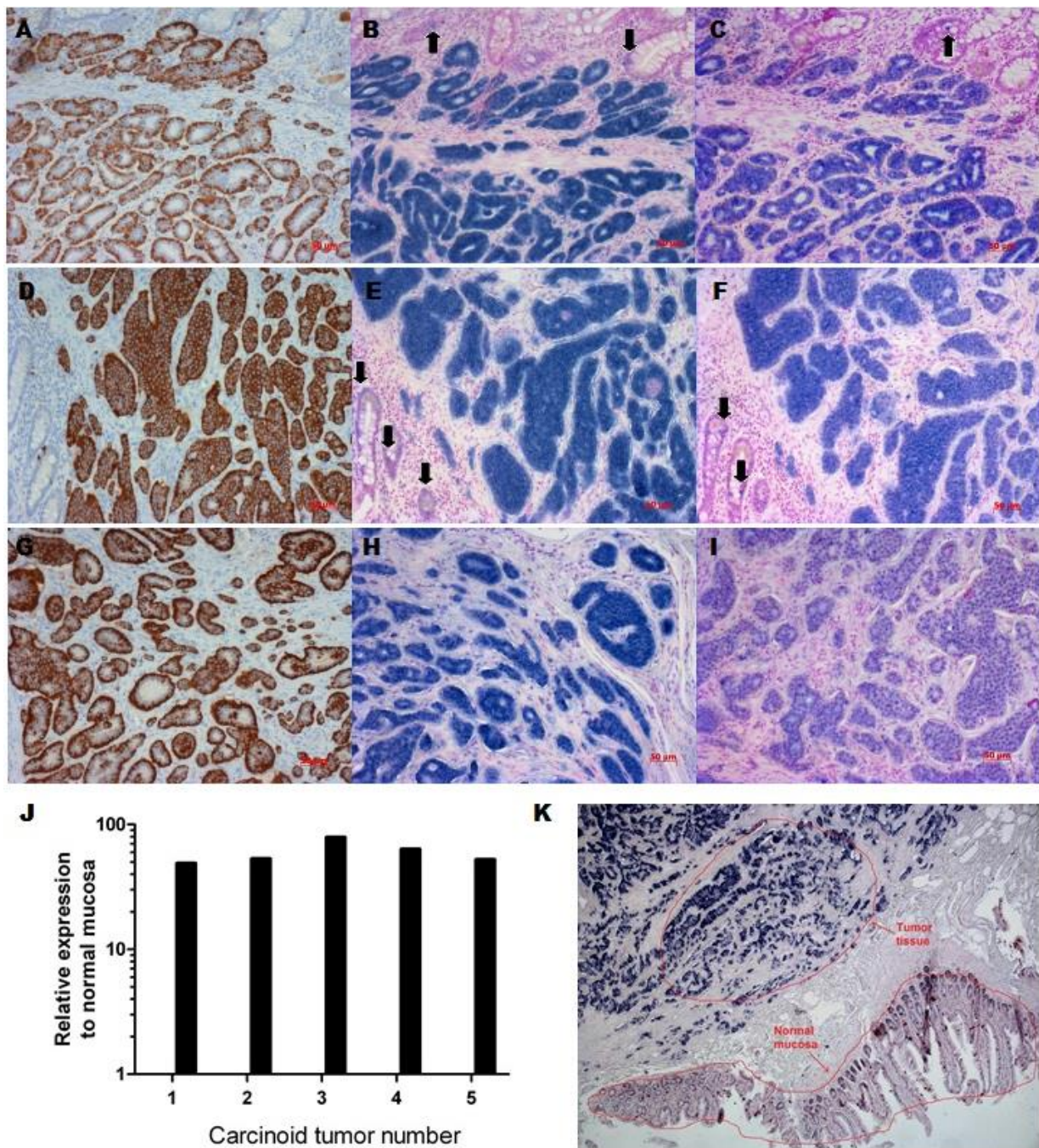
Figure 16: *In situ* hybridization of miR-375 and miR-7-5p and relative expression of miR-375 in carcinoid tissue. A-I: left panel: CgA IHC staining (brown) 10x; middle panel miR-375 (blue) ISH 10x; right panel: miR-7-5p (blue) ISH 10x. A-C: shows the strong expression of CgA protein, miR-375 and miR-7-5p in colon carcinoid tissue. D-F shows the strong expression of CgA protein, miR-375 and miR-7-5p in carcinoid located in the distal Ileum. G-I: shows the strong expression of CgA protein, miR-375, miR-7-5p in another carcinoid located in the ascending colon. Arrows indicate single endocrine cells of normal tissue, which are stained by *in situ* hybridization. J: Laser Capture Microdissection and qPCR of small intestine carcinoids from different patients, using normal mucosa to compare the miRNA expression. The relative expression is in folds. K: A drawing that shows how the tissue was dissected by LCM. The upper part shows the dissection of tumor tissue (red line) whereas the lower part is dissection of the mucosa (red line). IHC: Immunohistochemistry, ISH: *In situ* hybridization.

4.3 MicroRNA-375 and microRNA-7-5p expression in gastroenteropancreatic neuroendocrine tumors

In order to fully investigate the miR expression in GEP-NETs, tumors other than carcinoids were stained by *in situ* hybridization. miR-375 and miR-7-5p expression were visualized at cellular level in three different PNETs; insulinoma, VIPoma and NF-PNET (Figure 17). In all PNETs investigated, miR-375 and miR-7-5p was observed in islet endocrine cells (indicated by arrows) as well as in amassed endocrine cells of the tumor tissue, which further confirm the endocrine specific character of miR-375 and miR-7-5p.
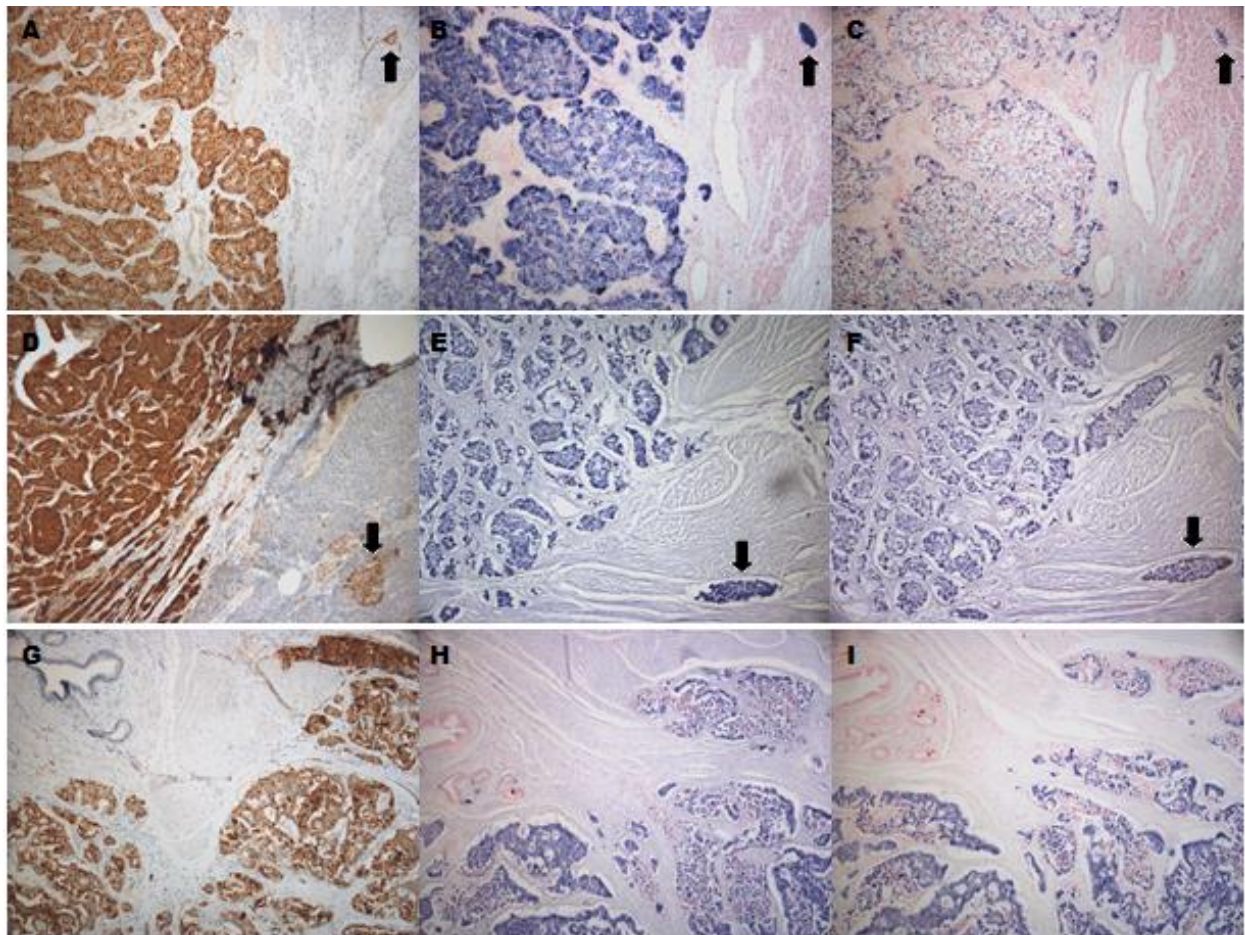
Figure 17: *In situ* hybridization of miR-375 and miR-7-5p in PNET tissue. A-I: left panel: CgA IHC staining (brown) 5x; middle panel miR-375 ISH (blue) 5x; right panel: miR-7-5p ISH (blue) 5x. A-C: shows the strong expression of CgA protein and miR-375, but lower expression of miR-7-5p in insulinoma tissue. D-F shows the strong expression of CgA protein, miR-375 and miR-7-5p in VIPoma. G-I: shows the strong expression of CgA protein, miR-375, miR-7-5p in a non-functional PNET. Arrows indicate isle of endocrine cells from healthy tissue, which are stained by *in situ* hybridization. IHC: Immunohistochemistry, ISH: *In situ* hybridization.

4.4 Assessment of the biological function of miR-375 and miR-7-5p in endocrine tumor cell lines

After determine that miR-375 and miR-7-5p are present at high levels in cells of neuroendocrine origin; including in several types of NETs as well as endocrine cells in normal tissue, I sought to find a reliable cell model system for investigating the biological action of both miRs in GEP-NETs. Considering that both miRs were highly expressed in our tumors found in vivo, I tried to find tumor cell lines of similar expression pattern. I therefore preformed qPCR measurement of miR-375 and miR-7-5p in a broad spectrum of human cell lines from normal lung (WI-38), normal skin (BJ) foreskin, osteosarcoma (U20S), melanoma (MDA-MD-435), seminoma (TCAM2), carcinomas from breast (T470 and MCF7), cervix (C33A), colon (RKO and HCT-116), stomach (SNU-638 and HFE145), foregut carcinoid cell lines in the lung (NCI-H720 and NCI-H727), pancreas (BON-1) and finally midgut carcinoid cell lines from the ileum (HC45 and CNDT2) as shown in Figure 18. The reason for including normal and non-NE tumor cell lines in our qPCR analysis is to see if both these miRs are expressed in normal or non-endocrine tumor cells and thereby exclude the possibility of these miRs are not endocrine specific.

When comparing miR-375 expression in carcinoid cell lines with expression in tumor- and normal cell lines, I could see a significantly higher expression of endogenous miR-375 in NCI-H720, NCI-H727 and BON-1 carcinoid tumor cell lines, suggesting that miR-375 expression is highly endocrine specific in endocrine tumors both *in vitro* and *in vivo*. Surprisingly, CNDT2 and HT45 showed a very low expression of miR-375. Interestingly, the breast cancer cell lines compared to other non-NE derived tumors express higher miR-375 levels, which could be because of their endocrine-related phenotype[492,493].

I therefore those to examine the biology of miR-375 and miR-7-5p in one endocrine cell line with high expression (NCI-H727) and one with low (CNDT2). Although BON-1 was also a good candidate, I did not choose it due to there has been disagreements of its use as an *in vitro* model system for EC cell-derived NETs[494].
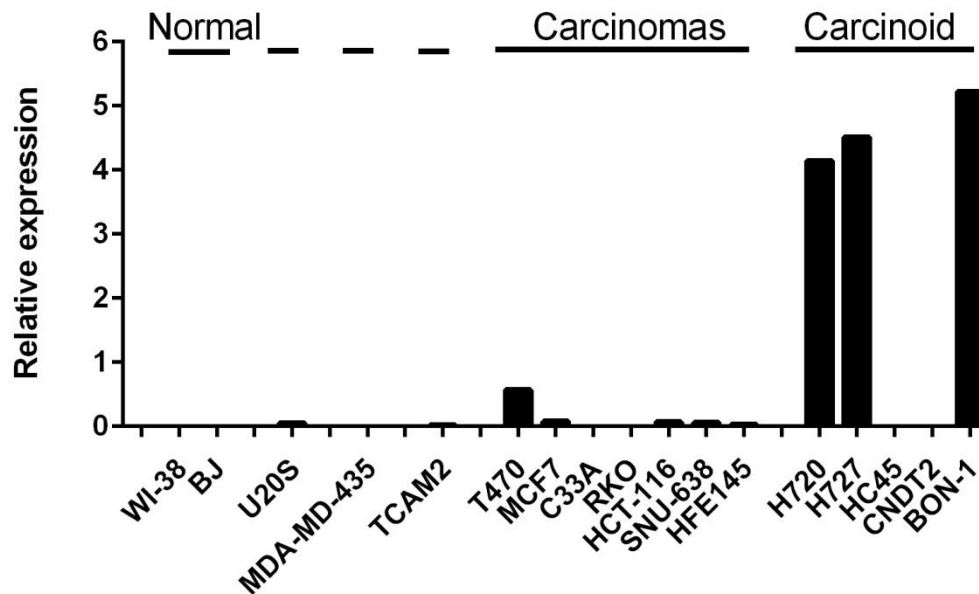
Figure 18: miR-375 expression profile in different cancer and non-cancer cell lines. The analysis of miR-375 expression by qPCR includes different cell lines that are derived from carcinoids, carcinomas and normal tissues as indicated. Moreover the analysis includes a human osteosarcoma, melanoma and seminoma cell line. From right panel: WI-38: Normal skin, BJ: Foreskin, U20S: Osteosarcoma, MDA-MD-435: Melanoma, TCAM2: Seminoma, T470 and MCF7: Breast carcinoma, C33A: Cervix carcinoma, RKO and HCT-116: Colon carcinoma, SNU-638 and HFE145: Gastric carcinoma, NCI-H720 and NCI-H727: Lung carcinoid, HC45 and CNDT2: Ileum carcinoid, BON-1: Pancreatic neuroendocrine tumor.

In order to transfect our chosen tumor cell lines, I sought to find the optimal miR transfection efficiency, using Turbofect transfection reagent. Therefore, I transfected CNDT2 cells with a transfection mix containing a constant amount of the cherry florescent miR, siGLO (50 nM), but a variable concentration of Turbofect reagent to find the optimal transfection efficiency. The transfection efficiency was assessed by the number of florescent cells visualized in each sample which was compared to a negative control without siGLO. The optimal transfection efficiency was obtained, using 10 µl of Turbofect reagent, were almost all cells showed cytoplasmic location of siGLO (Figure 19B and D).
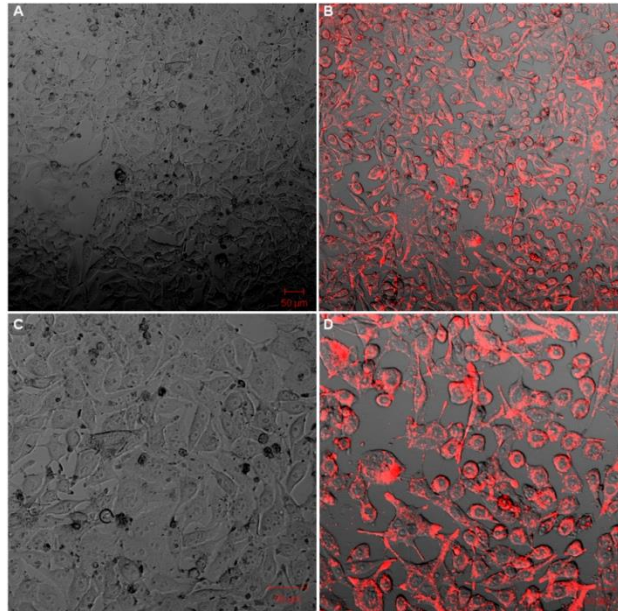
Figure 19: Transfection optimization, using Turbofect reagent in different concentration and siGLO for visual indication of the delivery. CNDT2 cells were transfected with 0, 5, 10, 15 or 20ul Turbofect reagent and transfection efficiency was assessed with a cherry-labeled RISC independent control siRNA (siGLO) the next day. For simplification only control sample without Turbofect and the optimal Turbofect concentration are shown. A: Control sample containing siGLO, but without Turbofect reagent showing no cellular localization of siGLO. B: Transfection with 10µl Turbofect reagent and siGLO, showing almost all cells transfected with the cherry-labeled siRNA. C and D show 2x zoom-in of A and B, respectively. Note that siGLO is localized in the cytoplasm of CNDT2 cells, when Turbofect is used.

As model systems for GEP-NETs, I transfected NCI-H727 and CNDT2 carcinoid cell lines with either pre-miR-375, miR-375 LNA inhibitor or pre-miR-7-5p and then monitored their effect on growth in long-term by comparing them to cells transfected with AllStars negative control siRNA. Before the initial growth experiment the optimal cell number for long-term growth measurement was found, using titration assay to monitor different number of cells growth pattern (Figure 27, Appendix). In NCI-H727 both miR-375 and miR-7-5p showed a statistical significant (P≤0.05), but minor increase in growth compared to post-transfected cell with negative control (Figure 20A and C). However, inhibition of miR-375 by using antisense inhibitor specific to target miR-375, increased growth of these cells significantly (P≤0.01) compared to control (Figure 20B). Interestingly, the opposite behavior was present in post-transfected CNDT2 cells. As shown in Figure 20D and F, both miR-375 and miR-7-5p increased the growth of CNDT2 cells significantly (P≤0.001 and P≤0.0001 respectively), while treatment with antisense miR-375 inhibitor reversed the miR-375 effect on growth (P≤0.05, Figure 20E).
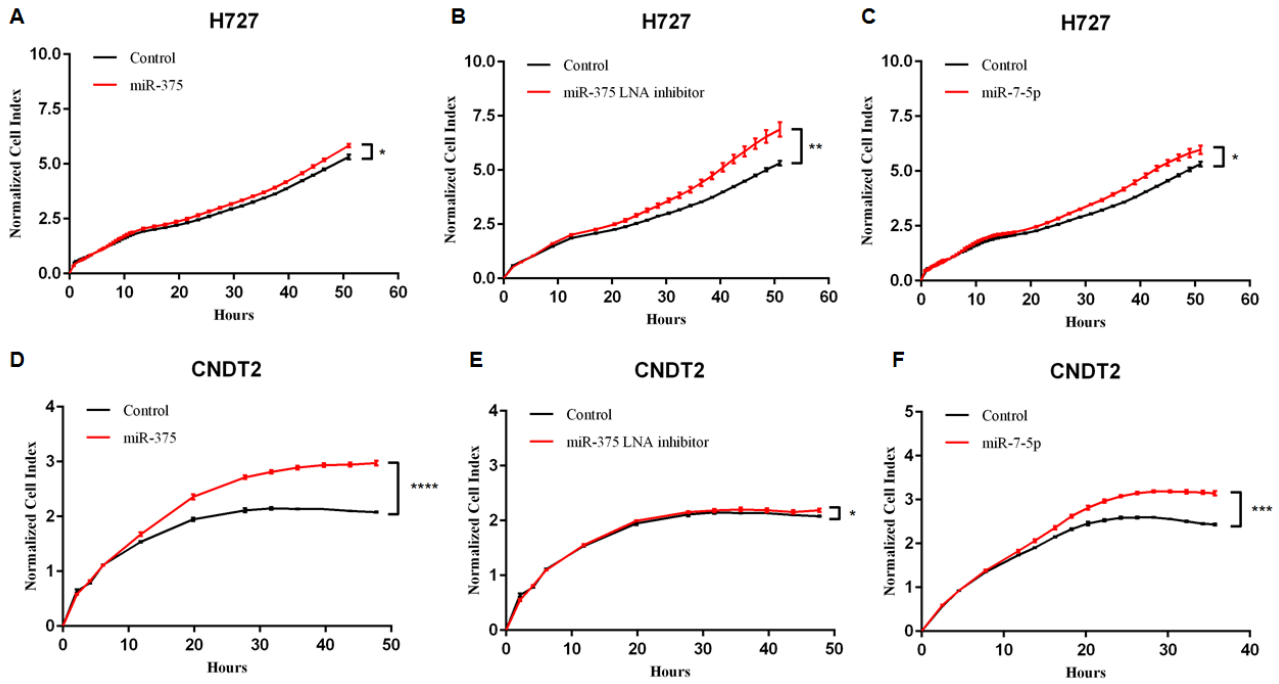
Figure 20: The effect of miR-375, miR-375 LNA inhibitor and miR-7-5p on long-term growth in NCI-H727 and CNDT2 cells. The cell index is normalized 5 hours after growth initiation to exclude adhering of cells. A-C: Growth curve of NCI-H727 cells monitored in 50 hours, comparing transfection with miR-375, miR-375 LNA inhibitor or miR-7-5p with control (AllStars siRNA). D-F: Growth curve of CNDT2 cells monitored in 40-50 hours, comparing transfection with miR-375, miR-375 LNA inhibitor or miR-7-5p with control (AllStars siRNA). After few passage of growth, NCI-H727 and CNDT2 were transfected with miR-375, miR-375 LNA inhibitor, miR-7-5p or AllStars for 24 hours, before trypsinization. 40.000 NCI-H727 or 15.000 CNDT2 cells were seeded into E-plates and adherence and proliferation were measured. *($P \leq 0.05$), ** ($P \leq 0.01$), ***($P \leq 0.001$), ****($P \leq 0.0001$).

4.5 Target prediction of microRNA-375

Having established that miR-375 and miR-7-5p effects proliferation in both cell lines, I focused next on target identification in GEP-NETs to elucidate their action. In order to do so, I performed a global analysis of the number of possible 6- and 7mer target sites of miR-375 in the known 3'UTRs. I found that mRNAs with predicted miRNA 7mer target sites in the 3'UTR were not significantly down-regulated compared to mRNAs with predicted 6mer target sites, after transfection with miR-375 in NCI-H727 cell line (p=0.39) as shown in Figure 21A. Therefore I examined the correlation between the number of 7mer and the number of 6mer 3'UTR sites associated with global miRNA target site. As shown in Figure 21C the number of 7mer sites in the 3'UTR was surprisingly low compared to 6mer target sites of miR-375, suggesting that low number of 7mer sites is the main cause, that I did not obtain significant results. Unbiased word analysis of all oligonucleotides of length 5-7 demonstrated that the miR-375 6mer (GAACAA) and 7mer (GAACAAA) sites in the 3'UTR were most correlated with down-regulation in NCI-H727 cell line.

To fully inspect the predictive function of miR-375, I performed a Gene Ontology (GO) term and KEGG pathway annotation using *GOstats* Bioconductor. GO term enrichment analysis showed that miR-375 mainly controlled the Notch signaling pathway in transfected NCI-H727 cell line. Other pathways noted were; the mTOR pathway and Insulin signaling pathway. The KEGG regulator pathway annotation showed that Notch signaling pathway was among the predicted targets Figure 21D where RBP-Jκ was predicted as the main target of miR-375 (not shown).
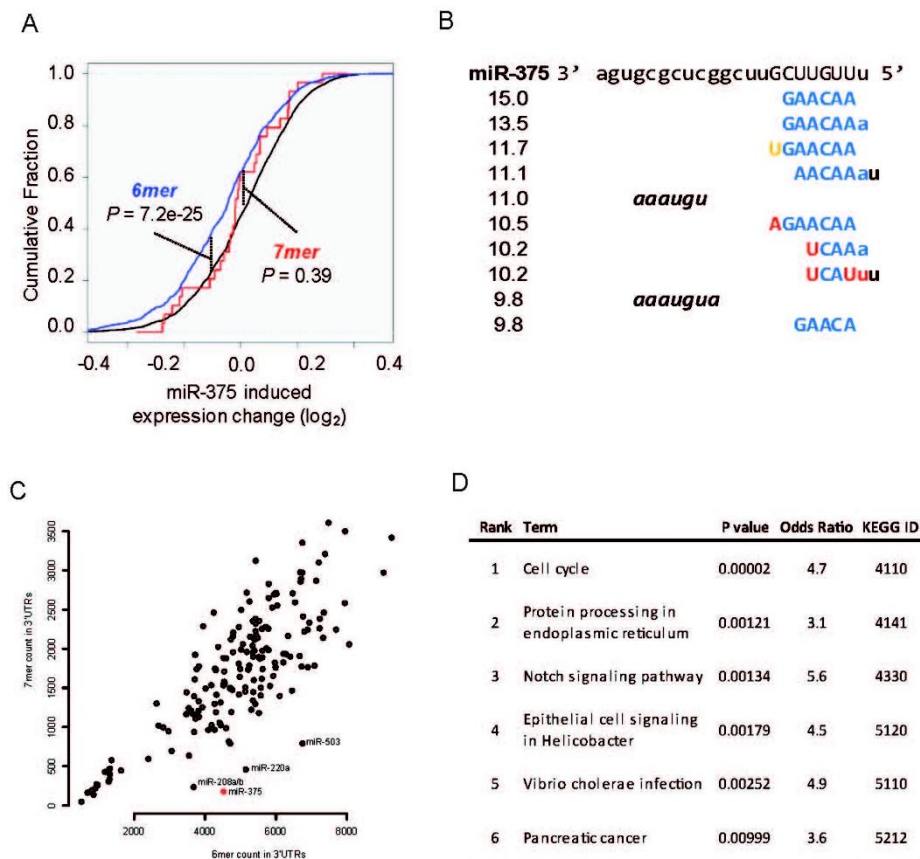
Figure 21: Bioinformatic results obtained from NCI-H727 cell lines, transfected with miR-375. A: The global changes of gene expression were the cumulative fraction of mRNA is plotted against miR-375 log₂ fold changes. B: Word-analysis of the down-regulated transcripts showed enrichment of transcripts containing 6mer and 7mer targets of words. C: Comparison plot that compare between the 7mer and 6mer counts in 3'UTR, showing that there is more substantial 6mer seed sites compared to 7mer sites for miR-375 (red dot). D: KEGG pathway analysis of NCI-H727 transfected cells with miR-375, showing that Notch signaling pathway is one of the most enriched pathways.

4.6 RBP-Jκ is a direct target of miR-375 and miR-7-5p by binding to 7mer site on RBP-Jκ mRNA

RBP-Jκ was among the predicted targets of miR-375. Using the TargetScan v. 6.2 bioinformatic algorithm, I confirmed that RBP-Jκ is a putative target of miR-375, but also for miR-7-5p. To confirm that these miRs have a direct interaction with the binding sequences, present at the 3'UTR site of the wild-type or mutated RBP-Jκ mRNA were cloned downstream the firefly luciferase reporter gene and co-transfected with Renilla as a control vector and either AllStars negative control siRNA, pre-miR-375 or pre-miR-7-5p into HEK293 cells. When pre-miR-375 was co-transfected, the relative luciferase expression of the reporter, containing miR-375 wild-type 3'UTR was significantly suppressed by about 40% compared to a reporter containing the mutated 3'UTR sequence of miR-375 (P≤0.001). In contrast, the relative luciferase expression of the reporter containing miR-375 wild-type or mutated 3'UTR was unaffected when co-transfected with AllStars negative control siRNA (Figure 22B). In addition to this miR-375 LNA inhibitor was co-transfected with reporter containing miR-375 wild-type 3'UTR sequence to inhibit endogenous miR-375 targeting the binding site in 3'UTR sequence. Indeed the relative luciferase expression increased significantly by about 20% (P≤0.001). Similarly, when pre-miR-7-5p was co-transfected, the relative luciferase expression of the reporter, containing miR-7-5p wild-type 3'UTR was significantly suppressed by 40% (P≤0.001) compared to a reporter containing the mutated 3'UTR sequence of miR-375 (Figure 22C). Also inhibition of endogenous miR-7-5p increased the relative luciferase expression (P≤0.001). Collectively these results suggest that miR-375 and miR-7-5p targets the binding sequence at the 3'UTR of RBP-Jκ.
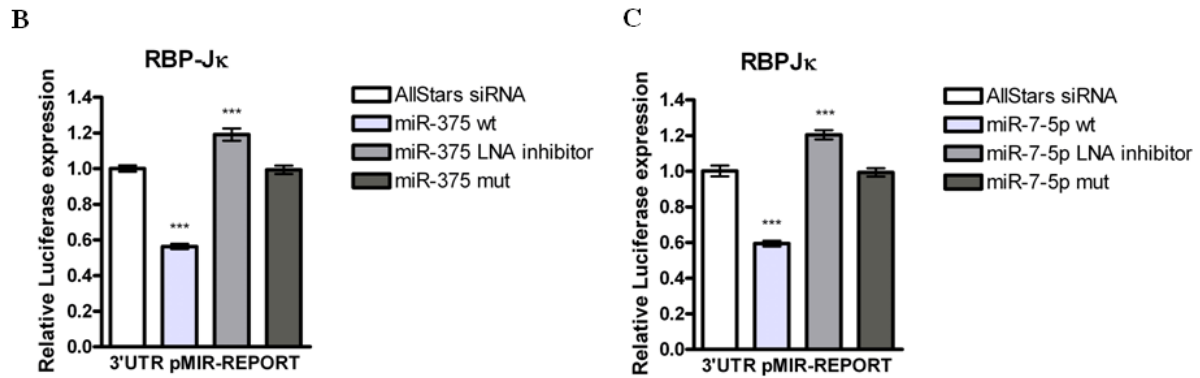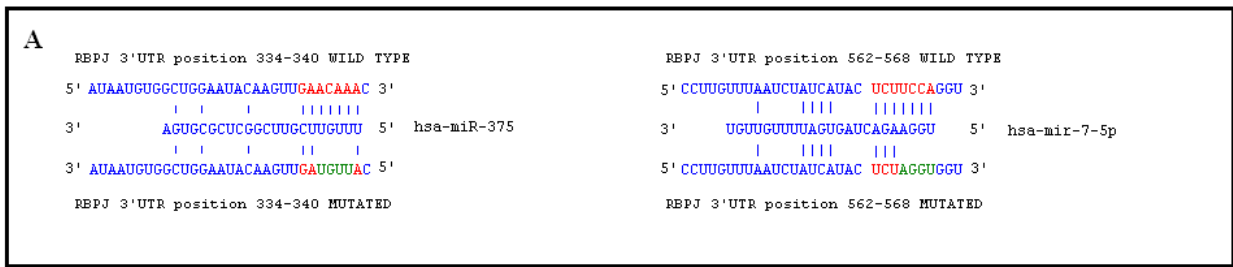
Figure 22: Sequence alignment and results from the dual-luciferase reporter assay, showing miR-375 and miR-7-5p function on RBP-Jκ. A: The sequence alignment of miR-375 and miR-7-5p, with wild-type and mutated RBP-Jκ 3'UTR sites. B: The verification of direct and functional target binding using luciferase plasmid construct, pMIR-REPORT holding wild-type or mutated 7mer site in 3'UTR sequence for RBP-Jκ. Constructs containing either wild-type or mutated 3'UTR site downstream to the firefly luciferase gene were co-transfected into HEK293 cells together with Renilla luciferase control plasmid and miR-375, miR-7-5p, respective inhibitors or control (AllStars siRNA). Co-transfection with Renilla plasmid was used as internal control for normalization of luciferase reporter construct. ***($P \leq 0.001$).

4.7 Inhibition of miR-375 and miR-7-5p does not alter RBP-Jκ protein levels in carcinoid cell line

To assess whether miR-375 and miR-7-5p actually suppresses RBP-Jκ at protein level, miR375 or miR-7-5p LNA inhibitors were transfected into NCI-H727 cells. These inhibitors should therefore down-regulate the high endogenous miR-375, previously found in the NCI-H727cell line and cease the suppression on the protein. Whether miR-7-5p is increased in NCI-H727 is still an open question, however the suppression of RBP-Jκ by miR-7-5p was assessed. At 6, 12, 48 and 72 hours after transfection, cell were subject to western blot using antibodies directed against RBP-Jκ and GAPDH which was used as internal control. As shown in Figure 23, ectopic expression of the LNA inhibitors for miR-375 or miR-7-5p did not cause any increase on the RBP-Jκ expression when compared with cells transfected with siGLO at defined transfection hours. However these results have not been independently confirmed by qPCR due to lack of time.
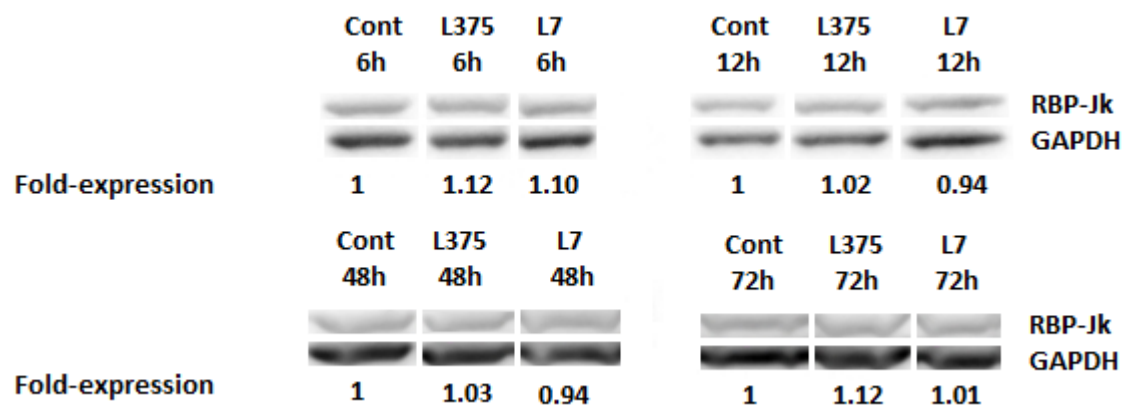
Figure 23: Western blot analysis in NCI-H727 cell line. NCI-H727 cells were treated with 50 mM siGLO (Cont), hsa-miR-375 LNA inhibitor (L375) or hsa-miR-7-5p LNA inhibitor (L7) and harvest after 6, 12, 48 and 72 hours. Antibodies directed against RBP-Jκ and GAPDH proteins were used to visualize the bands and fold-expression was calculated. All experiments were performed as duplicates.

5   Discussion

5.1   MicroRNA-375 and microRNA-7-5p is overexpressed in GEP-NET tumor tissue

In contrast to many other tumor types, the current knowledge about miRNA expression pattern in GEP-NETs is very little. Like coding genes, miRNA can either be up- or down regulated and act as oncogene or tumor suppressor, based on the downstream target that the miRNA controls[495]. There are miRNAs that are generally found over-expressed in cancers and therefore act as general oncogenes; particularly miR-21 is highly upregulated in many cancer tissues[496,497], other miRNAs are more specific oncogenes such as miR-125, miR-133a and miR-99 between PNETs and pancreatic acinar carcinoma[457]. According to others, miR-375 and miR-7-5p are found to be down-regulated in several types of cancers, including gastric-, liver carcinoma and colorectal cancer. In the present study it was shown that several miRNAs are differentially expressed in primary NETs compared to corresponding normal tissues. Among these differentially expressed miRNAs, miR-375 was upregulated in most carcinoid cell lines *in vitro*, which was independently confirmed by LCM of carcinoid tissue (Figure 18 and Figure 16J). These results are in good agreement with previously reported cases of miR-375 expression in SCLC cell line and different types of PNETs, including insulinomas and NF PNETs[457,464], and miR-7-5p in colonic carcinoids[454].

In the introduction it was argued that NETs of the GI-tract and pancreas (GEP-NETs) are caused by malignant transformation of neuroendocrine cells. In this thesis, expression of miR-375 and miR-7-5p were found to be highly restricted to endocrine cells of normal tissue, but also tumor tissue of ileum and colon carcinoids, NF PNET, insulinoma and VIPoma using *in situ* hybridization technique (Figure 16- and Figure 17B, E, H, C, F and I). Therefore it was suspected that the down-regulation observed in other cancer types does not reflect a down-regulation of miR-375 and miR-7-5p in cancer, but rather reflect absence of endocrine cells in the cancer tissue. Thus experiments trying to induce miR-375 or miR-7-5p do not make biological sense as they are trying to induce something which is not naturally present in the cancer. Moreover identification of targets in these cases is not relevant given the artificial setup. This research highlights the importance of not only determining expression levels but also the cellular origin of the gene expression. When examining alterations in gene expression using tissue homogenates it is important to differentiate between changes caused by the amount of RNA/protein in each cell and changes caused by the number of cells expressing the gene.

5.2 MicroRNA-375 and microRNA-7-5p overexpression may be related to secretory hyperplasia

Different pathways are thought to influence neuroendocrine tumorigenesis. The PI3K/AKT/mTOR pathway has been suggested to be involved in PNET tumorigenesis and progression. Hyper activation of Akt and mTOR due to gain or loss of mediators has been observed in large numbers of human cancers[498]. Particularly, inhibitors of the mTOR pathway, TSC2 and PTEN are observed to be lost in 30-60% of PNETs cases. Furthermore low expression of either TSC2 or PTEN correlates with significantly poorer prognosis and overall survival rate, given the higher tumor aggressiveness, Ki67 index, non-functional status and presence of liver metastasis at diagnosis that is present[499]. Other pathways are the growth factor signaling pathways, such as VEGF, TGFβ and IGF1/2, which are found to be overexpressed in different types of GEP-NETs[500–502].

In this thesis, I examined if miR-375 and miR-7-5p regulates the Notch signaling pathway by directly targeting RBP-Jκ. As mentioned in the introduction, RBP-Jκ is a known downstream factor of the Notch cascade which is important for transducing the signal between Notch activated component, NICD and Hes1 target repression of neuroendocrine differentiation. These miRNAs showed to interact with the 7mer target site located in the 3'UTR of RBP-Jκ, suggesting that mRNA of RBP-Jκ is post-translationally inhibited by miR-375 and miR-7-5p. The miR-375 possibly targeting 7mer site on RBP-Jκ was proposed using global analysis of the number of possible 6- and 7mer target sites and KEGG pathway enrichment. It was found that the target 7mer sites showed to be not significant due to the number of 7mer sites was very low, suggesting 7mer target sites to be more specific than the 6mer sites. Among the sites, RBP-Jκ was predicted as a target of miR-375. It should be mentioned however that the global analysis was only done for miR-375 in NCI-H727, but not miR-7-5p.

Genetic depletion studies of Notch components, including RBP-Jκ results in decrease proliferation of intestinal cells of the crypt and induce secretory cell hyperplasia[127,130,503]. Secretory cells hyperplasia in the intestine were also seen in mice defective for protein fucosylation, important for Notch receptor and ligand interactions[504]. As Notch activation is absent or low in several types of GEP-NETs[428,439] it was hypothesized that GEP-NETs can be caused by the absence of Notch components to regulate cell homeostasis. When Notch is not permitted, the lateral inhibition is abolished so progenitor cells within the epithelial compartment cannot influence nearby cells. Thus more progenitor cells differentiate into neuroendocrine cells as a consequence of proendocrine bHLH transcription factors, mainly Mash1, ngn3 and NeuroD are no longer inhibited. It is therefore proposed that the notable expression of miR-375 and miR-7-5p found

neuroendocrine cells of GEP-NETs may assist in directing progenitor cells to neuroendocrine cell fate through decreasing *Hes1* repression of bHLH transcriptions factors by targeting RBP-Jκ.

5.3   MicroRNA-375 and microRNA-7-5p effects growth in Carcinoid cell lines

In several types of non-neuroendocrine cancers the role miR-375 and miR-7-5p is to act as tumor suppressor where overexpression of miR-375 suppresses growth and inducing apoptosis[459,460,467,505]. In this thesis proliferation was investigated *in vitro* for NCI-H727 and CNDT2 to see if miR-375 and miR-7-5p affects growth. In NCI-H727, no variation in growth from the control was observed after inducing miR-375 or miR-7-5p, which may be explained by miR-375 already overexpressed in these cells. Instead inhibition of miR-375 showed to increase proliferation significantly. It was therefore speculated that the increase in growth, could be because miR-375 is no longer inhibiting Notch expression. Thus cells are switching from differentiation to a proliferative state. The opposite was true for CNDT2 cell lines, cells with induced miR-375 and miR-7-5p expression, increased proliferation, while inhibition of miR-375 showed no difference of growth compared to control cells. The difference between NCI-H727 and CNDT2 could be caused by the different expression of miR-375 (Figure 18) and possibly miR-7-5p, which was not examined. Therefore the authenticity of CNDT2 as a human midgut carcinoid cell line can be questioned, since this cell line resembles more carcinoma (low miR-375 expression) than NETs in tissue with high miR-375 expression. Others have questioned the authenticity of CNDT2 mainly because it do not express CgA, which is a fundamental protein in cell of endocrine phenotype[478].

5.4   MicroRNA-375 and microRNA-7-5p as potential biomarkers

The majority of GEP-NETs reveal no notable symptoms where the rest are often related to syndromes caused by tumors-related excess hormone production and secretion[506]. Early detection increases the chances for successful treatment and therefore biomarkers for early diagnosis and disease outcome are of great importance[507]. There are a vast number of potential biomarkers for GEP-NETs, including CgA which is often considered as a universal marker of this disease[294,508,509] and miRNA have a great potential in GEP-NETs as predictive and prognostic biomarker or as therapeutics[510].

Although a growing number of potential oncogenic and tumor suppressor miRNAs have been identified, the use of miRNAs as biomarkers are currently not available for diagnostic purposes[511]. In this thesis, the use of miR-375 and miR-7-5p as biomarkers for early detection and diagnostic of GEP-NETs was not investigated, however these miRs showed to hold a great potential compared to the novel biomarker CgA. As previously said high level of miR-375 expression was found in carcinoid tissues of the intestine, cut and captured with LCM. Similarly, high expression levels of CgA were previously detected in gastric and small intestine carcinoids by RT-PCR[512]. Furthermore *in situ* hybridization argues that both these miRs are highly endocrine

specific when compared to CgA immunohistochemistry, suggesting that these miRs are found in neuroendocrine cells throughout the gastroenteropancreatic tract, but not in non-endocrine cells. This is supported by the observation that miR-375 and miR-7-5p are both highly expressed in pancreatic islets[513] and PNETs[457], but decreased in non-neuroendocrine cancers, such as gastric carcinoma[514,515] and colorectal cancer[516,517]. Biomarkers used today for diagnosis, includes CgA, NSE and Synaptophysin are markers present in terminally differentiated endocrine cells, thus progenitor cells that are in the process of endocrine differentiation cannot be identified by these markers, since they are not able to synthesis or secrete hormones. This limits the use of some of these biomarkers in poorly differentiated GEP-NETs with high Ki67 proliferation index where dedifferentiation is abundantly present[191]. In contrast it is proposed that miR-375 and miR-7-5p are both markers of endocrine lineage and involved in regulating the endocrine differentiation. Using these markers may decrease the risk of GEP-NETs to lose markers that are inherited to the endocrine phenotype and differentiation.

To further determine the use of miR-375 and miR-7-5p as biomarkers, the expression levels of these has first to be detected in plasma or serum of GEP-NETs patients and healthy controls to verify that these are present in the circulation and are differentially expressed in cancer patients. Then differentially expressed miRs in plasma or serum has to be exploited prognostic and diagnostically by correlating them with demographic data, such as survival time or risk of metastasis. Also the correlation between circulating miR levels in response to treatment is useful to predict miRs as biomarkers[518,519].

6 Concluding remarks

In this thesis, I have characterized the differential expression of miRNAs between tumor and surrounding normal tissue. However, the expression profile was limited to only small intestine carcinoids, thus did not include other GEP-NETs. Among the most expressed miRNAs, I chose miR-375 and miR-7-5p because there are previously reported to affect endocrine differentiation. LCM and real-time RT-PCR confirmed the up-regulation of miR-375 in carcinoid tissue and *in situ* hybridization revealed; miR-375 and miR-7-5p were only present in endocrine cells (CgA+ cells) of normal and tumor tissue. Thus, I conclude that in carcinoid tissue is miR-375 upregulated and these two miRs cellular expression is limited to endocrine cells. Because of their specific cellular location miR-375 and miR-7-5p may be used as a more sensitive and specific biomarker than conventional endocrine markers such as CgA and Synaptophysin for clinical diagnosis of GEP-NETs.

As a model system for cellular growth *in vitro*, the carcinoid cell lines; NCI-H727 and CNDT2 were chosen because of their differences in endogenous expression of miR-375. Not surprisingly miR-375 and miR-7-5p up-regulation in NCI-H727 did not result in increase of growth, however it's down-regulation did. Conversely, up-regulation of miR-375 and miR-7-5p in CNDT2 increased growth, but not inhibition of miR-375, I conclude that miR-375 affects growth in these tumors. Finally, I examine pathways and a potential target for these miRs. Global analysis of targets after NCI-H727 was transfected with miR-375 revealed that 7mer targets were more specific, and miR-375 targets Notch signaling pathway, Insulin signaling pathway and mTOR pathway. As Notch signaling pathway is important for enteroendocrine differentiation in the small intestine, miR-375 main target was RBP-Jκ. I did not evaluate miR-7-5p pathways or targets. A Dual-luciferase reporter assay revealed that miR-375 and miR-7-5p binds to the 7mer 3'UTR site of RBP-Jκ. However, I was unsuccessful in showing that these miRs inhibit protein levels of RBP-Jκ in NCI-H727 by western blot. I conclude that these miRs may be important for endocrine differentiation in tumors by negatively regulate RBP-Jκ and keeping endocrine progenitor cells in differential state.

7 Perspectives

In future studies it could be interesting to elucidate if miR-375 and miR-7-5p are involved in endocrine differentiation by investigating their behavior in the gut. This could be done using transgenic mice containing a GFP construct with miR-375[461] or miR-7-5p mouse locus. Then paraffinized sections of the whole length of the small intestine could be retrieved and immunofluorescent stained with anti-bodies for GFP and CgA to see for co-localization. Other secretory cell types could also be stained to exclude the possibility of the miR appear in other terminally differentiated cells, but not progenitor cells.

In respect to investigate miR-375 and miR-7-5p activation of the Notch modulator, RBP-Jκ it could be interesting to perform the Cignal Reporter luciferase assay (Qiagen) were the reporter, containing an inducible transcription factor responsive construct, under the control of a basal promoter element (TATA box) is downstream to several tandem repeats of RBP-Jκ transcriptional response elements (TRE). For normalization, a constitutive expressing Renilla construct, under control of CMV promoter is used as internal control. Using this type of assay I will be able to confirm our results that RBP-Jκ expression is down-regulated by miR-375 and miR-7-5p, during direct repression of the firefly luciferase reporter transcription that is mediated by miRNA binding to the TRE sequence. In addition qPCR measurements of miR-375, miR-7-5p and RBP-Jκ transcript in NCI-H727 cells transfected with respective miR LNA inhibitor could be helpful in confirming target inhibition.

To investigate how these miRs regulate endocrine cell development, chicken embryos can be electroporated with plasmid construct containing the miR controlled by wild-type or mutant NeuroD promoter. Then frozen sections of the gut at different time periods can be obtained and visualized by immunohistochemistry to see if there are any changes in endocrine cells development. Furthermore it would be interesting to examine the biomarker potential of these miRs in patients with untreated GEP-NETs. This could be done by taking plasma samples from a large cohort of age- and gender matched healthy individuals and GEP-NET patients in different stages of the disease (G1, G2 and G3). RNA is extracted from plasma and miR-375 and miR-7-5p expression can be measured by qPCR and normalized with internal controls. The correlation between miR expression in normal and GEP-NET patients or different clinical stages of GEP-NETs can be analyzed by Wilcoxon two-sample tests[520]. Furthermore validation as biomarker can be performed by determining the sensitivity and specificity of the miR as biomarker and its ability to predict prognosis.

8 Reference

1. Rennert, H. & Fischer, R. T. Generation of Regulatory Oxysterols: 26-Hydroxylation of Cholesterol by Ovarian Mitochondria. *Endocrinology* **127,** 738–746 (1990).

2. Smith, P. D., Ochsenbauer-Jambor, C. & Smythies, L. E. Intestinal macrophages: Unique effector cells of the innate immune system. *Immunological Reviews* **206,** 149–159 (2005).

3. Tore, F. & Tuncel, N. Mast cells: target and source of neuropeptides. *Curr. Pharm. Des.* **15,** 3433–3445 (2009).

4. Grube, D. The endocrine cells of the digestive system: amines, peptides, and modes of action. *Anat. Embryol. (Berl).* 151–162 (1986).

5. Loevner, L. A. Imaging of the thyroid gland. *Semin. Ultrasound, CT MRI* **124,** 82–88 (1996).

6. Kershaw, E. E. & Flier, J. S. Adipose tissue as an endocrine organ. *J. Clin. Endocrinol. Metab.* **89,** 2548–2556 (2004).

7. Rindi, G., Leiter, A. B., Kopin, A. S., Bordi, C. & Solcia, E. The 'Normal' Endocrine Cell of the Gut: Changing Concepts and New Evidences. *Ann. N. Y. Acad. Sci.* **1014,** 1–12 (2004).

8. Modlin, I. M., Champaneria, M. C., Bornschein, J. & Kidd, M. Evolution of the diffuse neuroendocrine system-clear cells and cloudy origins. *Neuroendocrinology* **84,** 69–82 (2006).

9. Capen, C. C. in *Cancer Cytogenetics* 607–609 (2008). doi:10.1002/9780470376928

10. Karabchevsky, A., Tsapovsky, L., Marks, R. & Abdulhalim, I. Study of Immobilization Procedure on Silver Nanolayers and Detection of Estrone with Diverged Beam Surface Plasmon Resonance (SPR) Imaging. *Biosensors* **3,** 157–170 (2013).

11. Kondo, S. *et al.* Somatostatin inhibits gastrin-induced histamine secretion and synthesis in the rat. *Regul. Pept.* **48,** 373–380 (1993).

12. Sandvik, A. K., Dimaline, R., Forster, E. R., Evans, D. & Dockray, G. J. Differential control of somatostatin messenger RNA in rat gastric corpus and antrum. Role of acid, food, and capsaicin-sensitive afferent neurons. *J. Clin. Invest.* **91,** 244–250 (1993).

13. Yang, L., Ji, W., Xue, Y. & Chen, L. Imaging beta-cell mass and function in situ and in vivo. *J. Mol. Med.* **91,** 929–938 (2013).

14. Thomas-Reetz, A. C. & De Camilli, P. A role for synaptic vesicles in non-neuronal cells: clues from pancreatic beta cells and from chromaffin cells. *FASEB J.* **8,** 209–216 (1994).

15. Silver, M. M., Hearn, S. A., Lines, L. D. & Troster, M. Calcitonin and chromogranin A localization in medullary carcinoma of the thyroid by immunoelectron microscopy. *J. Histochem. Cytochem.* **36,** 1031–1036 (1988).

16.   O'Connor, D. T. & Deftos, L. J. Secretion of chromogranin A by peptide-producing endocrine neoplasms. *N. Engl. J. Med.* **314,** 1145–1151 (1986).

17.   Fischer-Colbrie, R., Hagn, C. & Schober, M. Chromogranins A, B, and C: widespread constituents of secretory vesicles. *Ann. N. Y. Acad. Sci.* **493,** 120–134 (1987).

18.   Munoz, D. G., Kobylinski, L., Henry, D. D. & George, D. H. Chromogranin A-like immunoreactivity in the human brain: Distribution in bulbar medulla and cerebral cortex. *Neuroscience* **34,** 533–543 (1990).

19.   Schmid, G. M. *et al.* Inhibition of insulin secretion by betagranin, an N-terminal chromogranin A fragment. *J. Biol. Chem.* **282,** 12717–12724 (2007).

20.   Hertelendyl, I., Patei, D. G. & Knitte, J. J. Pancreastatin inhibits insulin secretion in RlNmSF cells through obstruction of mediated, directed exocytosis. **19,** 125–132 (1996).

21.   Kim, T., Tao-Cheng, J. H., Eiden, L. E. & Loh, Y. P. Chromogranin A, an 'on/off' switch controlling dense-core secretory granule biogenesis. *Cell* **106,** 499–509 (2001).

22.   Azar, Y. & Eyal-Giladi, H. Interaction of epiblast and hypoblast in the formation of the primitive streak and the embryonic axis in chick, as revealed by hypoblast-rotation experiments. *J. Embryol. Exp. Morphol.* **61,** 133–144 (1981).

23.   Schoenwolf, G., Bleyl, S., Brauer, P. & Francis-West, P. *Larsen's Human Embryology.* (Churchill Livingstone Elsevier, 2008).

24.   Conlon, F. L. *et al.* A primary requirement for nodal in the formation and maintenance of the primitive streak in the mouse. *Development* **120,** 1919–1928 (1994).

25.   Aoki, T. O. *et al.* Molecular integration of casanova in the Nodal signalling pathway controlling endoderm formation. *Development* **129,** 275–286 (2002).

26.   Liu, P. *et al.* Requirement for Wnt3 in vertebrate axis formation. *Nat. Genet.* **22,** 361–365 (1999).

27.   Sun, X., Meyers, E. N., Lewandoski, M. & Martin, G. R. Targeted disruption of Fgf8 causes failure of cell migration in the gastrulating mouse embryo. *Genes Dev.* **13,** 1834–1846 (1999).

28.   Duband, J. L., Monier, F., Delannet, M. & Newgreen, D. Epithelium-mesenchyme transition during neural crest development. *Acta Anat. (Basel).* **154,** 63–78 (1995).

29.   Villanueva, S., Glavic, A., Ruiz, P. & Mayor, R. Posteriorization by FGF, Wnt, and retinoic acid is required for neural crest induction. *Dev. Biol.* **241,** 289–301 (2002).

30.   Grapin-Botton, A. & Melton, D. A. Endoderm development: From patterning to organogenesis. *Trends in Genetics* **16,** 124–130 (2000).

31.   Kanai-Azuma, M. *et al.* Depletion of definitive gut endoderm in Sox17-null mutant mice. *Development* **129,** 2367–2379 (2002).

32.   Som, P. M. & Naidich, T. P. Illustrated review of the embryology and development of the facial region, part 1: Early face and lateral nasal cavities. *Am. J. Neuroradiol.* **34,** 2233–2240 (2013).

33. Nievelstein, R. A., van der Werff, J. F., Verbeek, F. J., Valk, J. & Vermeij-Keers, C. Normal and abnormal embryonic development of the anorectum in human embryos. *Teratology* **57,** 70–78 (1998).

34. Fagman, H. & Nilsson, M. Morphogenetics of early thyroid development. *J. Mol. Endocrinol.* **46,** R33–R42 (2010).

35. Grosse, A. S. *et al.* Cell dynamics in fetal intestinal epithelium: implications for intestinal growth and morphogenesis. *Development* **138,** 4423–4432 (2011).

36. Saotome, I., Curto, M. & McClatchey, A. I. Ezrin is essential for epithelial organization and villus morphogenesis in the developing intestine. *Dev. Cell* **6,** 855–864 (2004).

37. Ockleford, C. D., Wakely, J. & Badley, R. A. Morphogenesis of human placental chorionic villi: cytoskeletal, syncytioskeletal and extracellular matrix proteins. *Proc. R. Soc. Lond. B. Biol. Sci.* **212,** 305–316 (1981).

38. Powell, D. W., Pinchuk, I. V, Saada, J. I., Chen, X. & Mifflin, R. C. Mesenchymal cells of the intestinal lamina propria. *Annu. Rev. Physiol.* **73,** 213–237 (2011).

39. Schröder, N. & Gossler, A. Expression of Notch pathway components in fetal and adult mouse small intestine. *Gene Expr. patterns* **2,** 247–250 (2002).

40. Jensen, J. *et al.* Control of endodermal endocrine development by Hes-1. *Nat. Genet.* **24,** 36–44 (2000).

41. Bettess, M. D. *et al.* c-Myc is required for the formation of intestinal crypts but dispensable for homeostasis of the adult intestinal epithelium. *Mol. Cell. Biol.* **25,** 7868–7878 (2005).

42. Wallace, K. N., Akhter, S., Smith, E. M., Lorent, K. & Pack, M. Intestinal growth and differentiation in zebrafish. *Mech. Dev.* **122,** 157–173 (2005).

43. Crosnier, C., Stamataki, D. & Lewis, J. Organizing cell renewal in the intestine: stem cells, signals and combinatorial control. *Nat. Rev. Genet.* **7,** 349–359 (2006).

44. Ramalho-Santos, M., Melton, D. A. & McMahon, A. P. Hedgehog signals regulate multiple aspects of gastrointestinal development. *Development* **127,** 2763–2772 (2000).

45. Madison, B. B. *et al.* Epithelial hedgehog signals pattern the intestinal crypt-villus axis. *Development* **132,** 279–289 (2005).

46. Karlsson, L., Lindahl, P., Heath, J. K. & Betsholtz, C. Abnormal gastrointestinal development in PDGF-A and PDGFR-(alpha) deficient mice implicates a novel mesenchymal structure with putative instructive properties in villus morphogenesis. *Development* **127,** 3457–3466 (2000).

47. Roberts, D. Molecular mechanisms of development of the gastrointestinal tract. *Dev. Dyn.* **120,** 109–120 (2000).

48. Auclair, B. A., Benoit, Y. D., Rivard, N., Mishina, Y. & Perreault, N. Bone morphogenetic protein signaling is essential for terminal differentiation of the intestinal secretory cell lineage. *Gastroenterology* **133,** 887–896 (2007).

49. Bienz, M. & Clevers, H. Linking colorectal cancer to Wnt signaling. *Cell* **103,** 311–320 (2000).

50. Booth, C., Brady, G. & Potten, C. S. Crowd control in the crypt. *Nat. Med.* **8,** 1360–1361 (2002).

51. He, X. C. *et al.* BMP signaling inhibits intestinal stem cell self-renewal through suppression of Wnt-beta-catenin signaling. *Nat. Genet.* **36,** 1117–1121 (2004).

52. Ahlman, H. & Nilsson. The gut as the largest endocrine organ in the body. *Ann. Oncol.* **12,** S63–S68 (2001).

53. Rehfeld, J. F. The new biology of gastrointestinal hormones. *Physiol. Rev.* **78,** 1087–1108 (1998).

54. Turner, J. R. Intestinal mucosal barrier function in health and disease. *Nat. Rev. Immunol.* **9,** 799–809 (2009).

55. Trier, J. S. & Rubin, C. E. Electron microscopy of the small intestine: a review. *Gastroenterology* **49,** 574–603 (1965).

56. Gabella, G. The cross-ply arrangement of collagen fibres in the submucosa of the mammalian small intestine. *Cell Tissue Res.* **248,** 491–497 (1987).

57. Krause, W. J. Brunner's glands: a structural, histochemical and pathological profile. *Prog. Histochem. Cytochem.* **35,** 259–367 (2000).

58. Cheng, H. & Leblond, C. P. Origin, differentiation and renewal of the four main epithelial cell types in the mouse small intestine. I. Columnar cell. *Am. J. Anat.* **141,** 461–479 (1974).

59. Schubert, M. L. & Peura, D. A. Control of gastric acid secretion in health and disease. *Gastroenterology* **134,** 1842–1860 (2008).

60. Bevins, C. L. & Salzman, N. H. Paneth cells, antimicrobial peptides and maintenance of intestinal homeostasis. *Nat. Rev. Microbiol.* **9,** 356–368 (2011).

61. Barker, N. *et al.* Identification of stem cells in small intestine and colon by marker gene Lgr5. *Nature* **449,** 1003–1007 (2007).

62. Potten, C. S. Stem cells in gastrointestinal epithelium: numbers, characteristics and death. *Philos. Trans. R. Soc. Lond. B. Biol. Sci.* **353,** 821–830 (1998).

63. Kaur, P. & Potten, C. S. Cell migration velocities in the crypts of the small intestine after cytotoxic insult are not dependent on mitotic activity. *Cell Tissue Kinet.* **19,** 601–610 (1986).

64. Bjerknes, M. & Cheng, H. The stem-cell zone of the small intestinal epithelium. III. Evidence from columnar, enteroendocrine, and mucous cells in the adult mouse. *Am. J. Anat.* **160,** 77–91 (1981).

65. Marshman, E., Booth, C. & Potten, C. S. The intestinal epithelial stem cell. *BioEssays* **24,** 91–98 (2002).

66. Cheng, H., Merzel, J. & Leblond, C. P. Renewal of Paneth cells in the small intestine of the mouse. *Am. J. Anat.* **126,** 507–525 (1969).

67. Potten, C. S. Extreme sensitivity of some intestinal crypt cells to X and [gamma] irradiation. *Nature* **269,** 518–521 (1977).

68. Potten, C. S., Owen, G. & Booth, D. Intestinal stem cells protect their genome by selective segregation of template DNA strands. *J. Cell Sci.* **115,** 2381–2388 (2002).

69. Van der Flier, L. G. *et al.* The Intestinal Wnt/TCF Signature. *Gastroenterology* **132,** 628–632 (2007).

70. Hsu, S. Y., Liang, S. G. & Hsueh, A. J. Characterization of two LGR genes homologous to gonadotropin and thyrotropin receptors with extracellular leucine-rich repeats and a G protein-coupled, seven-transmembrane region. *Mol. Endocrinol.* **12,** 1830–1845 (1998).

71. Carmon, K. S., Gong, X., Lin, Q., Thomas, A. & Liu, Q. R-spondins function as ligands of the orphan receptors LGR4 and LGR5 to regulate Wnt/beta-catenin signaling. *Proc. Natl. Acad. Sci. U. S. A.* **108,** 11452–11457 (2011).

72. De Lau, W. *et al.* Lgr5 homologues associate with Wnt receptors and mediate R-spondin signalling. *Nature* **476,** 293–297 (2011).

73. Kim, T. H., Escudero, S. & Shivdasani, R. A. Intact function of Lgr5 receptor-expressing intestinal stem cells in the absence of Paneth cells. *Proc. Natl. Acad. Sci.* **109,** 3932–3937 (2012).

74. Potten, C. S. Radiation, the ideal cytotoxic agent for studying the cell biology of tissues such as the small intestine. *Radiat. Res.* **161,** 123–136 (2004).

75. Sato, T. *et al.* Single Lgr5 stem cells build crypt-villus structures in vitro without a mesenchymal niche. *Nature* **459,** 262–265 (2009).

76. Sato, T. *et al.* Paneth cells constitute the niche for Lgr5 stem cells in intestinal crypts. *Nature* **469,** 415–418 (2011).

77. Lopez-Garcia, C., Klein, A. M., Simons, B. D. & Winton, D. J. Intestinal stem cell replacement follows a pattern of neutral drift. *Science* **330,** 822–825 (2010).

78. Snippert, H. J. *et al.* Intestinal crypt homeostasis results from neutral competition between symmetrically dividing Lgr5 stem cells. *Cell* **143,** 134–144 (2010).

79. Uchida, T., Takada, T., Ammori, B. J., Suda, K. & Takahashi, T. Three-dimensional reconstruction of the ventral and dorsal pancreas: a new insight into anatomy and embryonic development. *J. Hepatobiliary. Pancreat. Surg.* **6,** 176–180 (1999).

80. Slack, J. M. Developmental biology of the pancreas. *Development* **121,** 1569–1580 (1995).

81. Le Borgne, R., Bardin, A. & Schweisguth, F. The roles of receptor and ligand endocytosis in regulating Notch signaling. *Development* **132,** 1751–1762 (2005).

82. Weinmaster, G. & Fischer, J. A. Notch ligand ubiquitylation: what is it good for? *Dev. Cell* **21,** 134–144 (2011).

83. Fleming, R. J. Structural conservation of Notch receptors and ligands. *Semin. Cell Dev. Biol.* **9,** 599–607 (1998).

84. Henderson, S. T., Gao, D., Lambie, E. J. & Kimble, J. Lag-2 may encode a signaling ligand for the GLP-1 and LIN-12 receptors of C. elegans. *Development* **120,** 2913–2924 (1994).

85. Hukriede, N. A., Gu, Y. & Fleming, R. J. A dominant-negative form of Serrate acts as a general antagonist of Notch activation. *Development* **124,** 3427–3437 (1997).

86. Kopan, R. & Ilagan, M. X. The canonical Notch signaling pathway: unfolding the activation mechanism. *Cell* **137,** 216–233 (2009).

87. Rebay, I. *et al.* Specific EGF repeats of Notch mediate interactions with Delta and Serrate: implications for Notch as a multifunctional receptor. *Cell* **67,** 687–699 (1991).

88. Cordle, J. *et al.* Localization of the delta-like-1-binding site in human Notch-1 and its modulation by calcium affinity. *J. Biol. Chem.* **283,** 11785–11793 (2008).

89. Okajima, T. & Irvine, K. D. Regulation of notch signaling by o-linked fucose. *Cell* **111,** 893–904 (2002).

90. Okajima, T., Xu, A., Lei, L. & Irvine, K. D. Chaperone activity of protein O-fucosyltransferase 1 promotes notch receptor folding. *Science* **307,** 1599–1603 (2005).

91. Logeat, F. *et al.* The Notch1 receptor is cleaved constitutively by a furin-like convertase. *Proc. Natl. Acad. Sci. U. S. A.* **95,** 8108–8112 (1998).

92. Greenwald, I. & Seydoux, G. Analysis of gain-of-function mutations of the lin-12 gene of Caenorhabditis elegans. *Nature* **346,** 197–199 (1990).

93. Sanchez-irizarry, C. *et al.* Notch Subunit Heterodimerization and Prevention of Ligand-Independent Proteolytic Activation Depend, Respectively, on a Novel Domain and the LNR Repeats Notch Subunit Heterodimerization and Prevention of Ligand-Independent Proteolytic Activation Depend. *Mol. Cell. Biol.* **24,** 9265–9273 (2004).

94. Gordon, W. R. *et al.* Structural basis for autoinhibition of Notch. *Nat. Struct. Mol. Biol.* **14,** 295–300 (2007).

95. Schroeter, E. H., Kisslinger, J. A. & Kopan, R. Notch-1 signalling requires ligand-induced proteolytic release of intracellular domain. *Nature* **393,** 382–386 (1998).

96. De Strooper, B. *et al.* A presenilin-1-dependent gamma-secretase-like protease mediates release of Notch intracellular domain. *Nature* **398,** 518–522 (1999).

97. Struhl, G. & Adachi, A. Requirements for presenilin-dependent cleavage of notch and other transmembrane proteins. *Mol. Cell* **6,** 625–636 (2000).

98. Tousseyn, T. *et al.* ADAM10, the rate-limiting protease of regulated intramembrane proteolysis of Notch and other proteins, is processed by ADAMS-9, ADAMS-15, and the gamma-secretase. *J. Biol. Chem.* **284,** 11738–11747 (2009).

99. Kovall, R. A. & Hendrickson, W. A. Crystal structure of the nuclear effector of Notch signaling, CSL, bound to DNA. *EMBO J.* **23,** 3441–3451 (2004).

100. Tamura, K. *et al.* Physical interaction between a novel domain of the receptor Notch and the transcription factor RBP-J kappa/Su(H). *Curr. Biol.* **5,** 1416–1423 (1995).

101. Kato, H. *et al.* Involvement of RBP-J in biological functions of mouse Notch1 and its derivatives. *Development* **124,** 4133–4141 (1997).

102. Nam, Y., Weng, A. P., Aster, J. C. & Blacklow, S. C. Structural requirements for assembly of the CSL.intracellular Notch1.Mastermind-like 1 transcriptional activation complex. *J. Biol. Chem.* **278,** 21232–21239 (2003).

103. Kannabiran, C., Zeng, X. & Vales, L. The mammalian transcriptional repressor RBP (CBF1) regulates interleukin-6 gene expression. *Mol. Cell. Biol.* **17,** 1–10 (1997).

104. Kao, H. Y. *et al.* A histone deacetylase corepressor complex regulates the Notch signal transduction pathway. *Genes Dev.* **12,** 2269–2277 (1998).

105. Taniguchi, Y., Furukawa, T., Tun, T., Han, H. & Honjo, T. LIM protein KyoT2 negatively regulates transcription by association with the RBP-J DNA-binding protein. *Mol. Cell. Biol.* (1998).

106. Hsieh, J. J., Zhou, S., Chen, L., Young, D. B. & Hayward, S. D. CIR, a corepressor linking the DNA binding factor CBF1 to the histone deacetylase complex. *Proc. Natl. Acad. Sci. U. S. A.* **96,** 23–28 (1999).

107. Zhou, S. *et al.* SKIP, a CBF1-associated protein, interacts with the ankyrin repeat domain of NotchIC To facilitate NotchIC function. *Mol. Cell. Biol.* **20,** 2400–2410 (2000).

108. Dou, G. R. *et al.* RBP-J, the transcription factor downstream of Notch receptors, is essential for the maintenance of vascular homeostasis in adult mice. *FASEB J.* **22,** 1606–1617 (2008).

109. Wu, L. *et al.* MAML1, a human homologue of Drosophila mastermind, is a transcriptional co-activator for NOTCH receptors. *Nat. Genet.* **26,** 484–489 (2000).

110. Smoller, D. *et al.* The Drosophila neurogenic locus mastermind encodes a nuclear protein unusually rich in amino acid homopolymers. *Genes Dev.* **4,** 1688–1700 (1990).

111. Barrick, D. & Kopan, R. The Notch transcription activation complex makes its move. *Cell* **124,** 883–885 (2006).

112. Oswald, F. *et al.* p300 acts as a transcriptional coactivator for mammalian Notch-1. *Mol. Cell. Biol.* **21,** 7761–7774 (2001).

113. Fryer, C. J., Lamar, E., Turbachova, I., Kintner, C. & Jones, K. A. Mastermind mediates chromatin-specific transcription and turnover of the notch enhancer complex. *Genes Dev.* **16,** 1397–1411 (2002).

114. Wallberg, A. E., Pedersen, K., Lendahl, U. & Roeder, R. G. p300 and PCAF act cooperatively to mediate transcriptional activation from chromatin templates by notch intracellular domains in vitro. *Mol. Cell. Biol.* **22,** 7812–7819 (2002).

115. Gu, W. & Roeder, R. G. Activation of p53 sequence-specific DNA binding by acetylation of the p53 C-terminal domain. *Cell* **90,** 595–606 (1997).

116. Saint Just Ribeiro, M., Hansson, M. L. & Wallberg, A. E. A proline repeat domain in the Notch co-activator MAML1 is important for the p300-mediated acetylation of MAML1. *Biochem. J.* **404,** 289–298 (2007).

117. Popko-Scibor, A. E., Lindberg, M. J., Hansson, M. L., Holmlund, T. & Wallberg, A. E. Ubiquitination of Notch1 is regulated by MAML1-mediated p300 acetylation of Notch1. *Biochem. Biophys. Res. Commun.* **416,** 300–306 (2011).

118. Lai, E. C. Notch signaling: control of cell communication and cell fate. *Development* **131,** 965–973 (2004).

119. Cabrera, C. V. Lateral inhibition and cell fate during neurogenesis in Drosophila: the interactions between scute, Notch and Delta. *Development* **110,** 733–742 (1990).

120. Parks, A. L., Huppert, S. S. & Muskavitch, M. A. The dynamics of neurogenic signalling underlying bristle development in Drosophila melanogaster. *Mech. Dev.* **63,** 61–74 (1997).

121. Chitnis, A., Henrique, D., Lewis, J., Ish-Horowicz, D. & Kintner, C. Primary neurogenesis in Xenopus embryos regulated by a homologue of the Drosophila neurogenic gene Delta. *Nature* **375,** 761–766 (1995).

122. Adam, J. *et al.* Cell fate choices and the expression of Notch, Delta and Serrate homologues in the chick inner ear: parallels with Drosophila sense-organ development. *Development* **125,** 4645–4654 (1998).

123. Lee, C. S. & Kaestner, K. H. Clinical endocrinology and metabolism. Development of gut endocrine cells. *Best Pract. Res. Clin. Endocrinol. Metab.* **18,** 453–462 (2004).

124. Kageyama, R., Ohtsuka, T., Shimojo, H. & Imayoshi, I. Dynamic regulation of Notch signaling in neural progenitor cells. *Curr. Opin. Cell Biol.* **21,** 733–740 (2009).

125. Stamataki, D. *et al.* Delta1 expression, cell cycle exit, and commitment to a specific secretory fate coincide within a few hours in the mouse intestinal stem cell system. *PLoS One* **6,** 1–11 (2011).

126. Salic, A. & Mitchison, T. J. A chemical method for fast and sensitive detection of DNA synthesis in vivo. *Proc. Natl. Acad. Sci. U. S. A.* **105,** 2415–2420 (2008).

127. Riccio, O. *et al.* Loss of intestinal crypt progenitor cells owing to inactivation of both Notch1 and Notch2 is accompanied by derepression of CDK inhibitors p27Kip1 and p57Kip2. *EMBO Rep.* **9,** 377–383 (2008).

128. Crosnier, C. *et al.* Delta-Notch signalling controls commitment to a secretory fate in the zebrafish intestine. *Development* **132,** 1093–1104 (2005).

129. Milano, J. *et al.* Modulation of Notch processing by gamma-secretase inhibitors causes intestinal goblet cell metaplasia and induction of genes known to specify gut secretory lineage differentiation. *Toxicol. Sci.* **82,** 341–358 (2004).

130. Van Es, J. H. *et al.* Notch/gamma-secretase inhibition turns proliferative cells in intestinal crypts and adenomas into goblet cells. *Nature* **435,** 959–963 (2005).

131. Ueo, T. *et al.* The role of Hes genes in intestinal development, homeostasis and tumor formation. *Development* **139,** 1071–1082 (2012).

132. Yang, Q., Bermingham, N. A., Finegold, M. J. & Zoghbi, H. Y. Requirement of Math1 for secretory cell lineage commitment in the mouse intestine. *Science* **294,** 2155–2158 (2001).

133. Mutoh, H. *et al.* The basic helix-loop-helix transcription factor BETA2/NeuroD is expressed in mammalian enteroendocrine cells and activates secretin gene expression. *Proc. Natl. Acad. Sci. U. S. A.* **94,** 3560–3564 (1997).

134. Hansen, T. V. Cholecystokinin gene transcription: promoter elements, transcription factors and signaling pathways. *Peptides* **22,** 1201–1211 (2001).

135. Naya, F. J. *et al.* Diabetes, defective pancreatic morphogenesis, and abnormal enteroendocrine differentiation in BETA2/NeuroD-deficient mice. *Genes Dev.* **11,** 2323–2334 (1997).

136. Bjerknes, M. & Cheng, H. Gastrointestinal stem cells. II. Intestinal stem cells. *Am. J. Physiol. Gastrointest. Liver Physiol.* **289,** G381–G387 (2005).

137. Schonhoff, S. E., Giel-Moloney, M. & Leiter, A. B. Neurogenin 3-expressing progenitor cells in the gastrointestinal tract differentiate into both endocrine and non-endocrine cell types. *Dev. Biol.* **270,** 443–454 (2004).

138. Jenny, M. *et al.* Neurogenin3 is differentially required for endocrine cell fate specification in the intestinal and gastric epithelium. *EMBO J.* **21,** 6338–6347 (2002).

139. Korinek, V. *et al.* Depletion of epithelial stem-cell compartments in the small intestine of mice lacking Tcf-4. *Nat. Genet.* **19,** 379–383 (1998).

140. Pinto, D., Gregorieff, A., Begthel, H. & Clevers, H. Canonical Wnt signals are essential for homeostasis of the intestinal epithelium. *Genes Dev.* **17,** 1709–1713 (2003).

141. Andreu, P. *et al.* Crypt-restricted proliferation and commitment to the Paneth cell lineage following Apc loss in the mouse intestine. *Development* **132,** 1443–1451 (2005).

142. Sansom, O. J. *et al.* Loss of Apc in vivo immediately perturbs Wnt signaling, differentiation, and migration. *Genes Dev.* **18,** 1385–1390 (2004).

143. Ohlsson, H., Karlsson, K. & Edlund, T. IPF1, a homeodomain-containing transactivator of the insulin gene. *EMBO J.* **12,** 4251–4259 (1993).

144. Gradwohl, G., Dierich, A., LeMeur, M. & Guillemot, F. Neurogenin3 Is Required for the Development of the Four Endocrine Cell Lineages of the Pancreas. *Proc. Natl. Acad. Sci. U. S. A.* **97,** 1607–1611 (2000).

145. Ahlgren, U., Jonsson, J. & Edlund, H. The morphogenesis of the pancreatic mesenchyme is uncoupled from that of the pancreatic epithelium in IPF1/PDX1-deficient mice. *Development* **122,** 1409–1416 (1996).

146. Ahlgren, U., Pfaff, S. L., Jessell, T. M., Edlund, T. & Edlund, H. Independent requirement for ISL1 in formation of pancreatic mesenchyme and islet cells. *Nature* **385,** 257–260 (1997).

147. Hart, A., Papadopoulou, S. & Edlund, H. Fgf10 maintains notch activation, stimulates proliferation, and blocks differentiation of pancreatic epithelial cells. *Dev. Dyn.* **228,** 185–193 (2003).

148. Jensen, J. *et al.* Independent development of pancreatic alpha- and beta-cells from neurogenin3-expressing precursors: a role for the notch pathway in repression of premature differentiation. *Diabetes* **49,** 163–176 (2000).

149. Apelqvist, A. *et al.* Notch signalling controls pancreatic cell differentiation. *Nature* **400,** 877–881 (1999).

150. Fujikura, J. *et al.* Notch/Rbp-j signaling prevents premature endocrine and ductal cell differentiation in the pancreas. *Cell Metab.* **3,** 59–65 (2006).

151. Sasai, Y., Kageyama, R., Tagawa, Y., Shigemoto, R. & Nakanishi, S. Two mammalian helix-loop-helix factors structurally related to Drosophila hairy and Enhancer of split. *Genes Dev.* **6,** 2620–2634 (1992).

152. Ishibashi, M. *et al.* Persistent expression of helix-loop-helix factor HES-1 prevents mammalian neural differentiation in the central nervous system. *EMBO J.* **13,** 1799–1805 (1994).

153. Grapin-Botton, A., Majithia, A. R. & Melton, D. A. Key events of pancreas formation are triggered in gut endoderm by ectopic expression of pancreatic regulatory genes. *Genes Dev.* **15,** 444–454 (2001).

154. Gasa, R. *et al.* Induction of pancreatic islet cell differentiation by the neurogenin-neuroD cascade. *Differentiation.* **76,** 381–391 (2008).

155. Sussel, L. *et al.* Mice lacking the homeodomain transcription factor Nkx2.2 have diabetes due to arrested differentiation of pancreatic beta cells. *Development* **125,** 2213–2221 (1998).

156. Sander, M. *et al.* Homeobox gene Nkx6.1 lies downstream of Nkx2.2 in the major pathway of beta-cell formation in the pancreas. *Development* **127,** 5533–5540 (2000).

157. Heremans, Y. *et al.* Recapitulation of embryonic neuroendocrine differentiation in adult human pancreatic duct cells expressing neurogenin 3. *J. Cell Biol.* **159,** 303–312 (2002).

158. Sosa-Pineda, B., Chowdhury, K., Torres, M., Oliver, G. & Gruss, P. The Pax4 gene is essential for differentiation of insulin-producing beta cells in the mammalian pancreas. *Nature* **386,** 399–402 (1997).

159. Lu, C. *et al.* Elucidation of the small RNA component of the transcriptome. *Science* **309,** 1567–1569 (2005).

160. Lee, Y. *et al.* MicroRNA genes are transcribed by RNA polymerase II. *EMBO J.* **23,** 4051–4060 (2004).

161. Borchert, G. M., Lanier, W. & Davidson, B. L. RNA polymerase III transcribes human microRNAs. *Nat. Struct. Mol. Biol.* **13,** 1097–1101 (2006).

162. Lee, Y. *et al.* The nuclear RNase III Drosha initiates microRNA processing. *Nature* **425,** 415–419 (2003).

163. Zeng, Y. & Cullen, B. R. Sequence requirements for micro RNA processing and function in human cells. *RNA* **9,** 112–123 (2003).

164. Bohnsack, M. T., Czaplinski, K. & Gorlich, D. Exportin 5 is a RanGTP-dependent dsRNA-binding protein that mediates nuclear export of pre-miRNAs. *RNA* **10,** 185–191 (2004).

165. Lund, E., Güttinger, S., Calado, A., Dahlberg, J. E. & Kutay, U. Nuclear export of microRNA precursors. *Science* **303,** 95–98 (2004).

166. Zeng, Y. & Cullen, B. R. Structural requirements for pre-microRNA binding and nuclear export by Exportin 5. *Nucleic Acids Res.* **32,** 4776–4785 (2004).

167. Yi, R., Qin, Y., Macara, I. G. & Cullen, B. R. Exportin-5 mediates the nuclear export of pre-microRNAs and short hairpin RNAs. *Genes Dev.* **17,** 3011–3016 (2003).

168. Lim, L. P. *et al.* The microRNAs of Caenorhabditis elegans. *Genes Dev.* **17,** 991–1008 (2003).

169. Kim, V. N. MicroRNA precursors in motion: Exportin-5 mediates their nuclear export. *Trends Cell Biol.* **14,** 156–159 (2004).

170. Hutvágner, G. *et al.* A cellular function for the RNA-interference enzyme Dicer in the maturation of the let-7 small temporal RNA. *Science* **293,** 834–838 (2001).

171. Ketting, R. F. *et al.* Dicer functions in RNA interference and in synthesis of small RNA involved in developmental timing in C. elegans. *Genes Dev.* **15,** 2654–2659 (2001).

172. Sasaki, T. & Shimizu, N. Evolutionary conservation of a unique amino acid sequence in human DICER protein essential for binding to Argonaute family proteins. *Gene* **396,** 312–320 (2007).

173. Macrae, I. J. *et al.* Structural basis for double-stranded RNA processing by Dicer. *Science* **311,** 195–198 (2006).

174. Song, J. J. *et al.* The crystal structure of the Argonaute2 PAZ domain reveals an RNA binding motif in RNAi effector complexes. *Nat. Struct. Biol.* **10,** 1026–1032 (2003).

175. Lee, Y. *et al.* The role of PACT in the RNA silencing pathway. *EMBO J.* **25,** 522–532 (2006).

176. Chendrimada, T. P. *et al.* TRBP recruits the Dicer complex to Ago2 for microRNA processing and gene silencing. *Nature* **436,** 740–744 (2005).

177. Haase, A. D. *et al.* TRBP, a regulator of cellular PKR and HIV-1 virus expression, interacts with Dicer and functions in RNA silencing. *EMBO Rep.* **6,** 961–967 (2005).

178. Forman, J. J., Legesse-Miller, A. & Coller, H. A. A search for conserved sequences in coding regions reveals that the let-7 microRNA targets Dicer within its coding sequence. *Proc. Natl. Acad. Sci. U. S. A.* **105,** 14879–14884 (2008).

179. Diederichs, S. & Haber, D. A. Dual Role for Argonautes in MicroRNA Processing and Posttranscriptional Regulation of MicroRNA Expression. *Cell* **131,** 1097–1108 (2007).

180. Song, J., Smith, S. K., Hannon, G. J. & Joshua-Tor, L. Crystal structure of Argonaute and its implications for RISC slicer activity. *Science* **305,** 1434–1437 (2004).

181. Liu, J. *et al.* Argonaute2 is the catalytic engine of mammalian RNAi. *Science* **305,** 1437–1441 (2004).

182. Robb, G. B. & Rana, T. M. RNA Helicase A Interacts with RISC in Human Cells and Functions in RISC Loading. *Mol. Cell* **26,** 523–537 (2007).

183. Meister, G. *et al.* Identification of novel argonaute-associated proteins. *Curr. Biol.* **15,** 2149–2155 (2005).

184. Salzman, D. W., Shubert-Coleman, J. & Furneaux, H. P68 RNA helicase unwinds the human let-7 microRNA precursor duplex and is required for let-7-directed silencing of gene expression. *J. Biol. Chem.* **282,** 32773–32779 (2007).

185. Nykänen, A., Haley, B. & Zamore, P. D. ATP requirements and small interfering RNA structure in the RNA interference pathway. *Cell* **107,** 309–321 (2001).

186. Khvorova, A., Reynolds, A. & Jayasena, S. D. Functional siRNAs and miRNAs exhibit strand bias. *Cell* **115,** 209–216 (2003).

187. Hutvágner, G. & Zamore, P. D. A microRNA in a multiple-turnover RNAi enzyme complex. *Science* **297,** 2056–2060 (2002).

188. Huang, Y. *et al.* Biological functions of microRNAs: A review. *Journal of Physiology and Biochemistry* **67,** 129–139 (2011).

189. Rindi, G. *et al.* Development of neuroendocrine tumors in the gastrointestinal tract of transgenic mice. Heterogeneity of hormone expression. *Am. J. Pathol.* **136,** 1349–1363 (1990).

190. Efrat, S., Teitelman, G., Anwar, M., Ruggiero, D. & Hanahan, D. Glucagon gene regulatory region directs oncoprotein expression to neurons and pancreatic alpha cells. *Neuron* **1,** 605–613 (1988).

191. Rindi, G., Villanacci, V. & Ubiali, A. Biological and molecular aspects of gastroenteropancreatic neuroendocrine tumors. *Digestion* **62,** 19–26 (2000).

192. Modlin, I. M. *et al.* Gastroenteropancreatic neuroendocrine tumours. *Lancet. Oncol.* **9,** 61–72 (2008).

193. Ramage, J. K. *et al.* Guidelines for the management of gastroenteropancreatic neuroendocrine (including carcinoid) tumours (NETs). *Gut* **61,** 6–32 (2012).

194. Barakat, M. T., Meeran, K. & Bloom, S. R. Neuroendocrine tumours. *Endocr. Relat. Cancer* **11,** 1–18 (2004).

195. Lawrence, B. *et al.* The epidemiology of gastroenteropancreatic neuroendocrine tumors. *Endocrinol. Metab. Clin. North Am.* **40,** 1–18 (2011).

196. Modlin, I. M., Lye, K. D. & Kidd, M. A 5-decade analysis of 13,715 carcinoid tumors. *Cancer* **97,** 934–959 (2003).

197. Ellis, L., Shale, M. J. & Coleman, M. P. Carcinoid tumors of the gastrointestinal tract: trends in incidence in England since 1971. *Am. J. Gastroenterol.* **105,** 2563–2569 (2010).

198. Oberndorfer, S. Karzinoide tumoren des dunndarms. *Frankfurt Z Pathol* **1,** 426–432 (1907).

199. Gosset, A. & Masson, P. Tumeurs endocrines de l'appendice. *Press. méd* **22,** 40 (1914).

200. Lembeck, F. 5-Hydroxytryptamine in a Carcinoid Tumour. *Nature* **172,** 910–911 (1953).

201. Thorson, Å., Biörck, G., Björkman, G. & Waldenström, J. Malignant carcinoid of the small intestine with metastases to the liver. *Am. Heart J.* **47,** 795–817 (1954).

202. Williams, E. The classification of carcinoid tumours. *Lancet* **281,** 238–239 (1963).

203. Klöppel, G., Heitz, P. U., Capella, C. & Solcia, E. The spectrum and classification of gastric and duodenal neuroendocrine tumours. *Curr. Diagnostic Pathol.* **2,** 10–14 (1995).

204. Klöppel, G., Heitz, P. U., Capella, C. & Solcia, E. Pathology and nomenclature of human gastrointestinal neuroendocrine (carcinoid) tumors and related lesions. *World J. Surg.* **20,** 132–141 (1996).

205. Capella, C., Heitz, P. U., Höfler, H., Solcia, E. & Klöppel, G. Revised classification of neuroendocrine tumours of the lung, pancreas and gut. *Virchows Arch.* **425,** 547–560 (1995).

206. Rindi, G. *et al.* TNM staging of foregut (neuro)endocrine tumors: a consensus proposal including a grading system. *Virchows Arch.* **449,** 395–401 (2006).

207. Solcia, E., Kloppel, G. & Sobin, L. *Histological Typing of Endocrine Tumours, World Health Organization International Histological Classification of Tumours*. (2000).

208. Ferrone, C. R. *et al.* Determining prognosis in patients with pancreatic endocrine neoplasms: can the WHO classification system be simplified? *J. Clin. Oncol.* **25,** 5609–5615 (2007).

209. Klöppel, G., Rindi, G., Perren, A., Komminoth, P. & Klimstra, D. S. The ENETS and AJCC/UICC TNM classifications of the neuroendocrine tumors of the gastrointestinal tract and the pancreas: a statement. *Virchows Arch.* **456,** 595–597 (2010).

210. Tang, L. H., Shia, J., Vakiani, E., Dhall, D. & Klimstra, D. S. High grade transformation of differentiated neuroendocrine neoplasms (NENs) of the enteropancreatic system - a unique entity distinct from de novo high grade neuroendocrine carcinoma (HGNECa) in pathogenesis and clinical behavior. *Lab. Investig.* **88,** 137A (2008).

211. Tang, L. H., Gonen, M., Hedvat, C., Modlin, I. M. & Klimstra, D. S. Objective Quantification of the Ki67 Proliferative Index in Neuroendocrine Tumors of the Gastroenteropancreatic System. *The American Journal of Surgical Pathology* **36,** 1761–1770 (2012).

212. Jalava, P. *et al.* Ki67 immunohistochemistry: a valuable marker in prognostication but with a risk of misclassification: proliferation subgroups formed based on Ki67 immunoreactivity and standardized mitotic index. *Histopathology* **48,** 674–682 (2006).

213.   Oberg, K., Knigge, U., Kwekkeboom, D. & Perren, A. Neuroendocrine gastro-entero-pancreatic tumors: ESMO Clinical Practice Guidelines for diagnosis, treatment and follow-up. *Ann. Oncol.* **23,** vii124–vii130 (2012).

214.   Rindi, G., Petrone, G. & Inzani, F. The 2010 WHO Classification of Digestive Neuroendocrine Neoplasms: a Critical Appraisal four years after Its Introduction. *Endocr. Pathol.* **25,** 186–192 (2014).

215.   Modlin, I. M., Kidd, M., Latich, I., Zikusoka, M. N. & Shapiro, M. D. Current Status of Gastrointestinal Carcinoids. *Gastroenterology* **128,** 1717–1751 (2005).

216.   Horton, K. M., Kamel, I., Hofmann, L. & Fishman, E. K. Carcinoid tumors of the small bowel: a multitechnique imaging approach. *AJR. Am. J. Roentgenol.* **182,** 559–567 (2004).

217.   Ha, J. Gastrointestinal Carcinoid Tumours: A Review. *J. Gastrointest. Dig. Syst.* **2,** 1–7 (2012).

218.   Strosberg, J. Neuroendocrine tumours of the small intestine. *Best Pract. Res. Clin. Gastroenterol.* **26,** 755–773 (2012).

219.   Burke, A. P., Thomas, R. M., Elsayed, A. M. & Sobin, L. H. Carcinoids of the jejunum and ileum: An immunohistochemical and clinicopathologic study of 167 cases. *Cancer* **79,** 1086–1093 (1997).

220.   Papadopoulos, V. *et al.* Carcinoid tumour of the appendix. *Surg. Chronicles* **11,** 151–156 (2006).

221.   Plöckinger, U. *et al.* Consensus guidelines for the management of patients with digestive neuroendocrine tumours: Well-differentiated tumour/carcinoma of the appendix and goblet cell carcinoma. *Neuroendocrinology* **87,** 20–30 (2007).

222.   Stinner, B. & Rothmund, M. Neuroendocrine tumours (carcinoids) of the appendix. *Best Pract. Res. Clin. Gastroenterol.* **19,** 729–738 (2005).

223.   Thompson, G. B. *et al.* Carcinoid tumors of the gastrointestinal tract: presentation, management, and prognosis. *Surgery* **98,** 1054–1063 (1985).

224.   Kulke, M. H. & Mayer, R. J. Carcinoid tumors. *N. Engl. J. Med.* **340,** 858–868 (1999).

225.   Modlin, I. M. & Öberg, K. in *A Century of Advances in Neuroendocrine Tumor Biology and Treatment* 124–133 (Felsenstein C.C.C.P, 2007). at <http://books.google.dk/books?id=RpB9lwEACAAJ>

226.   Matsui, K., Iwase, T. & Kitagawa, M. Small, polypoid-appearing carcinoid tumors of the rectum: clinicopathologic study of 16 cases and effectiveness of endoscopic treatment. *Am. J. Gastroenterol.* **88,** 1949–1953 (1993).

227.   Kaminski, M., Polkowski, M. & Regula, J. Prevalence and endoscopic features of rectal neuroendocrine tumors (carcinoids) among 50148 participants of the Polish colorectal−cancer screening programme. *Gut* **56,** A310 (2007).

228.   Mani, S., Modlin, I. M., Ballantyne, G., Ahlman, H. & West, B. Carcinoids of the rectum. *Journal of the American College of Surgeons* **179,** 231–248 (1994).

229. McDermott, F. D., Heeney, A., Courtney, D., Mohan, H. & Winter, D. Rectal carcinoids: A systematic review. *Surg. Endosc. Other Interv. Tech.* **28,** 2020–2026 (2014).

230. Scherübl, H. Rectal carcinoids are on the rise: Early detection by screening endoscopy. *Endoscopy* **41,** 162–165 (2009).

231. Caplin, M. *et al.* ENETS Consensus Guidelines for the management of patients with digestive neuroendocrine neoplasms: colorectal neuroendocrine neoplasms. *Neuroendocrinology* **95,** 88–97 (2012).

232. Kobayashi, K. *et al.* Indications of endoscopic polypectomy for rectal carcinoid tumors and clinical usefulness of endoscopic ultrasonography. *Dis. Colon Rectum* **48,** 285–291 (2005).

233. Park, H. W. *et al.* Endoscopic submucosal dissection for treatment of rectal carcinoid tumors. *Gastrointest. Endosc.* **72,** 143–149 (2010).

234. Heah, S. M., Eu, K. W., Ooi, B. S., Ho, Y. H. & Seow-Choen, F. Tumor size is irrelevant in predicting malignant potential of carcinoid tumors of the rectum. *Tech. Coloproctol.* **5,** 73–77 (2001).

235. Shields, C. J., Tiret, E. & Winter, D. C. Carcinoid tumors of the rectum: a multi-institutional international collaboration. *Ann. Surg.* **252,** 750–755 (2010).

236. Caplin, M. E. *et al.* Carcinoid tumour. *Lancet* **352,** 799–805 (1998).

237. Kaltsas, G. A., Besser, G. M. & Grossman, A. B. The diagnosis and medical management of advanced neuroendocrine tumors. *Endocr. Rev.* **25,** 458–511 (2004).

238. Vinik, A. I. *et al.* Clinical features, diagnosis, and localization of carcinoid tumors and their management. *Gastroenterol. Clin. North Am.* **18,** 865–896 (1989).

239. Williams, E. D. & Sandler, M. The classification of carcinoid tumours. *Lancet* **281,** 238–239 (1963).

240. Ganim, R. B. & Norton, J. A. Recent advances in carcinoid pathogenesis, diagnosis and management. *Surg. Oncol.* **9,** 173–179 (2000).

241. Davis, Z., Moertel, C. G. & McIlrath, D. C. The malignant carcinoid syndrome. *Surg. Gynecol. Obstet.* **137,** 637–644 (1973).

242. De Herder, W. W. Tumours of the midgut (jejunum, ileum and ascending colon, including carcinoid syndrome). *Best Pract. Res. Clin. Gastroenterol.* **19,** 705–715 (2005).

243. Tomassetti, P. *et al.* Epidemiology, clinical features and diagnosis of gastroenteropancreatic endocrine tumours. *Ann. Oncol.* **12,** S95–S99 (2001).

244. Sarraj, A., Duarte, J., Dominguez, L. & Pun, Y. W. Resection of metastatic pulmonary lesion of ossifying fibromyxoid tumor extending into the left atrium and ventricle via pulmonary vein. *Eur. J. Echocardiogr.* **8,** 384–386 (2007).

245. Service, F. J., McMahon, M. M., O'Brien, P. C. & Ballard, D. J. Functioning insulinoma-incidence, recurrence, and long-term survival of patients: a 60-year study. *Mayo Clin. Proc.* **66,** 711–719 (1991).

246. Oberg, K. & Eriksson, B. Endocrine tumours of the pancreas. *Best Pract. Res. Clin. Gastroenterol.* **19,** 753–781 (2005).

247. Doherty, G. M. Multiple endocrine neoplasia type 1. *J. Surg. Oncol.* **89,** 143–150 (2005).

248. Patel, S., Narwari, M., Parekh, D. & Shah, V. Insulinoma: case report and review of diagnostic and treatment modalities. *J. Assoc. Physicians India* **61,** 423–436 (2013).

249. Ashton, M. A. Strumal carcinoid of the ovary associated with hyperinsulinaemic hypoglycaemia and cutaneous melanosis. *Histopathology* **27,** 463–467 (1995).

250. Shin, J. J., Gorden, P. & Libutti, S. K. Insulinoma: pathophysiology, localization and management. *Future Oncol.* **6,** 229–237 (2010).

251. Boukhman, M. P. *et al.* Insulinoma-experience from 1950 to 1995. *West. J. Med.* **169,** 98–104 (1998).

252. Hirshberg, B. *et al.* Malignant insulinoma: Spectrum of unusual clinical features. *Cancer* **104,** 264–272 (2005).

253. Ellison, E. C. *et al.* 50-Year Appraisal of Gastrinoma: Recommendations for Staging and Treatment. *J. Am. Coll. Surg.* **202,** 897–905 (2006).

254. Roy, P. K. *et al.* Zollinger-Ellison syndrome. Clinical presentation in 261 patients. *Medicine (Baltimore).* **79,** 379–411 (2000).

255. Phan, G. Q. *et al.* Surgical experience with pancreatic and peripancreatic neuroendocrine tumors: Review of 125 patients. *J. Gastrointest. Surg.* **2,** 473–482 (1998).

256. Pipeleers-Marichal, M., Donow, C., Heitz, P. U. & Klöppel, G. Pathologic aspects of gastrinomas in patients with Zollinger-Ellison syndrome with and without multiple endocrine neoplasia type I. *World J. Surg.* **17,** 481–488 (1993).

257. Donow, C. *et al.* Surgical pathology of gastrinoma. Site, size, multicentricity, association with multiple endocrine neoplasia type 1, and malignancy. *Cancer* **68,** 1329–1334 (1991).

258. Wu, P. C. *et al.* A prospective analysis of the frequency, location, and curability of ectopic (nonpancreaticoduodenal, nonnodal) gastrinoma. *Surgery* **122,** 1176–1182 (1997).

259. Norton, J. A. *et al.* Surgery increases survival in patients with gastrinoma. *Annals of surgery* **244,** 410–419 (2006).

260. Anlauf, M. *et al.* Sporadic versus hereditary gastrinomas of the duodenum and pancreas: Distinct clinico-pathological and epidemiological features. *World J. Gastroenterol.* **12,** 5440–5446 (2006).

261. Klöppel, G., Willemer, S., Stamm, B., Häcki, W. H. & Heitz, P. U. Pancreatic lesions and hormonal profile of pancreatic tumors in multiple endocrine neoplasia type I. An immunocytochemical study of nine patients. *Cancer* **57,** 1824–1832 (1986).

262. Lévy-Bohbot, N. *et al.* Prevalence, characteristics and prognosis of MEN 1-associated glucagonomas, VIPomas, and somatostatinomas: study from the GTE (Groupe des Tumeurs Endocrines) registry. *Gastroenterol. Clin. Biol.* **28,** 1075–1081 (2004).

263.	Chastain, M. A. The glucagonoma syndrome: a review of its features and discussion of new perspectives. *Am. J. Med. Sci.* **321,** 306–320 (2001).

264.	Noone, T. C., Hosey, J., Zeynep, F. & Semelka, R. C. Imaging and localization of islet-cell tumours of the pancreas on CT and MRI. *Best Pract. Res. Clin. Endocrinol. Metab.* **19,** 195–211 (2005).

265.	Mignon, M. Natural history of neuroendocrine enteropancreatic tumors. *Digestion* **62,** 51–58 (2000).

266.	Soga, J. & Yakuwa, Y. Glucagonomas/diabetico-dermatogenic syndrome (DDS): a statistical evaluation of 407 reported cases. *J. Hepatobiliary. Pancreat. Surg.* **5,** 312–319 (1998).

267.	Van Beek, A. P. *et al.* The glucagonoma syndrome and necrolytic migratory erythema: A clinical review. *Eur. J. Endocrinol.* **151,** 531–537 (2004).

268.	Wermers, R. A., Fatourechi, V., Wynne, A. G., Kvols, L. K. & Lloyd, R. V. The glucagonoma syndrome. Clinical and pathologic features in 21 patients. *Medicine (Baltimore).* **75,** 53–63 (1996).

269.	Fang, S., Li, S. & Cai, T. Glucagonoma syndrome : a case report with focus on skin disorders. *Onco. Targets. Ther.* **9,** 1449–1453 (2014).

270.	Frankton, S. & Bloom, S. R. Gastrointestinal endocrine tumours. Glucagonomas. *Baillieres. Clin. Gastroenterol.* **10,** 697–705 (1996).

271.	Ghaferi, A. A., Chojnacki, K. A., Long, W. D., Cameron, J. L. & Yeo, C. J. Pancreatic VIPomas: Subject review and one institutional experience. *J. Gastrointest. Surg.* **12,** 382–393 (2008).

272.	Park, S. K., O'Dorisio, M. S. & O'Dorisio, T. M. Vasoactive intestinal polypeptide-secreting tumours: Biology and therapy. *Baillieres. Clin. Gastroenterol.* **10,** 673–696 (1996).

273.	Lundstedt, C., Linjawi, T. & Amin, T. Liver VIPoma: report of two cases and literature review. *Abdom. Imaging* **19,** 433–437 (1994).

274.	Long, R. G. *et al.* Clinicopathological study of pancreatic and ganglioneuroblastoma tumours secreting vasoactive intestinal polypeptide (vipomas). *Br. Med. J. (Clin. Res. Ed).* **282,** 1767–1771 (1981).

275.	Soga, J. & Yakuwa, Y. Vipoma/diarrheogenic syndrome: a statistical evaluation of 241 reported cases. *J. Exp. Clin. Cancer Res.* **17,** 389–400 (1998).

276.	Polak, J. M. & Bloom, S. R. Somatostatin localization in tissues. *Scand. J. Gastroenterol. Suppl.* **119,** 11–21 (1986).

277.	Mao, C., Shah, A., Hanson, D. J. & Howard, J. M. Von Recklinghausen's disease associated with duodenal somatostatinoma: Contrast of duodenal versus pancreatic somatostatinomas. *J. Surg. Oncol.* **59,** 67–73 (1995).

278.	Soga, J. & Yakuwa, Y. Somatostatinoma/inhibitory syndrome: a statistical evaluation of 173 reported cases as compared to other pancreatic endocrinomas. *J. Exp. Clin. Cancer Res.* **18,** 13–22 (1999).

279.	Masulović, D., Stevic, R., Filipović, A., Micev, M. & Ivanović, A. Somatostatin-producing duodenal carcinoma Clinicopathological description of a case. *Acta Chir. Iugosl.* **60,** 61–64 (2013).

280. Tanaka, S. *et al.* Duodenal somatostatinoma: A case report and review of 31 cases with special reference to the relationship between tumor size and metastasis. *Pathol. Int.* **50,** 146–152 (2000).

281. Zhang, B., Xie, Q., Gao, S., Fu, Y. & Wu, Y. Pancreatic somatostatinoma with obscure inhibitory syndrome and mixed pathological pattern. *J. Zhejiang Univ. Sci. B* **11,** 22–26 (2010).

282. He, X., Wang, J., Wu, X., Kang, L. & Lan, P. Pancreatic somatostatinoma manifested as severe hypoglycemia. *J. Gastrointest. Liver Dis.* **18,** 221–224 (2009).

283. Jensen, R. T. Pancreatic endocrine tumors: recent advances. *Ann. Oncol.* **10,** 170–176 (1999).

284. Kann, P. H. *et al.* Natural course of small, asymptomatic neuroendocrine pancreatic tumours in multiple endocrine neoplasia type 1: An endoscopic ultrasound imaging study. *Endocr. Relat. Cancer* **13,** 1195–1202 (2006).

285. Jensen, R. T., Berna, M. J., Bingham, D. B. & Norton, J. A. Inherited pancreatic endocrine tumor syndromes: Advances in molecular pathogenesis, diagnosis, management, and controversies. *Cancer* **113,** 1807–1843 (2008).

286. Eriksson, B. & Oberg, K. in *Endocrine Tumors of the Pancreas: Recent Advances in Research and Management. Frontiers of Gastrointestinal Research.* (eds. Mignon, M. & Jensen, R.) 208–222 (Karger, 1995).

287. Qiao, X. W. *et al.* Chromogranin A is a reliable serum diagnostic biomarker for pancreatic neuroendocrine tumors but not for insulinomas. *BMC Endocr. Disord.* **14,** 1–10 (2014).

288. Nobels, F. R. *et al.* Chromogranin A as serum marker for neuroendocrine neoplasia: Comparison with neuron-specific enolase and the α-subunit of glycoprotein hormones. *J. Clin. Endocrinol. Metab.* **82,** 2622–2628 (1997).

289. Zatelli, M. C. *et al.* Chromogranin A as a marker of neuroendocrine neoplasia: An Italian Multicenter Study. *Endocr. Relat. Cancer* **14,** 473–482 (2007).

290. Bílek, R., Šafařík, L., Ciprová, V., Vlček, P. & Lisá, L. Chromogranin A, a member of neuroendocrine secretory proteins as a selective marker for laboratory diagnosis of pheochromocytoma. *Physiol. Res.* **57,** 171–179 (2008).

291. Oberg, K. Circulating biomarkers in gastroenteropancreatic neuroendocrine tumours. *Endocr. Relat. Cancer* **18,** S17–S25 (2011).

292. Eurodiagnostica. EURIA Chromogranin B - improved diagnosis of neuroendocrine tumours in combination with Chromogranin A. (2012). at <http://www.eurodiagnostica.com>

293. Panzuto, F. *et al.* Utility of combined use of plasma levels of chromogranin A and pancreatic polypeptide in the diagnosis of gastrointestinal and pancreatic endocrine tumors. *J. Endocrinol. Invest.* **27,** 6–11 (2004).

294. Bajetta, E. *et al.* Chromogranin A, neuron specific enolase, carcinoembryonic antigen, and hydroxyindole acetic acid evaluation in patients with neuroendocrine tumors. *Cancer* **86,** 858–865 (1999).

295. Perri, M. *et al.* Octreo-SPECT/CT imaging for accurate detection and localization of suspected neuroendocrine tumors. *Q. J. Nucl. Med. Mol. Imaging* **52,** 323–333 (2008).

296. Gouya, H. *et al.* CT, endoscopic sonography, and a combined protocol for preoperative evaluation of pancreatic insulinomas. *Am. J. Roentgenol.* **181,** 987–992 (2003).

297. Van Eijck, C. H. *et al.* Somatostatin receptor imaging and therapy of pancreatic endocrine tumors. *Ann. Oncol.* **10 Suppl 4,** 177–181 (1999).

298. Koopmans, K. P. *et al.* Molecular imaging in neuroendocrine tumors: Molecular uptake mechanisms and clinical results. *Crit. Rev. Oncol. Hematol.* **71,** 199–213 (2009).

299. Öberg, K. *et al.* Guidelines for the management of gastroenteropancreatic neuroendocrine tumours (including bronchopulmonary and thymic neoplasms). Part II-specific NE tumour types. *Acta Oncol. (Madr).* **43,** 626–636 (2004).

300. Jamar, F., Fiasse, R., Leners, N. & Pauwels, S. Somatostatin receptor imaging with indium-111-pentetreotide in gastroenteropancreatic neuroendocrine tumors: safety, efficacy and impact on patient management. *J. Nucl. Med.* **36,** 542–549 (1995).

301. Gibril, F. *et al.* Somatostatin receptor scintigraphy: Its sensitivity compared with that of other imaging methods in detecting primary and metastatic gastrinomas: A prospective study. *Ann. Intern. Med.* **125,** 26–34 (1996).

302. Shi, W. *et al.* Localization of neuroendocrine tumours with [111In] DTPA-octreotide scintigraphy (Octreoscan): a comparative study with CT and MR imaging. *QJM* **91,** 295–301 (1998).

303. Krenning, E. P. *et al.* Somatostatin receptor scintigraphy with [111In-DTPA-d-Phe1]- and [123I-Tyr3]-octreotide: the Rotterdam experience with more than 1000 patients. *Eur. J. Nucl. Med.* **20,** 716–731 (1993).

304. Zimmer, T. *et al.* Endoscopic ultrasonography and somatostatin receptor scintigraphy in the preoperative localisation of insulinomas and gastrinomas. *Gut* **39,** 562–568 (1996).

305. Meko, J. B., Doherty, G. M., Siegel, B. A. & Norton, J. A. Evaluation of somatostatin-receptor scintigraphy for detecting neuroendocrine tumors. *Surgery* **120,** 975–983 (1996).

306. Ramage, J. K. *et al.* Guidelines for the management of gastroenteropancreatic neuroendocrine (including carcinoid) tumours. *Gut* **54,** iv1–iv16 (2005).

307. Frilling, A. *et al.* Use of somatostatin receptor scintigraphy to image extrahepatic metastases of neuroendocrine tumors. *Surgery* **124,** 1000–1004 (1998).

308. Ramage, J. K., Williams, R. & Buxton-Thomas, M. Imaging secondary neuroendocrine tumours of the liver: comparison of I123 metaiodobenzylguanidine (MIBG) and In111-labelled octreotide (Octreoscan). *QJM* **89,** 539–542 (1996).

309. Chiti, A. *et al.* Comparison of somatostatin receptor imaging, computed tomography and ultrasound in the clinical management of neuroendocrine gastro-entero-pancreatic tumours. *Eur. J. Nucl. Med.* **25,** 1396–1403 (1998).

310. Gibril, F. *et al.* Specificity of somatostatin receptor scintigraphy: a prospective study and effects of false-positive localizations on management in patients with gastrinomas. *J. Nucl. Med.* **40,** 539–553 (1999).

311. Lamberts, S. W. *et al.* Parallel in vivo and in vitro detection of functional somatostatin receptors in human endocrine pancreatic tumors: Consequences with regard to diagnosis, localization, and therapy. *J. Clin. Endocrinol. Metab.* **71,** 566–574 (1990).

312. Papotti, M. *et al.* Expression of somatostatin receptor types 1-5 in 81 cases of gastrointestinal and pancreatic endocrine tumors: A correlative immunohistochemical and reverse-transcriptase polymerase chain reaction analysis. *Virchows Arch.* **440,** 461–475 (2002).

313. Reubi, J. C., Waser, B., Schaer, J. C. & Laissue, J. A. Somatostatin receptor sst1-sst5 expression in normal and neoplastic human tissues using receptor autoradiography with subtype-selective ligands. *Eur. J. Nucl. Med.* **28,** 836–846 (2001).

314. Ezziddin, S. *et al.* Factors predicting tracer uptake in somatostatin receptor and MIBG scintigraphy of metastatic gastroenteropancreatic neuroendocrine tumors. *J. Nucl. Med.* **47,** 223–233 (2006).

315. Binderup, T. *et al.* Functional imaging of neuroendocrine tumors: a head-to-head comparison of somatostatin receptor scintigraphy, 123I-MIBG scintigraphy, and 18F-FDG PET. *J. Nucl. Med.* **51,** 704–712 (2010).

316. Kaltsas, G. *et al.* Comparison of somatostatin analog and meta-iodobenzylguanidine radionuclides in the diagnosis and localization of advanced neuroendocrine tumors. *J. Clin. Endocrinol. Metab.* **86,** 895–902 (2001).

317. Gambhir, S. S. Molecular imaging of cancer with positron emission tomography. *Nat. Rev. Cancer* **2,** 683–693 (2002).

318. Czernin, J. & Phelps, M. E. Positron emission tomography scanning: current and future applications. *Annu. Rev. Med.* **53,** 89–112 (2002).

319. Kayani, I. *et al.* Functional imaging of neuroendocrine tumors with combined PET/CT using 68Ga-DOTATATE (Dota-DPhe1, Tyr3-octreotate) and 18F-FDG. *Cancer* **112,** 2447–2455 (2008).

320. Belhocine, T. *et al.* Fluorodeoxyglucose positron emission tomography and somatostatin receptor scintigraphy for diagnosing and staging carcinoid tumours: correlations with the pathological indexes p53 and Ki-67. *Nucl. Med. Commun.* **23,** 727–734 (2002).

321. Al-Nahhas, A. *et al.* What can gallium-68 PET add to receptor and molecular imaging? *Eur. J. Nucl. Med. Mol. Imaging* **34,** 1897–1901 (2007).

322. Srirajaskanthan, R. *et al.* The role of 68Ga-DOTATATE PET in patients with neuroendocrine tumors and negative or equivocal findings on 111In-DTPA-octreotide scintigraphy. *J. Nucl. Med.* **51,** 875–882 (2010).

323. Kayani, I. *et al.* A comparison of 68Ga-DOTATATE and 18F-FDG PET/CT in pulmonary neuroendocrine tumors. *J. Nucl. Med.* **50,** 1927–1932 (2009).

324. Săftoiu, A. & Vilmann, P. Role of endoscopic ultrasound in the diagnosis and staging of pancreatic cancer. *J. Clin. Ultrasound* **37,** 1–17 (2009).

325. Puli, S. R. *et al.* Diagnostic accuracy of endoscopic ultrasound in pancreatic neuroendocrine tumors: a systematic review and meta analysis. *World J. Gastroenterol.* **19,** 3678–3684 (2013).

326. Zimmer, T. *et al.* Endosonography of neuroendocrine tumors of the stomach, duodenum, and pancreas. *Ann. N. Y. Acad. Sci.* **733,** 425–436 (1994).

327. Ruszniewski, P. *et al.* Localization of gastrinomas by endoscopic ultrasonography in patients with Zollinger-Ellison syndrome. *Surgery* **117,** 629–635 (1995).

328. Rösch, T. *et al.* Localization of pancreatic endocrine tumors by endoscopic ultrasonography. *N. Engl. J. Med.* **326,** 1721–1726 (1992).

329. Ginès, A., Vazquez-Sequeiros, E., Soria, M. T., Clain, J. E. & Wiersema, M. J. Usefulness of EUS-guided fine needle aspiration (EUS-FNA) in the diagnosis of functioning neuroendocrine tumors. *Gastrointest. Endosc.* **56,** 291–296 (2002).

330. Zimmer, T. *et al.* Endoscopic ultrasonography of neuroendocrine tumours. *Digestion* **62,** 45–50 (2000).

331. Service, F. J. Hypoglycemias. *West. J. Med.* **154,** 442–454 (1991).

332. Service, F. J. *et al.* C-peptide suppression test for insulinoma. *J. Lab. Clin. Med.* **90,** 180–186 (1977).

333. Vezzosi, D., Bennet, A., Fauvel, J. & Caron, P. Insulin, C-peptide and proinsulin for the biochemical diagnosis of hypoglycaemia related to endogenous hyperinsulinism. *Eur. J. Endocrinol.* **157,** 75–83 (2007).

334. Dhillo, W. S. *et al.* Plasma gastrin measurement cannot be used to diagnose a gastrinoma in patients on either proton pump inhibitors or histamine type-2 receptor antagonists. *Ann. Clin. Biochem.* **43,** 153–155 (2006).

335. Roy, P. K. *et al.* Gastric secretion in Zollinger-Ellison syndrome. Correlation with clinical expression, tumor extent and role in diagnosis-a prospective NIH study of 235 patients and a review of 984 cases in the literature. *Medicine (Baltimore).* **80,** 189–222 (2001).

336. El-Omar, E., Penman, I., Dorrian, C. A., Ardill, J. E. & McColl, K. E. Eradicating Helicobacter pylori infection lowers gastrin mediated acid secretion by two thirds in patients with duodenal ulcer. *Gut* **34,** 1060–1065 (1993).

337. Korman, M. G., Strickland, R. G. & Hansky, J. Serum gastrin in chronic gastritis. *Br. Med. J.* **2,** 16–18 (1971).

338. Rakic, S., Hinder, R. A., Adanja, G. & DeMeester, T. R. Elevated serum gastrin levels in patients with gastric cancer. *J. Surg. Oncol.* **47,** 79–81 (1991).

339. Guzzo, J. L., Duncan, M., Bass, B. L., Bochicchio, G. V. & Napolitano, L. M. Severe and refractory peptic ulcer disease: The diagnostic dilemma. Case report and comprehensive review. *Digestive Diseases and Sciences* **50,** 1999–2008 (2005).

340. Frucht, H. *et al.* Secretin and calcium provocative tests in the Zollinger-Ellison syndrome: A prospective study. *Ann. Intern. Med.* **111,** 713–722 (1989).

341. Berna, M. J., Hoffmann, K. M., Serrano, J., Gibril, F. & Jensen, R. T. Serum gastrin in Zollinger-Ellison syndrome: I. Prospective study of fasting serum gastrin in 309 patients from the National Institutes of Health and comparison with 2229 cases from the literature. *Medicine (Baltimore).* **85,** 295–330 (2006).

342. Wada, M., Komoto, I., Doi, R. & Imamura, M. Intravenous calcium injection test is a novel complementary procedure in differential diagnosis for gastrinoma. *World J. Surg.* **26,** 1291–1296 (2002).

343. Kheir, S. M., Omura, E. F., Grizzle, W. E., Herrera, G. A. & Lee, I. Histologic variation in the skin lesions of the glucagonoma syndrome. *The American journal of surgical pathology* **10,** 445–453 (1986).

344. Waeber, G. *et al.* In vivo and in vitro effects of somatostatin and insulin on glucagon release in a human glucagonoma. *Clin. Endocrinol. (Oxf).* **46,** 637–642 (1997).

345. Economopoulos, P. & Christopoulos, C. Glucagonoma. *Ann. Gastroenterol.* **14,** 99–108 (2001).

346. Brelian, D. & Tenner, S. Diarrhoea due to pancreatic diseases. *Best Pract. Res. Clin. Gastroenterol.* **26,** 623–631 (2012).

347. Nikou, G. C. *et al.* VIPomas: an update in diagnosis and management in a series of 11 patients. *Hepatogastroenterology.* **52,** 1259–1265 (2005).

348. Song, S., Shi, R., Li, B. & Liu, Y. Diagnosis and treatment of pancreatic vasoactive intestinal peptide endocrine tumors. *Pancreas* **38,** 811–814 (2009).

349. Angeletti, S. *et al.* Use of the somatostatin analogue octreotide to localise and manage somatostatin-producing tumours. *Gut* **42,** 792–794 (1998).

350. Suzuki, H. *et al.* Diagnostic usefulness of FDG-PET for malignant somatostatinoma of the pancreas. *Hepatogastroenterology.* **55,** 1242–1245 (2008).

351. Nesi, G., Marcucci, T., Rubio, C. A., Brandi, M. L. & Tonelli, F. Somatostatinoma: Clinico-pathological features of three cases and literature reviewed. *J. Gastroenterol. Hepatol.* **23,** 521–526 (2008).

352. Stelow, E. B. *et al.* Fine-needle aspiration cytology of pancreatic somatostatinoma: The importance of immunohistochemistry for the cytologic diagnosis of pancreatic endocrine neoplasms. *Diagn. Cytopathol.* **33,** 100–105 (2005).

353. Shah, T. *et al.* α-Fetoprotein and human chorionic gonadotrophin-β as prognostic markers in neuroendocrine tumour patients. *Br. J. Cancer* **99,** 72–77 (2008).

354. Gullo, L. Nonfunctioning pancreatic endocrine tumors: a multicenter clinical study. *Am. J. Gastroenterol.* **98,** 2435–2439 (2003).

355. Thomas-Marques, L. *et al.* Prospective endoscopic ultrasonographic evaluation of the frequency of nonfunctioning pancreaticoduodenal endocrine tumors in patients with multiple endocrine neoplasia type 1. *Am. J. Gastroenterol.* **101,** 266–273 (2006).

356. Wamsteker, E. J., Gauger, P. G., Thompson, N. W. & Scheiman, J. M. EUS detection of pancreatic endocrine tumors in asymptomatic patients with type 1 multiple endocrine neoplasia. *Gastrointest. Endosc.* **58,** 531–535 (2003).

357. Limmer, S. *et al.* Radiofrequency ablation of solitary pancreatic insulinoma in a patient with episodes of severe hypoglycemia. *Eur. J. Gastroenterol. Hepatol.* **21,** 1097–1101 (2009).

358. Rott, G., Biggemann, M. & Pfohl, M. Embolization of an insulinoma of the pancreas with trisacryl gelatin microspheres as definitive treatment. *Cardiovasc. Intervent. Radiol.* **31,** 659–662 (2008).

359. Jürgensen, C. *et al.* EUS-guided alcohol ablation of an insulinoma. *Gastrointest. Endosc.* **63,** 1059–1062 (2006).

360. Soga, J., Yakuwa, Y. & Osaka, M. Insulinoma/hypoglycemic syndrome: a statistical evaluation of 1085 reported cases of a Japanese series. *J. Exp. Clin. Cancer Res.* **17,** 379–388 (1998).

361. Crippa, S. *et al.* Middle pancreatectomy: indications, short- and long-term operative outcomes. *Ann. Surg.* **246,** 69–76 (2007).

362. Falconi, M. *et al.* Surgical strategy in the treatment of pancreatic neuroendocrine tumors. *J. pancreas* **7,** 150–156 (2006).

363. Kishikawa, H. *et al.* Successful treatment of insulinoma by a single daily dose of octreotide in two elderly female patients. *Endocr. J.* **53,** 79–85 (2006).

364. Katabami, T., Kato, H., Shirai, N., Naito, S. & Saito, N. Successful long-term treatment with once-daily injection of low-dose octreotide in an aged patient with insulinoma. *Endocr. J.* **52,** 629–634 (2005).

365. Brodows, R. G. & Campbell, R. G. Control of refractory fasting hypoglycemia in a patient with suspected insulinoma with diphenylhydantoin. *J. Clin. Endocrinol. Metab.* **38,** 159–161 (1974).

366. Bourcier, M. E., Sherrod, A., DiGuardo, M. & Vinik, A. I. Successful control of intractable hypoglycemia using rapamycin in an 86-year-old man with a pancreatic insulin-secreting islet cell tumor and metastases. *J. Clin. Endocrinol. Metab.* **94,** 3157–3162 (2009).

367. Gillams, A., Cassoni, A., Conway, G. & Lees, W. Radiofrequency ablation of neuroendocrine liver metastases: The Middlesex experience. *Abdom. Imaging* **30,** 435–441 (2005).

368. Bégu-Le Corroller, A. *et al.* Aggressive multimodal therapy of sporadic malignant insulinoma can improve survival: A retrospective 35-year study of 12 patients. *Diabetes Metab.* **34,** 343–348 (2008).

369. Schütt, M. *et al.* Recurrent hypoglycemia caused by malignant insulinoma: chemoembolization as a therapeutic option. *Med. Klin.* **96,** 632–636 (2001).

370. Norton, J. A. & Jensen, R. T. Current surgical management of Zollinger-Ellison syndrome (ZES) in patients without multiple endocrine neoplasia-type 1 (MEN1). *Surg. Oncol.* **12,** 145–151 (2003).

371. Sugg, S. L. *et al.* A prospective study of intraoperative methods to diagnose and resect duodenal gastrinomas. *Ann. Surg.* **218,** 138–144 (1993).

372. Franz, R. C. & Penzhorn, H. O. Is total gastrectomy still a viable option in the management of patients with the Zollinger-Ellison syndrome? *South African J. Surg.* **45,** 58–60 (2007).

373. Hung, P. D., Schubert, M. L. & Mihas, A. A. Zollinger-Ellison syndrome. *Current Treatment Options in Gastroenterology* **6,** 163–170 (2003).

374. Fishbeyn, V. A. *et al.* Assessment and prediction of long-term cure in patients with the Zollinger-Ellison syndrome: The best approach. *Ann. Intern. Med.* **119,** 199–206 (1993).

375. Shojamanesh, H. *et al.* Prospective study of the antitumor efficacy of long-term octreotide treatment in patients with progressive metastatic gastrinoma. *Cancer* **94,** 331–343 (2002).

376. Alexander, E. K., Robinson, M., Staniec, M. & Dluhy, R. G. Peripheral amino acid and fatty acid infusion for the treatment of necrolytic migratory erythema in the glucagonoma syndrome. *Clin. Endocrinol. (Oxf).* **57,** 827–831 (2002).

377. Edney, J. A., Hofmann, S., Thompson, J. S. & Kessinger, A. Glucagonoma syndrome is an underdiagnosed clinical entity. *Am. J. Surg.* **160,** 625–628 (1990).

378. Holmes, A., Kilpatrick, C., Proietto, J. & Green, M. D. Reversal of a neurologic paraneoplastic syndrome with octreotide (Sandostatin) in a patient with glucagonoma. *Am. J. Med.* **91,** 434–436 (1991).

379. Kindmark, H. *et al.* Endocrine pancreatic tumors with glucagon hypersecretion: A retrospective study of 23 cases during 20 years. *Med. Oncol.* **24,** 330–337 (2007).

380. De Mestier, L. *et al.* Dramatic efficacy of chemotherapy with 5-fluorouracil and dacarbazine in a patient with metastatic glucagonoma and cardiac insufficiency. *Gastroenterol. Clin. Biol.* **34,** 106–110 (2010).

381. Vinik, A. I. & Raymond, E. Pancreatic neuroendocrine tumors: approach to treatment with focus on sunitinib. *Therap. Adv. Gastroenterol.* **6,** 396–411 (2013).

382. Oberg, K. Neuroendocrine tumors of the digestive tract: impact of new classifications and new agents on therapeutic approaches. *Curr. Opin. Oncol.* **24,** 433–440 (2012).

383. Yao, J. C. *et al.* Everolimus for advanced pancreatic neuroendocrine tumors. *N. Engl. J. Med.* **364,** 514–523 (2011).

384. Akerström, G. *et al.* ENETS consensus guidelines for the standards of care in neuroendocrine tumors: Pre- and perioperative therapy in patients with neuroendocrine tumors. *Neuroendocrinology* **90,** 203–208 (2009).

385. Schoevaerdts, D., Favet, L., Zekry, D., Sieber, C. C. & Michel, J. P. Vipoma: Effective treatment with octreotide in the oldest old. *Journal of the American Geriatrics Society* **49,** 496–497 (2001).

386. Nguyen, H. N. *et al.* Long-term survival after diagnosis of hepatic metastatic VIPoma: Report of two cases with disparate courses and review of therapeutic options. *Dig. Dis. Sci.* **44,** 1148–1155 (1999).

387. Case, C. C., Wirfel, K. & Vassilopoulou-Sellin, R. Vasoactive intestinal polypeptide-secreting tumor (VIPoma) with liver metastases: dramatic and durable symptomatic benefit from hepatic artery embolization, a case report. *Med. Oncol.* **19,** 181–187 (2002).

388. Bramley, P. N., Lodge, J. P., Losowsky, M. S. & Giles, G. R. Treatment of metastatic Vipoma by liver transplantation. *Clin. Transplant.* **4,** 276–278 (1990).

389. Moertel, C. G., Lefkopoulo, M., Lipsitz, S., Hahn, R. G. & Klaassen, D. Streptozocin-doxorubicin, streptozocin-fluorouracil or chlorozotocin in the treatment of advanced islet-cell carcinoma. *N. Engl. J. Med.* **326,** 519–523 (1992).

390. Bourcier, M. E. & Vinik, A. I. Sunitinib for the treatment of metastatic paraganglioma and vasoactive intestinal polypeptide-producing tumor (VIPoma). *Pancreas* **42,** 348–352 (2013).

391. Gagner, M. & Palermo, M. Laparoscopic Whipple procedure: Review of the literature. *J. Hepatobiliary. Pancreat. Surg.* **16,** 726–730 (2009).

392. Garbrecht, N. *et al.* Somatostatin-producing neuroendocrine tumors of the duodenum and pancreas: Incidence, types, biological behavior, association with inherited syndromes, and functional activity. *Endocr. Relat. Cancer* **15,** 229–241 (2008).

393. Falconi, M. *et al.* ENETS Consensus Guidelines for the management of patients with digestive neuroendocrine neoplasms of the digestive system: well-differentiated pancreatic non-functioning tumors. *Neuroendocrinology* **95,** 120–134 (2012).

394. Falconi, M. *et al.* Parenchyma-preserving resections for small nonfunctioning pancreatic endocrine tumors. *Ann. Surg. Oncol.* **17,** 1621–1627 (2010).

395. Öberg, K. *et al.* Consensus report on the use of somatostatin analogs for the management of neuroendocrine tumors of the gastroenteropancreatic system. *Ann. Oncol.* **15,** 966–973 (2004).

396. Cwikla, J. B. *et al.* Efficacy of radionuclide treatment DOTATATE Y-90 in patients with progressive metastatic gastroenteropancreatic neuroendocrine carcinomas (GEP-NETs): a phase II study. *Ann. Oncol.* **21,** 787–794 (2010).

397. Valkema, R. *et al.* Survival and Response After Peptide Receptor Radionuclide Therapy With [90Y-DOTA0,Tyr3]Octreotide in Patients With Advanced Gastroenteropancreatic Neuroendocrine Tumors. *Semin. Nucl. Med.* **36,** 147–156 (2006).

398. Imhof, A. *et al.* Response, survival, and long-term toxicity after therapy with the radiolabeled somatostatin analogue [90Y-DOTA]-TOC in metastasized neuroendocrine cancers. *J. Clin. Oncol.* **29,** 2416–2423 (2011).

399. Sabet, A. *et al.* Specific efficacy of peptide receptor radionuclide therapy with 177Lu-octreotate in advanced neuroendocrine tumours of the small intestine. *Eur. J. Nucl. Med. Mol. Imaging* Ahead of print (2015).

400. De Jong, M., Breeman, W. A., Valkema, R., Bernard, B. F. & Krenning, E. P. Combination radionuclide therapy using 177Lu- and 90Y-labeled somatostatin analogs. *J. Nucl. Med.* **46,** 13S–17S (2005).

401. Ellisen, L. W. *et al.* TAN-1, the human homolog of the Drosophila notch gene, is broken by chromosomal translocations in T lymphoblastic neoplasms. *Cell* **66,** 649–661 (1991).

402. Weng, A. P., Ferrando, A. A., Lee, W. & Morris, J. P. Activating Mutations of NOTCH1 in Human T Cell Acute Lymphoblastic Leukemia. *Sci. (New York, NY)* **306,** 269–272 (2004).

403. Thompson, B. J. *et al.* Control of hematopoietic stem cell quiescence by the E3 ubiquitin ligase Fbw7. *J. Exp. Med.* **205,** 1395–1408 (2008).

404. Sjölund, J. *et al.* Suppression of renal cell carcinoma growth by inhibition of Notch signaling in vitro and in vivo. *J. Clin. Invest.* **118,** 217–228 (2008).

405. Stylianou, S., Clarke, R. B. & Brennan, K. Aberrant activation of Notch signaling in human breast cancer. *Cancer Res.* **66,** 1517–1525 (2006).

406. Wang, Z. *et al.* Down-regulation of Notch-1 contributes to cell growth inhibition and apoptosis in pancreatic cancer cells. *Mol. Cancer Ther.* **5,** 483–493 (2006).

407. Reedijk, M. *et al.* High-level coexpression of JAG1 and NOTCH1 is observed in human breast cancer and is associated with poor overall survival. *Cancer Res.* **65,** 8530–8537 (2005).

408. Santagata, S. *et al.* JAGGED1 expression is associated with prostate cancer metastasis and recurrence. *Cancer Res.* **64,** 6854–6857 (2004).

409. Nicolas, M. *et al.* Notch1 functions as a tumor suppressor in mouse skin. *Nat. Genet.* **33,** 416–421 (2003).

410. Rangarajan, A. *et al.* Notch signaling is a direct determinant of keratinocyte growth arrest and entry into differentiation. *EMBO J.* **20,** 3427–3436 (2001).

411. Mammucari, C. *et al.* Integration of notch 1 and calcineurin/NFAT signaling pathways in keratinocyte growth and differentiation control. *Dev. Cell* **8,** 665–676 (2005).

412. Sriuranpong, V., Borges, M. W. & Ravi, R. K. Notch signaling induces cell cycle arrest in small cell lung cancer cells. *Cancer Res.* **61,** 3200–3205 (2001).

413. Zheng, Q. *et al.* Notch signaling inhibits growth of the human lung adenocarcinoma cell line A549. *Oncol. Rep.* **17,** 847–852 (2007).

414. Reedijk, M. *et al.* Activation of Notch signaling in human colon adenocarcinoma. *Int. J. Oncol.* **33,** 1223–1229 (2008).

415. Fre, S. *et al.* Notch and Wnt signals cooperatively control cell proliferation and tumorigenesis in the intestine. *Proc. Natl. Acad. Sci. U. S. A.* **106,** 6309–6314 (2009).

416. Peignon, G. *et al.* Complex interplay between β-catenin signalling and Notch effectors in intestinal tumorigenesis. *Gut* **60,** 166–176 (2011).

417. Guilmeau, S., Flandez, M., Mariadason, J. M. & Augenlicht, L. H. Heterogeneity of Jagged1 expression in human and mouse intestinal tumors: implications for targeting Notch signaling. *Oncogene* **29,** 992–1002 (2010).

114

418. Weijzen, S. *et al.* Activation of Notch-1 signaling maintains the neoplastic phenotype in human Ras-transformed cells. *Nat. Med.* **8,** 979–986 (2002).

419. Mittal, S., Subramanyam, D., Dey, D., Kumar, R. V & Rangarajan, A. Cooperation of Notch and Ras/MAPK signaling pathways in human breast carcinogenesis. *Mol. Cancer* **8,** 128–139 (2009).

420. Di Magliano, M. P. *et al.* Hedgehog/Ras interactions regulate early stages of pancreatic cancer. *Genes Dev.* **20,** 3161–3173 (2006).

421. Massagué, J., Blain, S. W. & Lo, R. S. TGFbeta signaling in growth control, cancer, and heritable disorders. *Cell* **103,** 295–309 (2000).

422. Rao, P. & Kadesch, T. The intracellular form of notch blocks transforming growth factor beta-mediated growth arrest in Mv1Lu epithelial cells. *Mol. Cell. Biol.* **23,** 6694–6701 (2003).

423. Masuda, S. *et al.* Notch1 oncoprotein antagonizes TGF-beta/Smad-mediated cell growth suppression via sequestration of coactivator p300. *Cancer Sci.* **96,** 274–282 (2005).

424. MacKenzie, F., Duriez, P., Wong, F., Noseda, M. & Karsan, A. Notch4 Inhibits Endothelial Apoptosis via RBP-Jkappa-dependent and -independent Pathways. *J. Biol. Chem.* **279,** 11657–11663 (2004).

425. Nair, P., Somasundaram, K. & Krishna, S. Activated Notch1 inhibits p53-induced apoptosis and sustains transformation by human papillomavirus type 16 E6 and E7 oncogenes through a PI3K-PKB/Akt-dependent pathway. *J. Virol.* **77,** 7106–7112 (2003).

426. Nickoloff, B. J. *et al.* Jagged-1 mediated activation of notch signaling induces complete maturation of human keratinocytes through NF-kappaB and PPARgamma. *Cell Death Differ.* **9,** 842–855 (2002).

427. Bash, J. *et al.* Rel/NF-κB can trigger the Notch signaling pathway by inducing the expression of Jagged1, a ligand for Notch receptors. *EMBO J.* **18,** 2803–2811 (1999).

428. Nakakura, E. K. *et al.* Regulation of neuroendocrine differentiation in gastrointestinal carcinoid tumor cells by notch signaling. *J. Clin. Endocrinol. Metab.* **90,** 4350–4356 (2005).

429. Sriuranpong, V. *et al.* Notch Signaling Induces Rapid Degradation of Achaete-Scute Homolog 1. *Mol. Cell. Biol.* **22,** 3129–3139 (2002).

430. Borges, M. *et al.* An achaete-scute homologue essential for neuroendocrine differentiation in the lung. *Nature* **386,** 852–855 (1997).

431. Kunnimalaiyaan, M., Vaccaro, A. M., Ndiaye, M. A. & Chen, H. Overexpression of the NOTCH1 intracellular domain inhibits cell proliferation and alters the neuroendocrine phenotype of medullary thyroid cancer cells. *J. Biol. Chem.* **281,** 39819–39830 (2006).

432. Chen, H. *et al.* Tissue-specific expression of human achaete-scute homologue-1 in neuroendocrine tumors: transcriptional regulation by dual inhibitory regions. *Cell Growth Differ.* **8,** 677–686 (1997).

433. Rapa, I. *et al.* Human ASH1 expression in prostate cancer with neuroendocrine differentiation. *Mod. Pathol.* **21,** 700–707 (2008).

434. Linnoila, R. I. *et al.* Constitutive achaete-scute homologue-1 promotes airway dysplasia and lung neuroendocrine tumors in transgenic mice. *Cancer Res.* **60,** 4005–4009 (2000).

435. Greenblatt, D. Y. *et al.* Valproic acid activates notch-1 signaling and regulates the neuroendocrine phenotype in carcinoid cancer cells. *Oncologist* **12,** 942–951 (2007).

436. Greenblatt, D. Y. *et al.* Valproic acid activates Notch1 signaling and induces apoptosis in medullary thyroid cancer cells. *Ann. Surg.* **247,** 1036–1040 (2008).

437. Johansson, T. A., Westin, G. & Skogseid, B. Identification of Achaete-scute complex-like 1 (ASCL1) target genes and evaluation of DKK1 and TPH1 expression in pancreatic endocrine tumours. *BMC Cancer* **9,** 321–333 (2009).

438. Osada, H. *et al.* Roles of achaete-scute homologue 1 in DKK1 and E-cadherin repression and neuroendocrine differentiation in lung cancer. *Cancer Res.* **68,** 1647–1655 (2008).

439. Krausch, M. *et al.* Notch 1 tumor expression is lacking in highly proliferative pancreatic neuroendocrine tumors. *Endocrine* **44,** 182–186 (2013).

440. Shida, T. *et al.* Aberrant expression of human achaete-scute homologue gene 1 in the gastrointestinal neuroendocrine carcinomas. *Clin. Cancer Res.* **11,** 450–458 (2005).

441. Shida, T. *et al.* The expression of NeuroD and mASH1 in the gastroenteropancreatic neuroendocrine tumors. *Mod. Pathol.* **21,** 1363–1370 (2008).

442. Tomasetti, C. & Vogelstein, B. Cancer etiology. Variation in cancer risk among tissues can be explained by the number of stem cell divisions. *Science* **347,** 78–81 (2015).

443. Calin, G. A. *et al.* MicroRNA profiling reveals distinct signatures in B cell chronic lymphocytic leukemias. *Proc. Natl. Acad. Sci. U. S. A.* **101,** 11755–11760 (2004).

444. Iorio, M. V *et al.* MicroRNA gene expression deregulation in human breast cancer. *Cancer Res.* **65,** 7065–7070 (2005).

445. Ambs, S. *et al.* Genomic profiling of microRNA and messenger RNA reveals deregulated microRNA expression in prostate cancer. *Cancer Res.* **68,** 6162–6170 (2008).

446. Reinhart, B. J. *et al.* The 21-nucleotide let-7 RNA regulates developmental timing in Caenorhabditis elegans. *Nature* **403,** 901–906 (2000).

447. Brennecke, J., Hipfner, D. R., Stark, A., Russell, R. B. & Cohen, S. M. bantam encodes a developmentally regulated microRNA that controls cell proliferation and regulates the proapoptotic gene hid in Drosophila. *Cell* **113,** 25–36 (2003).

448. Xu, P., Vernooy, S. Y., Guo, M. & Hay, B. A. The Drosophila microRNA mir-14 suppresses cell death and is required for normal fat metabolism. *Curr. Biol.* **13,** 790–795 (2003).

449. Michael, M. Z., O' Connor, S. M., van Holst Pellekaan, N. G., Young, G. P. & James, R. J. Reduced accumulation of specific microRNAs in colorectal neoplasia. *Mol. Cancer Res.* **1,** 882–891 (2003).

450. Akao, Y. *et al.* Role of anti-oncomirs miR-143 and -145 in human colorectal tumors. *Cancer Gene Ther.* **17,** 398–408 (2010).

451. Yu, F. *et al.* let-7 Regulates Self Renewal and Tumorigenicity of Breast Cancer Cells. *Cell* **131,** 1109–1123 (2007).

452. Ruebel, K. *et al.* MicroRNA expression in ileal carcinoid tumors: downregulation of microRNA-133a with tumor progression. *Mod. Pathol.* **23,** 367–375 (2010).

453. Li, S. C. *et al.* Global microRNA profiling of well-differentiated small intestinal neuroendocrine tumors. *Mod. Pathol.* **26,** 685–696 (2013).

454. Hamfjord, J. *et al.* Differential expression of miRNAs in colorectal cancer: Comparison of paired tumor tissue and adjacent normal mucosa using high-throughput sequencing. *PLoS One* **7,** 1–9 (2012).

455. Olson, P. *et al.* MicroRNA dynamics in the stages of tumorigenesis correlate with hallmark capabilities of cancer. *Genes Dev.* **23,** 2152–2165 (2009).

456. Li, A. *et al.* MicroRNA array analysis finds elevated serum miR-1290 accurately distinguishes patients with low-stage pancreatic cancer from healthy and disease controls. *Clin. Cancer Res.* **19,** 3600–3610 (2013).

457. Roldo, C. *et al.* MicroRNA expression abnormalities in pancreatic endocrine and acinar tumors are associated with distinctive pathologic features and clinical behavior. *J. Clin. Oncol.* **24,** 4677–4684 (2006).

458. Poy, M. N. *et al.* A pancreatic islet-specific microRNA regulates insulin secretion. *Nature* **432,** 226–230 (2004).

459. Ding, L. *et al.* MiR-375 frequently downregulated in gastric cancer inhibits cell proliferation by targeting JAK2. *Cell Res.* **20,** 784–793 (2010).

460. Liu, A. M., Poon, R. T. & Luk, J. M. MicroRNA-375 targets Hippo-signaling effector YAP in liver cancer and inhibits tumor properties. *Biochem. Biophys. Res. Commun.* **394,** 623–627 (2010).

461. Avnit-Sagi, T., Kantorovich, L., Kredo-Russo, S., Hornstein, E. & Walker, M. D. The promoter of the pri-miR-375 gene directs expression selectively to the endocrine pancreas. *PLoS One* **4,** 1–9 (2009).

462. Keller, D. M. *et al.* Characterization of pancreatic transcription factor Pdx-1 binding sites using promoter microarray and serial analysis of chromatin occupancy. *J. Biol. Chem.* **282,** 32084–32092 (2007).

463. Nishikawa, E. *et al.* miR-375 is activated by ASH1 and inhibits YAP1 in a lineage-dependent manner in lung cancer. *Cancer Res.* **71,** 6165–6173 (2011).

464. Zhao, H. *et al.* miR-375 is highly expressed and possibly transactivated by achaete-scute complex homolog 1 in small-cell lung cancer cells. *Acta Biochim. Biophys. Sin. (Shanghai).* **44,** 177–182 (2012).

465. Correa-Medina, M. *et al.* MicroRNA miR-7 is preferentially expressed in endocrine cells of the developing and adult human pancreas. *Gene Expr. Patterns* **9,** 193–199 (2009).

466. Nieto, M. *et al.* Antisense miR-7 impairs insulin expression in developing pancreas and in cultured pancreatic buds. *Cell Transplant.* **21,** 1761–1774 (2012).

467. Zhang, N. *et al.* microRNA-7 is a novel inhibitor of YY1 contributing to colorectal tumorigenesis. *Oncogene* **32,** 5078–5088 (2013).

468. Li, Y. *et al.* PAX6, a novel target of microRNA-7, promotes cellular proliferation and invasion in human colorectal cancer cells. *Dig. Dis. Sci.* **59,** 598–606 (2014).

469. Nicholson, S., Whitehouse, H., Naidoo, K. & Byers, R. J. Yin Yang 1 in human cancer. *Crit. Rev. Oncog.* **16,** 245–260 (2011).

470. Zong, X. *et al.* Possible role of Pax-6 in promoting breast cancer cell proliferation and tumorigenesis. *BMB Rep.* **44,** 595–600 (2011).

471. Miko, E. *et al.* Differentially expressed microRNAs in small cell lung cancer. *Exp. Lung Res.* **35,** 646–664 (2009).

472. Workman, C. *et al.* A new non-linear normalization method for reducing variability in DNA microarray experiments. *Genome Biol.* **3,** 1–17 (2002).

473. Brandt, D. W., Pandol, S. J. & Deftos, L. J. Calcium-stimulated parathyroid hormone-like protein secretion: potentiation through a protein kinase-C pathway. *Endocrinology* **128,** 2999–3004 (1991).

474. Giaccone, G. *et al.* Neuromedin B is present in lung cancer cell lines. *Cancer Res.* **52,** 2732s–2736s (1992).

475. Pitt, S. C., Chen, H. & Kunnimalaiyaan, M. Phosphatidylinositol 3-kinase-Akt signaling in pulmonary carcinoid cells. *J. Am. Coll. Surg.* **209,** 82–88 (2009).

476. Ball, D. W. *et al.* Identification of a human achaete-scute homolog highly expressed in neuroendocrine tumors. *Proc. Natl. Acad. Sci. U. S. A.* **90,** 5648–5652 (1993).

477. Van Buren, G. *et al.* The development and characterization of a human midgut carcinoid cell line. *Clin. Cancer Res.* **13,** 4704–4712 (2007).

478. Ellis, L. M., Samuel, S. & Sceusi, E. Varying opinions on the authenticity of a human midgut carcinoid cell line-letter. *Clin. Cancer Res.* **16,** 5365–5366 (2010).

479. Welin, S., Fjällskog, M. L., Saras, J., Eriksson, B. & Janson, E. T. Expression of tyrosine kinase receptors in malignant midgut carcinoid tumors. *Neuroendocrinology* **84,** 42–48 (2006).

480. Dean, D. A. & Gasiorowski, J. Z. Liposome-mediated transfection. *Cold Spring Harb. Protoc.* **6,** 55–83 (2011).

481. Atienza, J. M. *et al.* Dynamic and label-free cell-based assays using the real-time cell electronic sensing system. *Assay Drug Dev. Technol.* **4,** 597–607 (2006).

482. Ozdemir, A. & Ark, M. xCELLigence Real Time Cell Analysis System: A New Method for Cell Proliferation and Cytotoxicity. *Niche J.* **2,** 15–17 (2014).

483. Gentleman, R. C. *et al.* Bioconductor: open software development for computational biology and bioinformatics. *Genome Biol.* **5,** R80–R95 (2004).

484. Irizarry, R. A. *et al.* Exploration, normalization, and summaries of high density oligonucleotide array probe level data. *Biostatistics* **4,** 249–264 (2003).

485. Gregersen, L. H. *et al.* MicroRNA-145 targets YES and STAT1 in colon cancer cells. *PLoS One* **5,** 1–10 (2010).

486. Jacobsen, A., Wen, J., Marks, D. S. & Krogh, A. Signatures of RNA binding proteins globally coupled to effective microRNA target sites. *Genome Res.* **20,** 1010–1019 (2010).

487. Zheng, L., Baumann, U. & Reymond, J. L. An efficient one-step site-directed and site-saturation mutagenesis protocol. *Nucleic Acids Res.* **32,** e115–e119 (2004).

488. Messer, W., Bellekes, U. & Lother, H. Effect of dam methylation on the activity of the E. coli replication origin, oriC. *EMBO J.* **4,** 1327–1332 (1985).

489. Fraga, H., Fernandes, D., Fontes, R. & Esteves da Silva, J. C. Coenzyme A affects firefly luciferase luminescence because it acts as a substrate and not as an allosteric effector. *FEBS J.* **272,** 5206–5216 (2005).

490. Sherf, B. A., Navarro, S. L., Hannah, R. R. & Wood, K. V. Dual-Luciferase Reporter Assay: An Advanced Co-Reporter Technology Integrating Firefly and Renilla Luciferase Assays. *Promega Notes* **57,** 1–8 (1996).

491. Bravo-Egana, V. *et al.* Quantitative differential expression analysis reveals miR-7 as major islet microRNA. *Biochem. Biophys. Res. Commun.* **366,** 922–926 (2008).

492. Vorherr, H. Endocrinology of breast cancer. *Maturitas* **9,** 113–122 (1987).

493. Rodríguez-Rodero, S. *et al.* Epigenetic alterations in endocrine-related cancer. *Endocr. Relat. Cancer* **21,** R319–R330 (2014).

494. Siddique, Z. L. *et al.* KRJ-I and bon cell lines: Defining an appropriate enterochromaffin cell neuroendocrine tumor model. *Neuroendocrinology* **89,** 458–470 (2009).

495. Di Leva, G. & Croce, C. M. miRNA profiling of cancer. *Curr. Opin. Genet. Dev.* **23,** 1–14 (2013).

496. Selcuklu, S. D., Donoghue, M. T. a & Spillane, C. miR-21 as a key regulator of oncogenic processes. *Biochem. Soc. Trans.* **37,** 918–925 (2009).

497. Medina, P. P., Nolde, M. & Slack, F. J. OncomiR addiction in an in vivo model of microRNA-21-induced pre-B-cell lymphoma. *Nature* **467,** 86–90 (2010).

498. Hay, N. The Akt-mTOR tango and its relevance to cancer. *Cancer Cell* **8,** 179–183 (2005).

499. Missiaglia, E. *et al.* Pancreatic endocrine tumors: Expression profiling evidences a role for AKT-mTOR pathway. *J. Clin. Oncol.* **28,** 245–255 (2010).

500. Terris, B. *et al.* Expression of vascular endothelial growth factor in digestive neuroendocrine tumours. *Histopathology* **32,** 133–138 (1998).

501. Chaudhry, A., Oberg, K., Gobl, A., Heldin, C. H. & Funa, K. Expression of transforming growth factors beta 1, beta 2, beta 3 in neuroendocrine tumors of the digestive system. *Anticancer Res.* **14,** 2085–2091 (1994).

502. Höpfner, M., Baradari, V., Huether, A., Schöfl, C. & Scherübl, H. The insulin-like growth factor receptor 1 is a promising target for novel treatment approaches in neuroendocrine gastrointestinal tumours. *Endocr. Relat. Cancer* **13,** 135–149 (2006).

503. Pellegrinet, L. *et al.* Dll1- and dll4-mediated notch signaling are required for homeostasis of intestinal stem cells. *Gastroenterology* **140,** 1230–1240 (2011).

504. Waterhouse, C. C. *et al.* Secretory Cell Hyperplasia and Defects in Notch Activity in a Mouse Model of Leukocyte Adhesion Deficiency Type II. *Gastroenterology* **138,** 1079–1090 (2010).

505. Xu, L. *et al.* MicroRNA-7-regulated TLR9 signaling-enhanced growth and metastatic potential of human lung cancer cells by altering the phosphoinositide-3-kinase, regulatory subunit 3/Akt pathway. *Mol. Biol. Cell* **24,** 42–55 (2013).

506. Rindi, G., Capella, C. & Solcia, E. Cell biology, clinicopathological profile, and classification of gastro-enteropancreatic endocrine tumors. *J. Mol. Med.* **76,** 413–420 (1998).

507. Scherübl, H., Jensen, R. T., Cadiot, G., Stölzel, U. & Klöppel, G. Management of early gastrointestinal neuroendocrine neoplasms. *World J. Gastrointest. Endosc.* **3,** 133–139 (2011).

508. Eriksson, B., Oberg, K. & Stridsberg, M. Tumor markers in neuroendocrine tumors. *Digestion* **62,** 33–38 (2000).

509. Nobels, F. R., Kwekkeboom, D. J., Bouillon, R. & Lamberts, S. W. Chromogranin A: its clinical value as marker of neuroendocrine tumours. *Eur. J. Clin. Invest.* **28,** 431–440 (1998).

510. Vicentini, C. *et al.* Clinical application of microRNA testing in neuroendocrine tumors of the gastrointestinal tract. *Molecules* **19,** 2458–2468 (2014).

511. Capdevila, J. *et al.* Molecular biology of neuroendocrine tumors: From pathways to biomarkers and targets. *Cancer Metastasis Rev.* **33,** 345–351 (2014).

512. Kidd, M., Modlin, I. M., Mane, S. M., Camp, R. L. & Shapiro, M. D. Q RT-PCR detection of chromogranin A: a new standard in the identification of neuroendocrine tumor disease. *Ann. Surg.* **243,** 273–280 (2006).

513. Joglekar, M. V., Joglekar, V. M. & Hardikar, A. A. Expression of islet-specific microRNAs during human pancreatic development. *Gene Expr. Patterns* **9,** 109–113 (2009).

514. Tsukamoto, Y. *et al.* MicroRNA-375 is downregulated in gastric carcinomas and regulates cell survival by targeting PDK1 and 14-3-3zeta. *Cancer Res.* **70,** 2339–2349 (2010).

515. Pan, H. W., Li, S. C. & Tsai, K. W. MicroRNA dysregulation in gastric cancer. *Curr. Pharm. Des.* **19,** 1273–1284 (2013).

516. Dai, X. *et al.* Expression levels of microRNA-375 in colorectal carcinoma. *Mol. Med. Rep.* **5,** 1299–1304 (2012).

517. Xu, K., Chen, Z., Qin, C. & Song, X. Mir-7 Inhibits Colorectal Cancer Cell Proliferation and Induces Apoptosis By Targeting Xrcc2. *Onco. Targets. Ther.* **7,** 325–332 (2014).

518. Allegra, A. *et al.* Circulating microRNAs: New biomarkers in diagnosis, prognosis and treatment of cancer (Review). *Int. J. Oncol.* **41,** 1897–1912 (2012).

519. Zheng, D. *et al.* Plasma microRNAs as novel biomarkers for early detection of lung cancer. *Int. J. Clin. Exp. Pathol.* **4,** 575–586 (2011).

520. Mitchell, P. S. *et al.* Circulating microRNAs as stable blood-based markers for cancer detection. *Proc. Natl. Acad. Sci. U. S. A.* **105,** 10513–10518 (2008).

521. Criqui, M. H., Fronek, A., Klauber, M. R., Barrett-Connor, E. & Gabriel, S. The sensitivity, specificity, and predictive value of traditional clinical evaluation of peripheral arterial disease: results from noninvasive testing in a defined population. *Circulation* **71,** 516–522 (1985).

522. Reitsma, J. B. *et al.* Bivariate analysis of sensitivity and specificity produces informative summary measures in diagnostic reviews. *J. Clin. Epidemiol.* **58,** 982–990 (2005).
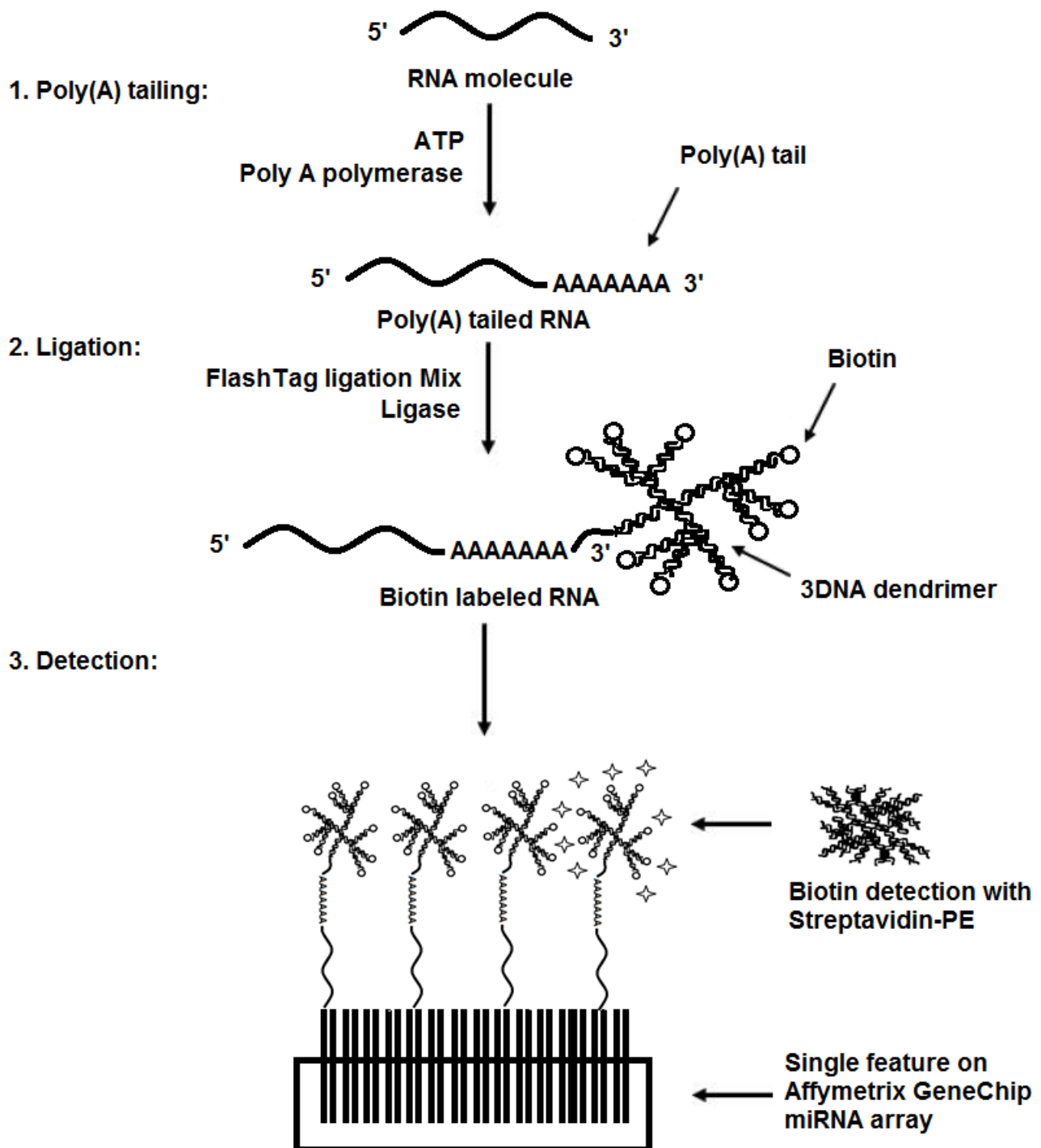
9 Appendix

Figure 24: A schematic overview of the following steps in Affymetrix miRNA array. To begin with RNA molecules are 1: poly(A) tailed by PolyA polymerase, followed by 2: ligation of biotin labeled 3DNA® dendrimer necessary for detection of hybridized miRNA to the GeneChip. After the FlashTag ligation, biotin label RNAs is hybridization to the Affymetrix Gene Chip and remaining unhybridized miRNAs are washed away. Hybridized miRNA is then 3: detected using Streptavidin conjugated with a reporter protein, such as Phycoerythrin (PE) which binds with high affinity to biotin and signal intensity is measured.

Differential expression of miRNAs in primary tumors versus normal tissue			
miRNA	*Fold-change*	*Regulation*	*p-value*
miR-183	42.2	up	0.0077
miR-7-5p	**39.0**	**up**	**0.0048**
miR-183-3p	36.8	up	0.0014
miR-615-3p	26.0	up	0.0006
miR-3065-3p	25.8	up	0.0043
miR-96	22.8	up	0.0001
miR-3065-5p	22.7	up	0.0059
miR-3200-3p	17.3	up	0.0026
miR-153	15.5	up	0.0035
miR-330-5p	14.0	up	0.0080
miR-708	12.0	up	0.0060
miR-182	11.8	up	0.0014
miR-301a	11.5	up	0.0008
miR-181d	10.8	up	0.0001
miR-181c-3p	9.4	up	0.0002
miR-330-3p	8.9	up	0.0083
miR-1250	7.5	up	0.0070
miR-1180	7.4	up	0.0072
miR-769-3p	6.8	up	0.0031
miR-2276	5.6	up	0.0044
miR-550a-3p	5.6	up	0.0041
miR-3200-5p	5.5	up	0.0071
miR-1301	5.5	up	0.0071
miR-375	**5.2**	**up**	**0.0093**
miR-615-5p	5.1	up	0.0069
miR-454	5.0	up	0.0052
miR-422a	17.2	down	0.0008
miR-378d	16.6	down	0.0006
miR-378g	16.3	down	0.0013
miR-378e	15.5	down	0.0017
miR-378a-5p	15.5	down	0.0020
miR-378i	14.7	down	0.0008
miR-378f	14.5	down	0.0008
miR-378c	11.9	down	0.0008
miR-378a	10.9	down	0.0009
miR-1184	3.0	down	0.0038
miR-4433	2.1	down	0.0039
miR-3656	2.1	down	0.0017

Table 3: Results from Affymetrix miRNA assay, showing miRNA profile of five different small intestine carcinoids versus four samples of normal tissue. The table shows 26 up-regulated and 12 down-regulated miRNAs, includes only miRNA with a 5-fold or greater change of expression compared to normal tissue and miRNA down regulated with a cut-off value of 2-fold. Only miRNA with a p-value below 0.01 are shown.
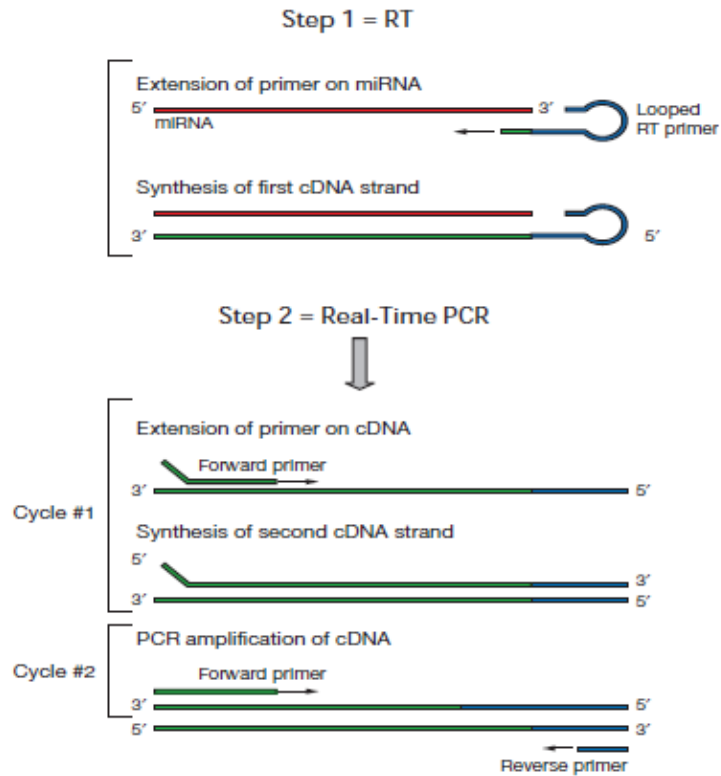
Figure 25: The overall principal of TaqMan® miRNA reverse transcription includes stem loop RT and RT-PCR.
Complimentary DNA (cDNA) is first reverse transcribed from total RNA using miRNA-specific looped primers for each miRNA. The looped 3'end primer binds at the 3'end of miRNA molecules and are reverse transcribed using reverse transcriptase. Then the PCR products are amplified from cDNA after denaturation step, using TaqMan® Universal PCR master mix. The advantages using this assay, is that the primers are only sensitive to mature miRNA, but not precursors, the assay requires only 1-10 ng of total RNA and it is a fast, reliable and simple to use (TaqMan manual).
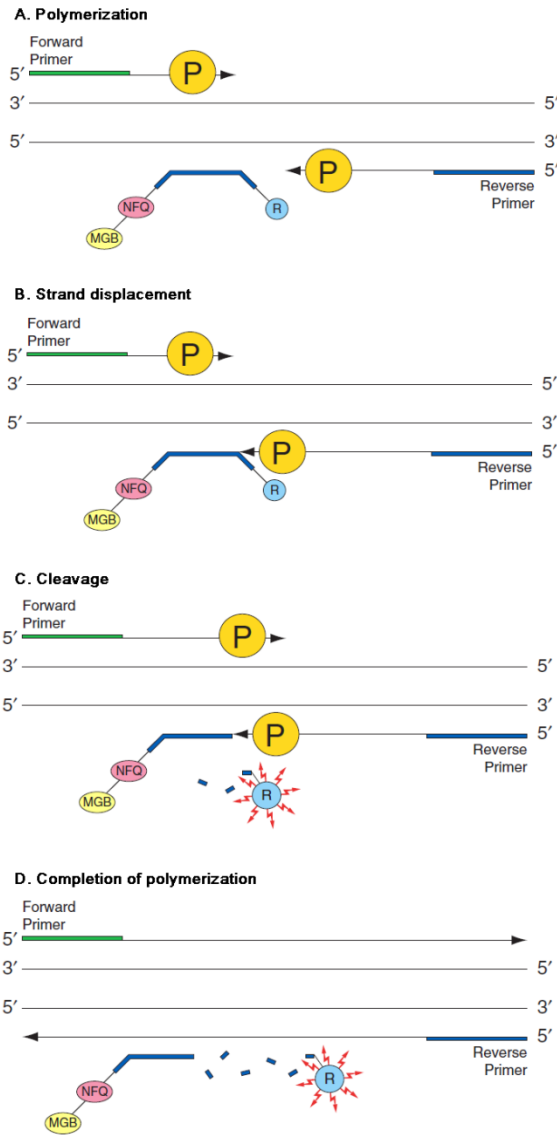
Figure 26: Following steps in TaqMan® qPCR reaction. A: During DNA amplification the probe anneals specifically to the complimentary sequence, between the forward and reverse primers. When the probe is intact and the reporter and quencher are at close proximity to each other, the fluorescence signal is suppressed. B-C: As the *Taq* polymerase reaches the probes it displaces and cleaves the hybridized probes, producing an exponential increase in cleaved reporter fluorescence emission and D: polymerization of the strand continues until completion. Because the 3'end of the probe is blocked, the probe is not extended. R: Reporter, NFQ: Non-fluorescent quencher, MGB: Minor groove binder, P: *Taq* polymerase (TaqMan manual).
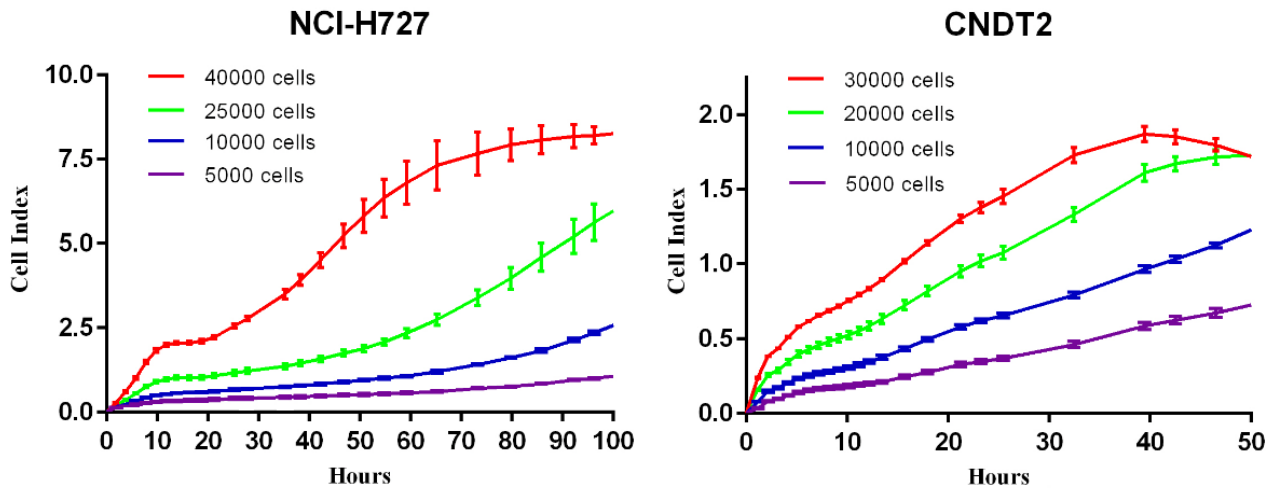
Figure 27: The titration assay used to determine the optimal cell number for growth measurement. A: The growth curve of NCI-H727 cells seeded in the numbers; 40.000 (red), 25.000 (green), 5000 (purple) and 2500 (black) cells per well. The wells with 40.000 cells showed most optimal growth rate were cells stop growing after 60 hours. B: The growth curve of CNDT2 cells seeded in the numbers; 30.000 (red), 20.000 (green), 10000 (blue) and 5000 (purple) cells per well. Because wells with 30.000 and 20.000 stop growing before 40 hours (become confluent), the number of 15.000 cells per well is considerate to be the most optimal for long-term growth measurement.
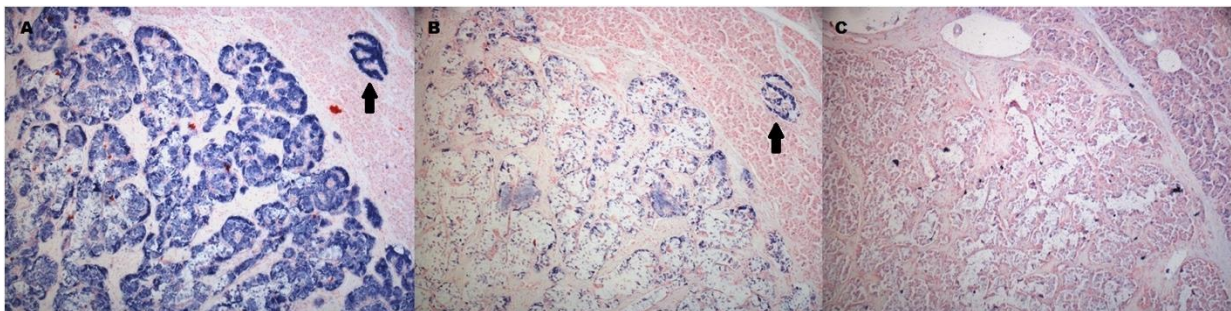

Figure 28: *In situ* **hybridization of miR-375, miR-7-5p and scramble miR in Insulinoma.** A-C: left panel: miR-375 ISH staining 5x; middle panel miR-7-5p ISH 5x; right panel: scramble miR ISH 5x. A and B: Note the specific binding of miR-375 and miR-7-5p LNA probes (blue) to endocrine cells located in the insulinoma and normal tissue (arrows), whereas C: the scramble miR do not bind to the tumor tissue. ISH: *In situ* hybridization.
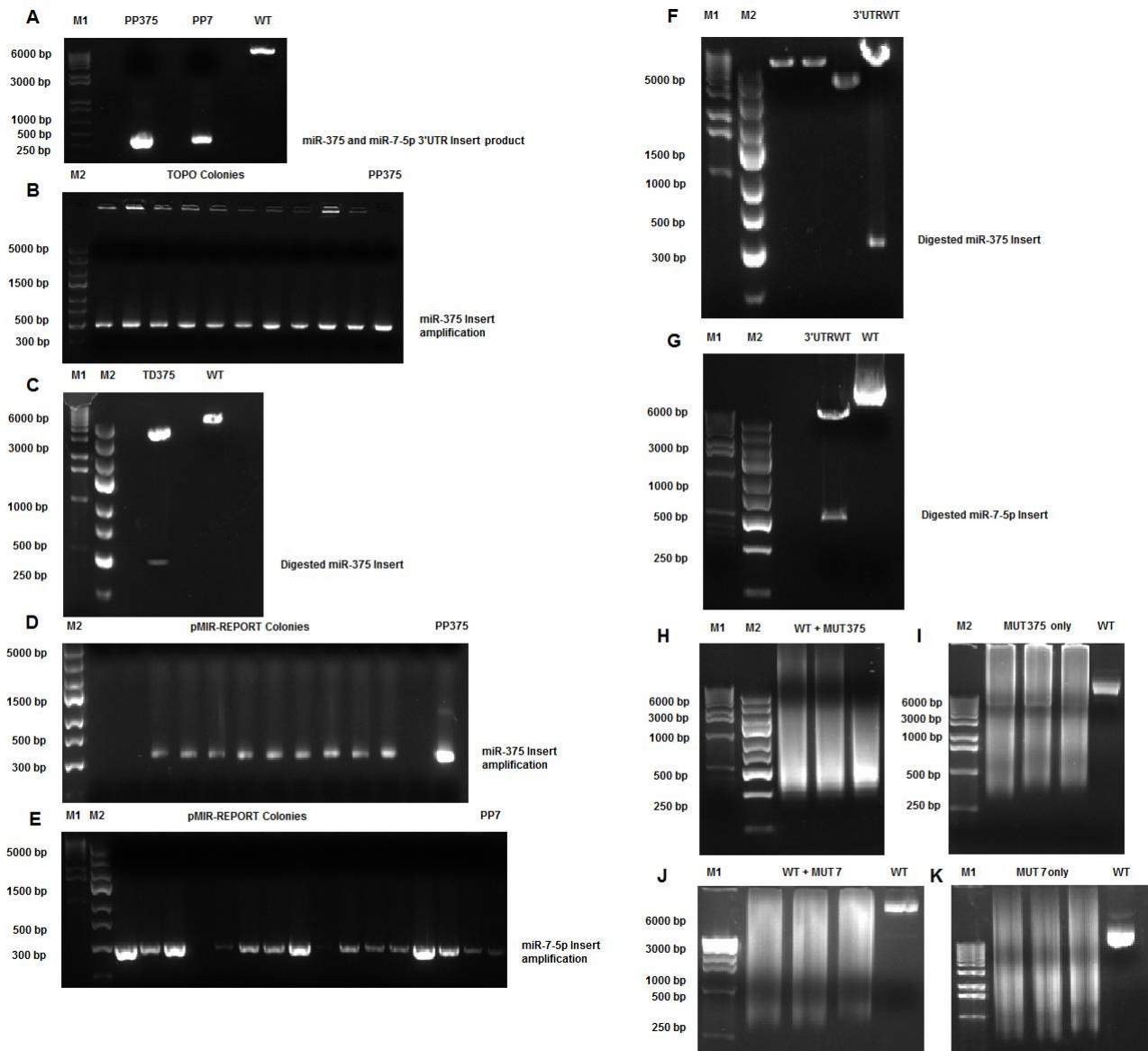
Figure 29: Validation of the PCR products and ligated inserts after digestion procedure. A: Agarose run confirm the presence of 3'UTR insert PCR products with binding site for miR-375 and miR-7-5p respectively, pMIR-REPORT without insert was used as negative control. B: Colony PCR of colonies containing possible recombinant pCR™-4-TOPO, 3'UTR insert with miR-375 binding site was used as positive control. C: After purifying the recombinant pCR™-4-TOPO by Maxi prep, the digestion of MluI/SpeI site confirm the presence of miR-375 3'UTR insert, pMIR-REPORT without insert was used as negative control. D: Colony PCR shows that most colonies contain the miR-375 3'UTR insert were miR-375 insert was used as positive control. E: Colony PCR shows that most colonies contain the miR-7-5p 3'UTR insert were miR-7-5p insert was used as positive control. F-G: Digestion of MluI/SpeI restriction sites in recombinant pMIR-REPORT showed that the plasmid contained the miR-375 or miR-7-5p 3'UTR insert which later was confirmed by sequencing. H and J: Results from site directed mutagenesis of pMIR-REPORT with 3'UTR for miR-375 and miR-7-5p respectively. No outlined bands, only 'smears' are shown. Nevertheless the DNA containing the nicked circular stand with incorporated mutation (pMIR-REPORT containing mutated 3'UTR site) and template strand (3'UTR pMIR-REPORT) was treated with DpnI (I and K) to remove template strand and then transformed into Top10 cells (shown in triplicates). M1: GeneRuler™ 1 kb DNA ladder (Cat. no. SM1163, Thermo Scientific), M2: GeneRuler™ Express DNA ladder (Cat. no. SM1551, Thermo Scientific), PP375: PCR-product insert of miR-375, PP7: PCR-product insert of miR-7-5p, WT: wild-type pMIR-REPORT, MUT: mutated pMIR-REPORT for miR-375 or miR-7-5p, TD375: Digestion of pCR™-4-TOPO with 3'UTR for miR-375, 3'UTRWT: wild-type pMIR-REPORT with 3'UTR for miR-375 or miR-7-5p.

PNET name	Primary/secondary hormone	Tumor location	Tumor Size, state	Associated syndrome	Clinical features	Diagnosis methods	Typical diagnosis age	Treatment	Malignant	MEN1 association
Insulinoma	Insulin	Pancreas Others: lung, duodenum, ileum, cervix and ovary	<2 cm, solid	Insulinoma	Hypoglycemia, neuroglycopenia (confusion, headache, visual changes, diaphoresis, tremor) and weight gain	The Whipple's criteria to establish hyperinsulinemia CT, MRI and EUS	30-60 years of age	Chance for curable surgery, Diazoxide octreotide, beta-blockers, emboli-zation, RFA, EUS-guided alcohol ablation	~10%	4-6%
Gastrinoma	Gastrin	Proximal duodenum Pancreas head Others: liver, bile duct, ovary, heart, pyloric canal, jejunum, and omentum	<1 cm, multiple 2-3 cm, solid	Zollinger-Ellison	Abdominal pain, diarrhea, gastroesophageal reflux and peptic ulcers	Measure FSG and the levels of gastric acid secretion. Secretin test and calcium test. Exclude other diseases with similar outcome SRS and EUS	40-50 years of age	Surgery, octreotide, H$_2$-receptor anta-gonists and PPIs	60-80%	25%
Glucagonoma	Glucagon Gastrin, Vasoactive intestinal peptide (VIP)	Pancreas tail	>6 cm	Glucagonoma	Necrolytic migratory erythema, mild glucose intolerance, weight loss, diarrhea, anemia and thromboembolism	Look after the presence of NME and measure serum Glucagon levels SRS and PET	40-60 years of age	Diet, Insulin, anticoagulation, surgery, octreotide, streptozotocin/fluorour acil, dacarbazine, sunitinib/bevacizumab and everolimus	60-70%	5-17%
VIPoma	VIP	Pancreas tail	4-5 cm	Verner-Morrison, WDHA	Watery diarrhea, hypokalemia, achlorhydria, hyperchloremic acidosis and dehydration	Look after the presence of watery diarrhoea/ watery stool and measure fasting VIP levels	50-60 years of age	Correction of fluid, acid-base and electrolyte abnormalities, octreotide, embolization, streptozocin/doxorubic in and sunitinib	50%	6-11%
Somatostatino ma	Somatostatin	Pancreas Duodenum Other: jejunum, cystic duct area	>2 cm <2 cm	Somatostatinoma	Hyperglycemia, gallbladder disease, diarrhea, steatorrhea, cholelithiasis and weight loss; typically only symptomatic with pancreatic lesions	Measure fasting serum Somatostatin levels. Histological examination. SRS and FDG-PET	~50 years of age	Diet, Insulin, pancreatic enzymes, surgery, octreotide and chemoembolization	~60%	5-10%
Non-functional PNET	None, pancreatic polypeptide	Pancreas head, other areas of pancreas	>3 cm	NF PNET	None, may be first diagnosed due to mass effects	Measure CgA, PP or hCG. SRS, MIBG and EUS	40-50 years of age	Surgery, octreotide, lanreotide and PRRT	>60%	20%, true incidence unknown

Table 4: Schematic representation of all PNETs with hormone secretion, tumor location, size, syndromes, clinical features, diagnosis, treatment, malignant and MEN1.